Generalized Modeling of Complex Dynamical Systems: An Application to the Stability of Ecological Networks

By

Stefan Awender

A Dissertation Presented in the Partial Fulfillment for
the Degree of

Doctor of Philosophy

in

Physics

University of Alaska Fairbanks
May 2023

APPROVED:

Renate Wackerbauer, Committee Co-Chair
Greg Breed, Committee Co-Chair
David Newman, Committee Member
Pat Doak, Committee Member
Martin Truffer, Chair
Physics Department
Karsten Hueffer, Interim Dean
College of Natural Science & Mathematics
Richard Collins, Director
Graduate School

Abstract

Understanding the stability of food webs is crucial for resource sustainability and conservation of ecosystems, especially in the context of climate change. Specific models describe the biomass flow in food webs by a set of ordinary differential equations that require the explicit reconstruction of a mathematical expression for each of the interactions or processes, like predator-prey interactions, primary production, and mortality. Although specific models are rich with time-evolution information, limited access for empirical observation of these typically immense systems induce uncertainty in the data and approximations in the corresponding models that can threaten robustness or relevance of results. Generalized models can produce the stability of all the equilibria of specific models that have the same vague structure and bypasses the requirement to specify every function by evoking a normalizing transformation. The analysis is subsequently computationally efficient and can be used to study large food webs with a great number of replicates.

Often generalized ecological network studies confine the scope to a small subset of the variable dynamical scenarios, but this limits the interpretations that can be inferred. With this in mind, we develop a deterministic food-web generator that can be used to compare large food webs that differ by only a single link and maintain an expansive dynamical scope. We found behavior that indicates the existence of critical links and a grander theory on topological equivalence. We explicitly show how we can create hypothetical paths the system may traverse upon enrichment of lower trophic levels using the expanded dynamical scope.

Generalized modeling is unable to produce evolution solutions among other things, but it has an unlimiting access to the stability of equilibria while specific models provide only a subset of stability data. Generalized modeling is a relatively new method and its relation to specific model outcomes/results is not clearly understood. Specific models can inform generalized modeling studies on properties like coexistence of fixed points or actually occurring relative weighting of flows between ecosystem members. We combined the methods and demonstrated the validity of the abstract technique of generalized modeling in emphasis to its usefulness/power for the analysis of network stability. The specific model provided a unifying explanation to a conglomerate of related microcosm experiments that showed conflicting results on enrichment and implied stabilization upon the hampering of predatory efficiency. We identified the conditions by which enrichment is stabilizing to a steady state when basal species are in a resource-deprived environment but destabilizing if resources become more abundant.

A prevalent issue in ecology involves discrepancies between simulation and empirical observation about food-web stability such as how intuition says enrichment or complexity in some way are favorable to stability but mathematical models find it predominately the oppo-

site. A common rationalization for these discrepancies includes discourse on reductionistic versus holistic rhetoric. The idea being that as models become better representations of ecosystems that capture more intricacies and detail, they will help to resolve the issue. We constructed over a million food webs that reveal positive effects on fixed-point stability from the incorporation of more realistic ecosystem features that include species specialization, habitat modularity, and predator's prey preferences.

Arctic warming is a portent to changes in species composition and ecological theory predicts the existence of key ecosystem members that have extraordinary influence on overall ecosystem function or the state of the system. Motivated by sea-ice loss and northward expansion of species distributions, ice-obligate species are removed from the food webs and southern competitors are introduced. Although it is common understanding that apex predators can enhance biodiversity, we find the presence of "super killers" significantly destabilizes food webs.

Ecosystems have immense complexity with thousands of species, but ecosystem models condense and consider only a few species that are of the most interest or abundance, neglecting the many weak interactions comprising the larger ecosystem. Considering this, we suppose a food web is subsumed by a larger phantom ecological network that represents hypothetically rare species or predator-prey relationships. Each link from the phantom network contributes a variably weak perturbation, but collectively, induce a net positive effect on the average stability of the food webs, considerably so near the optimal perturbation strength.

Table of Contents

List of Figures

List of Tables

Page

Acknowledgements

I assert that I was the principle investigator for all work of this thesis, but without the ample literary help and the scrupulous advice from Greg Breed and Renate Wackerbauer this work would not have achieved this form.

Despite the many sleepless nights and incessant work sessions, I cherish all that I learned while studying physics at UAF. I feel blessed with my family and friends for their undying support and I relish the new memories of the fantastic minds and wonderful company that I was fortunate enough to have crossed my path.

I would like to thank the Institute of Arctic Biology for awarding me Graduate Summer Research Award a few times and the Graduate School for awarding me a Dissertation Completion Fellowship.

Chapter 1 Introduction

The vitalness natural ecosystems provide to human life cannot be overstated. The benefits they provide include materials (e.g. food security, lumber, biofuel, water treatment), supportive services (e.g. economic prosperity, genetic biodiversity, dilution of pathogens, decomposition of waste), and cultural services (Costanza et al.; 1997). They operate as powerful agents in global-scale carbon cycles and sequestration (Borges and Abril; 2011; Polimene et al.; 2017; Basu and Mackey; 2018), as well as, host a variety of organisms that offer cures for maladies and influence for technological advances (Drew et al.; 2007; Marmottant et al.; 2013). It is prudent that the conservation and understanding of these valuable marvels are among our most heightened concerns.

1.1 Ecological Background

An ecosystem (Jorgensen; 2009) is a natural environment that hosts a complex of interplay between a variety of organisms and habitats. Matter and energy is held in the constituents and transfers may occur amongst each other or between the abiotic environment. A basic description of an ecosystem's biotic constituents includes producer organisms that create complex organic substances from simple inorganic substances through various biosynthetic processes and consumer organisms that get nutrients and/or energy from ingesting performed organic substances. Also, organisms are found to use the various combinations of sources for energy, electron donors, and carbon, and their distinctions make up the primary nutritional groups. The ecosystem models in this work are a community network of Chemoorganoheterotrophs, e.g. predators, decomposers, and detrivores. Species traits further refine the species' description, namely, morphology and behavior can be unique to each member of the community. For instance, different types of predators include true predators, grazers, parasites, and parasitoids. Other member attributes can include, body size, habitat, cannibalism, etc. Nutritional groups and species traits are determinative of the possible connections and the physical/ecological processes that drive the flows. Some other types of interactions include competition and symbiosis.

Different environments host different species compositions and affect the topology or network structure. For instance, terrestrial environments are characterized with macrophytic producers that are marked with cellulose and lignin to support their structural integrity with typical trophic consumers (primary, secondary, tertiary, etc.) and decomposition, while marine environments are dominated with microphtytic plankters and the subsequent consumer

agents. Marine and terrestrial systems both form a kind of monocyclic system, while lacustrine environments are characterised by plankters and macrophytic pond weeds as primary producers forming a kind of bi-cyclic system (Hazen; 1975). In a furtherance of this discourse, sympagic or partial sympagic systems could feature ice-algae as a primary producer (Hop and Gjøsæter; 2013).

Ecological networks (Pascual et al.; 2006; De Ruiter et al.; 2005; Winemiller and Polis; 1996; Polis and Winemiller; 2013) are expressed by having the biotic constituents be the nodes of the network and the connections or links embody the flows of various ecological processes. A node of an ecological network could represent an individual organism that begins at birth and maintains a time-dependant in-flux and out-flux of energy until terminating in death. However, a macroscopic perspective, that permits autonomous modeling (not explicitly dependant on time) and intrinsically reduces the size of the system, treats nodes as populations. Albeit, a population has a life history in which different life stages may have different connections and processes. Often, modelers of animal communities attempt to resolve this aspect by segmenting the population into two or more nodes (e.g. adults and juveniles). Many ecological networks are described with a few hundred species (Elmgren and Hill; 1997; Gaichas and Francis; 2008). From this macroscopic perspective, the sizes of the networks would still be huge. There have been over five million animal species classified, with the most depauperate ecosystems (e.g. the Arctic marine ecosystem) recording thousands of species (Boenigk et al.; 2015). To combat the problem of too many nodes, subsets of the community are taken into consideration and the ignored constituents are assumed to be part of the ecosystem that has negligible impact to the functioning of the considered system. Additionally, some taxonomically different species may have very similar functions or roles in an ecosystem (e.g. similar prey, similar predators) so they can be coalesced into one node, these are referred to as trophospecies. Typically, few to a few tens of species are considered when ecosystems are modeled as dynamical systems. In light of this, some real systems that have a few species are found in agricultural systems, experimental ecosystems (microcosms) (Karam et al.; 2012), and natural systems in isolated areas.

Ecology is often concerned with understanding ecosystem functioning and the features that impact said functioning. For instance, consider an observation that predators are more generalists than prey. This motivates the claim that this feature, in effect, enhances the survival of prey when predators are numerous and enhances the survival of predators when prey is scarce. This feature manifests in the topology; higher trophic levels become less discrete and the average chain length is shortened. Other topological features studied are network size (number of nodes) and connectance (link density). These two topological features and link-strength variance are also the main features of discourse on the complexity of ecological

networks.

In the study of ecological networks as dynamical systems, typical questions are concerned with how a particular feature in the ecological system impacts other features or the long-term fate of the system. For example: Does the presence of apex predators (e.g. wolf introductions (Ripple and Beschta; 2012)) or increasing a limiting nutrient (e.g. iron fertilization (Coale et al.; 1996)) impact the system's size (biodiversity), capacity (overall biomass), and/or likelihood it will approach a steady state? Will each species survive forever? There are examples of competitive exclusion (Lotka; 1932) which describes systems in which there will be one survivor of two competing species. On the other hand, change some of the parameters in such a system and it can be found that both survive at a stable steady state. Many ecological systems that allow each species to persist might exhibit stable steady state dynamics, cycles, or chaos.

In the study of ecosystems, population dynamics has demonstrated to be a prolific and eminent source of ecological insight. These mathematical simulations offer a means to study key processes and distinguished properties driving ecosystem behavior. The popularly studied period-4 salmon population cycles in the Fraser river (with a high year, an intermediate year, and followed with 2 low years) is an exceptional example of how simple ecosystem models have met success in discerning that a periodic attractor imitates, in silico, the complicated cycles observed from nature (Guill et al.; 2011). However, ecosystems in general are too complex to make such accurate predictions from overly simplified models. The amount of computations and derivations required increases superlinearly as complexities are added to the models. However, the development of a framework in the analysis of generalized models offers a means to extensively gain local stability insights from large, multi-process ecological models (Gross et al.; 2009).

1.2 Dynamical Systems

Dynamical systems are used in a diverse group of disciplines, but have roots in physics. The subject was conceived in the mid-1600s, when Newton invented differential equations and solved the gravitating two-body problem. Later, efforts to extend the analytics to the three-body problem were unsuccessful. It was not until the late 1800s when Poincaré provided the context of modern dynamical systems theory through geometric thinking. Instead of explicitly solving the problem, he instead asked qualitative question, like will the system remain for all time (Koon et al.; 2000). It is now a vast interdisciplinary field that has been extended to economics, ecology, chemical reactors, and engineering, to name a few.

A typical dynamical system is the mathematical formalization of a deterministic process,

by which the present state of the system moves in accord with an evolution law (Kuznetsov; 1998). An evolution operator $\phi^t : \mathbb{X} \to \mathbb{X}$ acts on points in an n-dimensional state space $\mathbb{X}$. Provided the initial state $\boldsymbol{x}_0 \in \mathbb{X}$ is known, the evolution operator maps $\boldsymbol{x}_0$ to the state $\boldsymbol{x}_t$ after some continuous or discrete time t,

$$\boldsymbol{x}_t = \phi^t \boldsymbol{x}_0. \tag{1.1}$$

In discrete time, the evolution operator is an iterated map, in which, for integer timescale $\phi^2 \boldsymbol{x}_0 = \phi^1(\phi^1 \boldsymbol{x}_0)$. In continuous time, the evolution operator is generally found by solving a set of differential equations called the flow. The forms of these differential equations may be partial differential equations that usually depict the state temporally and spatially or they may be expressed as an autonomous (time-independent) coupled set of ordinary differential equations of the velocities of the state variables and parameterized by a set of system parameters $\boldsymbol{p}$,

$$\dot{\boldsymbol{x}} = f(\boldsymbol{x}; \boldsymbol{p}), \tag{1.2}$$

where $\boldsymbol{x} \in \mathbb{X}$ and f is generally a nonlinear function. If there exists a point $\boldsymbol{x}^* \in \mathbb{X}$ such that $f(\boldsymbol{x}^*) = 0$, then $\boldsymbol{x}^*$ is an equilibrium point or fixed point. If a system is in the state $\boldsymbol{x}^*$, it will stay there for all time. At the fixed point, if the system receives a sufficiently small perturbing kick, the state will evolve in time and follow its trajectory, $\boldsymbol{x}(t)$. Numerical techniques estimate discretized solutions of $\boldsymbol{x}(t)$ with time step $\Delta\tau$. The crudest estimate has its n^{th} element

$$\boldsymbol{x}_n = \boldsymbol{x}_{n-1} + f(\boldsymbol{x}_{n-1})\Delta\tau, \tag{1.3}$$

known as the forward Euler method. The error of this estimation approaches zero as $\Delta\tau \to 0$. If the trajectory eventually returns to the fixed point from any perturbation direction, then the fixed point is attracting. If trajectories do not eventually return but remain close, then the fixed point is Lyapunov stable. A fixed point can be either or, but if it is both attracting and Lyapunov stable, it is asymptotically stable (or just stable). A fixed point is unstable if it is neither.

A fixed point is a type of invariant set. An invariant set, $S \subset \mathbb{X}$, is a subset of the state space such that any trajectory $\boldsymbol{x}(t)$ that starts in S stays in S for all time. More complicated than a fixed point, a closed cycle is also an invariant set. Also, there are invariant manifolds, such as the two-torus or chaotic attractor, that can contain an infinite number of periodic or nonperiodic orbits. When the invariant set attracts an open set of initial conditions and is minimal it is called an attractor.

1.2.1 Example: One-Dimensional Flows

Consider an organism's population $x \geq 0$ such that the per-capita birth rate $\dot{x}/x$ is a constant, then the population will undergo exponential growth and the flow is linear. The only fixed point, $x^* = 0$, is a repellor (unstable). If population is limited to a finite resource, then intraspecific competition would act to decrease the per-capita birth rate as the population increases. A per-capita birth rate that decreases linearly, becoming negative after some population k called the carrying capacity, is known as logistic growth and has a differential form

$$\dot{x} = rx\left(1 - \frac{x}{k}\right), \tag{1.4}$$

where r is a growth rate. Although the solution $x(t)$ can be solved analytically with separation of variables and direct integration, we can qualitatively gain insight with a geometrical analysis from just plotting the flow. If $0 < x < k$, the flow is positive and x is increasing, for $x > k$ the flow is negative and x is decreasing. In any case, $x(t)$ approaches k as $t \to \infty$ for any $x_0 > 0$, Fig. 1.1a. For initial conditions $0 < x_0 < k/2$ the trajectory is accelerating until $x = k/2$ at the maximal growth after which the flow slows down and asymptotically approaches the fixed point. This yields a sigmoid curve in a time series diagram, Fig 1.1b. If $k/2 < x_0 < k$, $x(t)$ is slowing down and moving in the positive direction for all time. If $x_0 > k$, $x(t)$ is slowing down and moving in the negative direction.

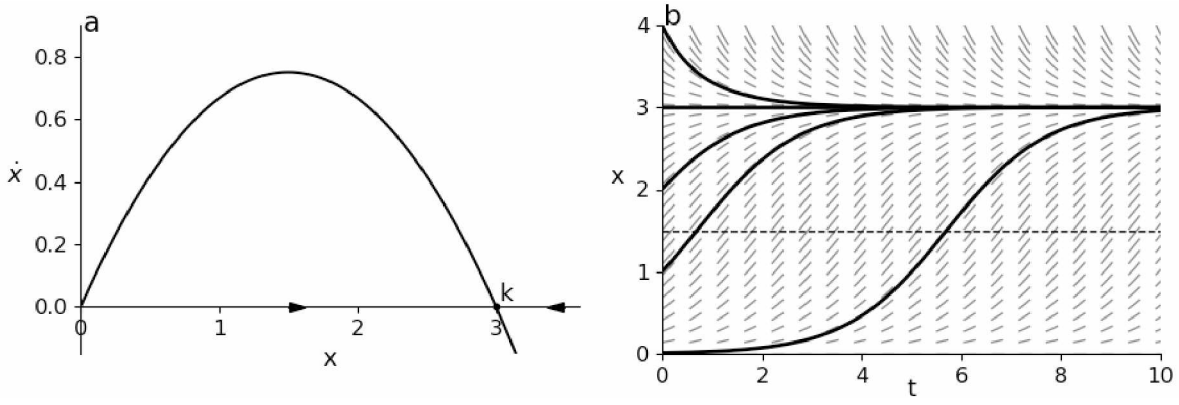

Figure 1.1: Flow and time series. a) Logistic growth flow, Eq. (1.4) and b) time series $x(t)$. $(r, k) = (1, 3)$. The dashed horizontal line is $x = k/2$.

In an environment with predators, a loss term is added to the flow that imitates a predator response. If the predator response is linear, this describes a predator limited by search or wait time. This function fits well with filter-feeders and is called Lokta-Voltera or Holling's type I predator response. When prey becomes so abundant that search time goes to zero, predator consumption is limited by handling time (the time it takes to process the food)

and the flow approaches a saturation (e.g. Holling's type II, Ivlev, Monod (Groß; 2004)). At saturation, the predators are eating as much as they can. When predators require practice to be apt at the hunt or prey can hide in limited hiding spots (this behavior is also consistent with prey switching), then when prey is scarce hunting efficiency is low and continues to decrease for decreasing prey. Combining the functionalities discussed so far, the response would have an S-shape, (e.g. Holling's type III, sigmoid). The inflection point on a Holling's type III response is at a prey population for which the loss flow is half its saturation flow. When prey have tough outer tissue, this would increase the handling time and decrease the max loss. When prey have camouflage, the search time is increased but handling time is unaffected resulting in a larger prey population for the half saturation. When prey exhibit collective defense, then after some prey population an increase of prey will decrease the response, e.g. Holling's type IV.

A population's flow that has logistic growth and a loss from a Holling's type III predator response is

$$\dot{x} = rx\left(1 - \frac{x}{k}\right) - \frac{x^2}{1 + x^2} \tag{1.5}$$

with carrying capacity k and growth rate r. Figure 1.2a depicts the flow increasing as the r values increase for fixed k. $x^* = 0$ is an unstable fixed point. Nontrivial fixed points are solutions to

$$r\left(1 - \frac{x}{k}\right) - \frac{x}{1 + x^2} = 0. \tag{1.6}$$

The number of nontrivial fixed points will be one, two, or three. For small r, there is one nontrivial fixed point and it is stable at low population. For sufficiently large k, increasing r will result in the creation of two higher-population fixed points, the smaller of the two is unstable and the larger one is stable. A bistable configuration of three nontrivial fixed points is set, dark line in Fig. 1.2a. The large-valued stable point is referred to as outbreak, the small-valued stable point is the refuge point. Increase k or r enough and an annihilation of the unstable point and the refuge point will leave only the outbreak point. This outbreak phenomenon is known as a cusp catastrophe (Strogatz; 2018). When there are two nontrivial fixed points, one of those fixed points corresponds to a blue-sky bifurcation, also known as a saddle-node bifurcation.

Blue-sky bifurcations are the creation or annihilation of two fixed points as a parameter is varied and the stability of this fixed point is sometimes called half stable since it attracts some of the state space and repels some. Figure 1.2b is a bifurcation diagram that plots the nontrivial fixed points as the two parameters, r and k, are varied. The projection of the bifurcations on the rk-plane depicts two lines that form a cusp. If system parameters are set to values between the two lines, then the system has a bistable configuration.

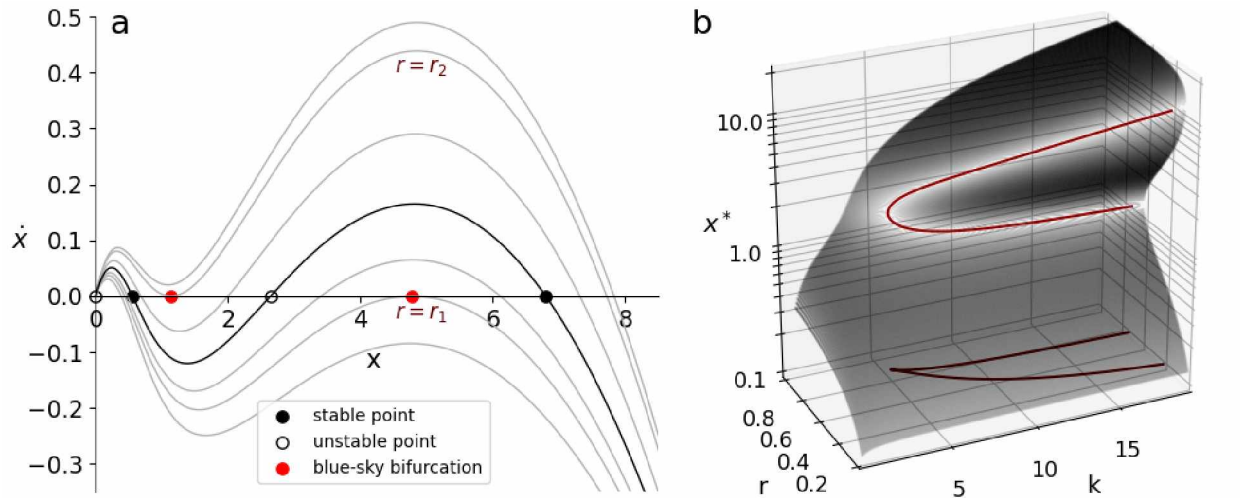

Figure 1.2: Logistic growth minus a predator response. (a) Flow of the population, Eq. (1.5), for different values of the intrinsic growth rate $r \in \{0.35, r_1, 0.41, 0.45, 0.5, r_2, 0.58\}$, where r_1 and r_2 are the bifurcation points and $k = 10$. (b) Bifurcation diagram with the fixed points as a function of system parameters, r and k. Fixed points are depicted with dark color and the bifurcations are depicted with red color and projected onto the rk-plane.

1.2.2 Example: Two-Dimensional Flows

Consider the two-species food chain with a Holling's type II predator response, species x has a logistic growth and its predator, species y, is affected with natural mortality

$$\dot{x} = rx\left(1 - \frac{x}{k}\right) - \frac{xy}{h+x} \tag{1.7}$$

$$\dot{y} = \eta\left(\frac{xy}{h+x} - y^2\right). \tag{1.8}$$

η is called an assimilation coefficient, and h is the half-saturation parameter.

The trivial fixed points are $(x^*, y^*) = (0,0)$ and $(k,0)$. The nontrivial fixed points are calculated from the intersections of the two nullclines. The x-nullcline is the curve for which $\dot{x} = 0$

$$y = \frac{r(k-x)(h+x)}{kx}. \tag{1.9}$$

The y-nullcline is the curve for which $\dot{y} = 0$

$$y = \frac{x}{h+x}. \tag{1.10}$$

The stability of these fixed points are acquired from the linearization of the system

(Strogatz; 2018). Consider the system

$$\dot{x} = f_1(x, y) \tag{1.11}$$

$$\dot{y} = f_2(x, y) \tag{1.12}$$

with a fixed point at (x^*, y^*). A Taylor expansion about the fixed point, using (x, y)=$(x^* + u$, $y^* + v)$, yields the linearized system

$$\begin{pmatrix} \dot{u} \\ \dot{v} \end{pmatrix} = \begin{pmatrix} \partial f_1/\partial x & \partial f_1/\partial y \\ \partial f_2/\partial x & \partial f_2/\partial y \end{pmatrix} \begin{pmatrix} u \\ v \end{pmatrix}. \tag{1.13}$$

The matrix of partial derivatives is known as the Jacobian matrix and has two eigenvalues, λ_1 and λ_2. If the eigenvalues are distinct, two linearly independent eigenvectors ($\boldsymbol{v}_1$ and $\boldsymbol{v}_2$) span the state space and the perturbation evolves as a linear combination of the eigenvectors,

$$\begin{pmatrix} u(t) \\ v(t) \end{pmatrix} = c_1 e^{\lambda_1 t} \boldsymbol{v}_1 + c_2 e^{\lambda_2 t} \boldsymbol{v}_2. \tag{1.14}$$

If the eigenvalues are purely real and both negative, then the fixed point is a stable node and the system asymptotically approaches the fixed point at a rate corresponding to the largest eigenvalue (slowest eigendirection). If both eigenvalues are positive, the fixed point is an unstable node. If one eigenvalue is positive and the other is negative, then the fixed point is called a saddle point and a typical perturbation will move away from the fixed point. If the eigenvalues are complex, then they are conjugate to each other and the state will evolve in time t as logarithmic spirals near the fixed point. In other words, time series represent exponentially decaying oscillations, if the real part is negative, and exponentially growing oscillations, if the real part is positive (Strogatz; 2018). The imaginary part quantifies the angular velocity.

Figure 1.3a is a bifurcation diagram that plots the fixed points and their stability as the half-saturation h is varied. For small h, the fixed point is an unstable spiral and typical initial conditions approach the stable limit cycle. Increasing h decreases the size of the limit cycle until the limit cycle collides with the fixed point at the critical h value, where the fixed point suddenly becomes a stable spiral. This critical parameter is called a supercritical Hopf bifurcation point. At the Hopf bifurcation point the two conjugate eigenvalues cross the imaginary axis, Fig. 1.3b.

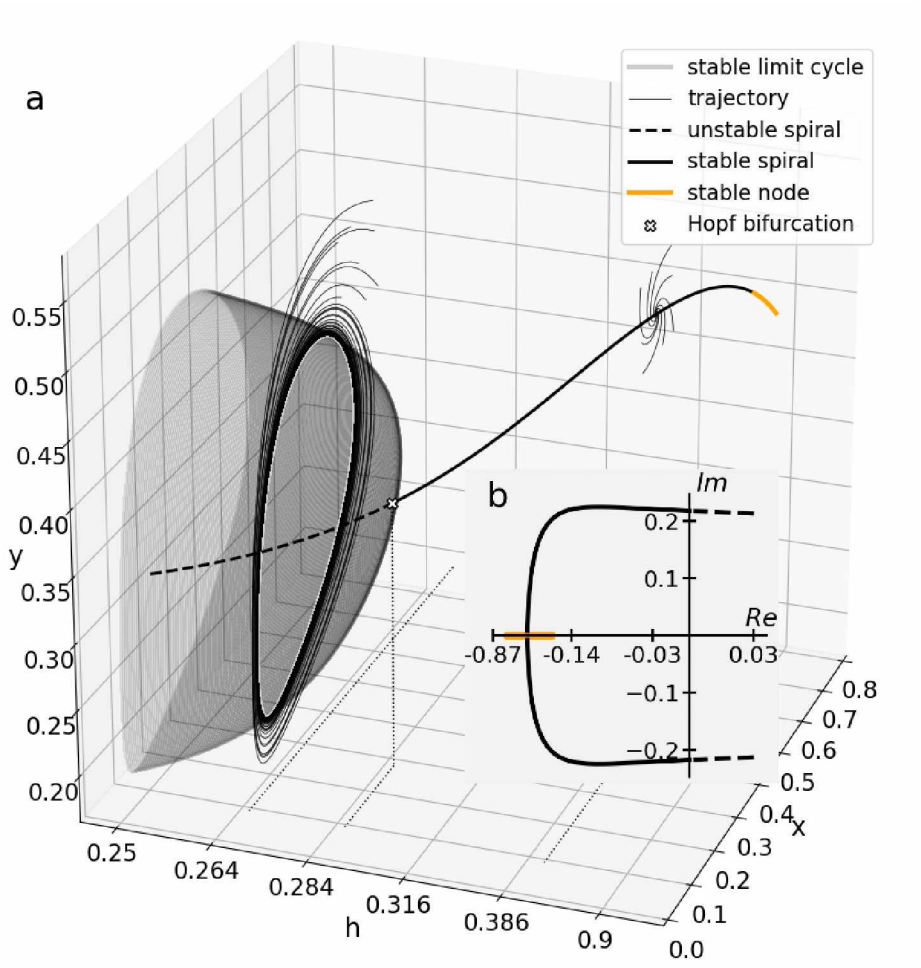

Figure 1.3: Bifurcation diagram and eigenvalues of a two-species food chain. a) Bifurcation diagram, Eq. (1.8). The Hopf bifurcation occurs at $h \approx 0.292$. Trajectories for a set of nine initial conditions are shown as thin, black lines for two different values of h, $\{0.27,0.45\}$. b) Eigenvalues of the Jacobian in the complex plane for each value of h, with Im the imaginary part and Re the real part. $k = 1$, $\eta = 0.333$, and $r = 1$.

1.3 Lotka-Volterra Competition

Large or poorly-parameterized systems are unsuited for conventional analysis, but abstract techniques can be employed for some analysis such as generalized modeling (GM) (Gross and Feudel; 2006), the primary focus of this thesis. To become accustomed with the basic mathematical framework of GM and introduce how it can be employed for scientific analysis, we consider a system with two competing species. First, a conventional analysis of a specific model is conducted in both a geometric and an analytic way. Following that, an alternative approach is used on the specific model that mimics the mathematical framework of GM before the fully-generalized Jacobian of such systems is derived.

1.3.1 Specific Model

In the early 20th century, Alfred Lotka, Vito Volterra, and Georgii Gause played significant roles in establishing modern ecology as a rigorous scientific discipline. They were the first to explore interspecific competition through quantitative methods (Volterra; 1926; Lotka; 1932) and these foundational contributions have been re-released in Gause (2019). The model that we discuss here is derived from these works and describes two species competing for resources, with each having logistic growth and a loss term that depends linearly on the competition. This model is known as the Lotka-Volterra competition equations.

$$\dot{X}_1 = \frac{r_1 X_1}{k_1}(k_1 - X_1 - a_1 X_2) \tag{1.15}$$

$$\dot{X}_2 = \frac{r_2 X_2}{k_2}(k_2 - X_2 - a_2 X_1) \tag{1.16}$$

where $X_i \geq 0$ and $r_i, k_i, a_i > 0$. The r_i is the growth rate and k_i is the carrying capacity of X_i. The competition coefficient, a_i, represents the interspecific competitive impact X_j has on X_i relative to the intraspecific competitive impact X_i has on itself, with $i, j \in \{1, 2\} | i \neq j$. The trivial fixed points are $(X_1^*, X_2^*) = (0, 0), (0, k_2), (k_1, 0)$. An isocline is a curve for which all the solutions of the ordinary differential equation intersecting that curve have the same slope. The isoclines can be found with $\dot{X}_2/\dot{X}_1 = dX_2/dX_1 = C$, for some constant C. The X_i-nullcline is the curve for $dX_i = 0$. The nullclines that determine the nontrivial fixed point are

$$X_i = k_i - a_i X_j, \tag{1.17}$$

and yield a fourth fixed point

$$X_i^* = \frac{k_i - a_i k_j}{1 - a_i a_j}. \tag{1.18}$$

If $a_1 a_2 = 1$, the nullclines are parallel and the equations of motion can be written in the form

$$\dot{X}_i = r_i X_i [1 - \rho_i (h_1 X_1 + h_2 X_2)]. \tag{1.19}$$

In this case, the species are competing for the same food source and both species together decrease the quantity of food by $h_1 x_1 + h_2 x_2$. Figure 1.4 displays three scenarios in which $a_1 a_2 = 1$. In the first scenario, Fig. 1.4a, the nullclines are the same and a line of Lyapunov stable fixed points exists. In the other scenarios, if one species has even the slightest advantage over the other, then the superior species will ultimately displace the competition entirely and hold the field in absolute monopoly, a phenomenon referred to as competitive

exclusion.

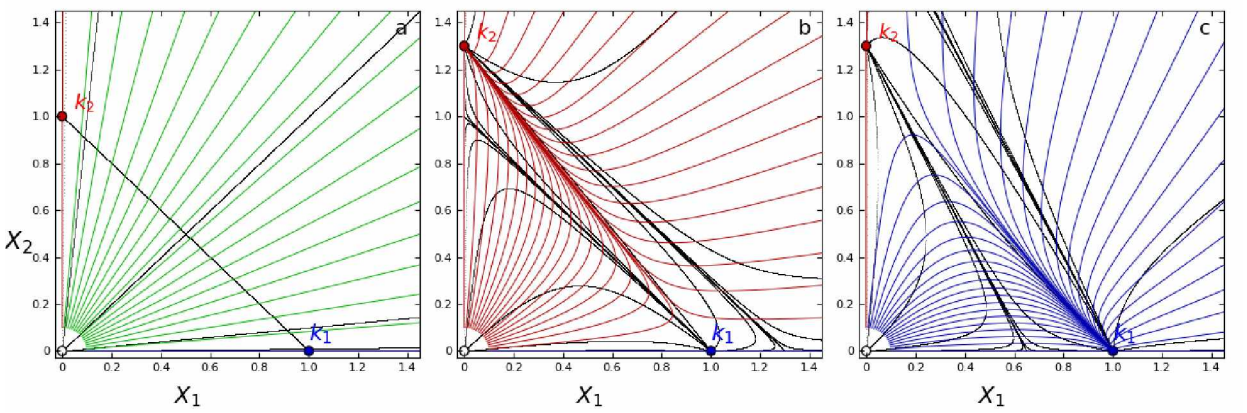

Figure 1.4: Isocline diagram and phase portraits for the competition model with single shared resource, Eq. (1.19). a) Nullclines are identical, b) parallel nullclines with $a_1 = a_2 = 1$ and increased k_2, c) parallel nullclines with $a_1 < a_2$. Isoclines are black with slope constants $\pm\{1000, 100, 10, 1, 0.1, 0.01, 0.001\}$ and the two nullclines are thickened. The trajectories are colored depending on which fixed point they are attracted to. Initial conditions of trajectories include 20 points at a radius of 0.1 from the origin and 20 points at a radius 2 from the origin.

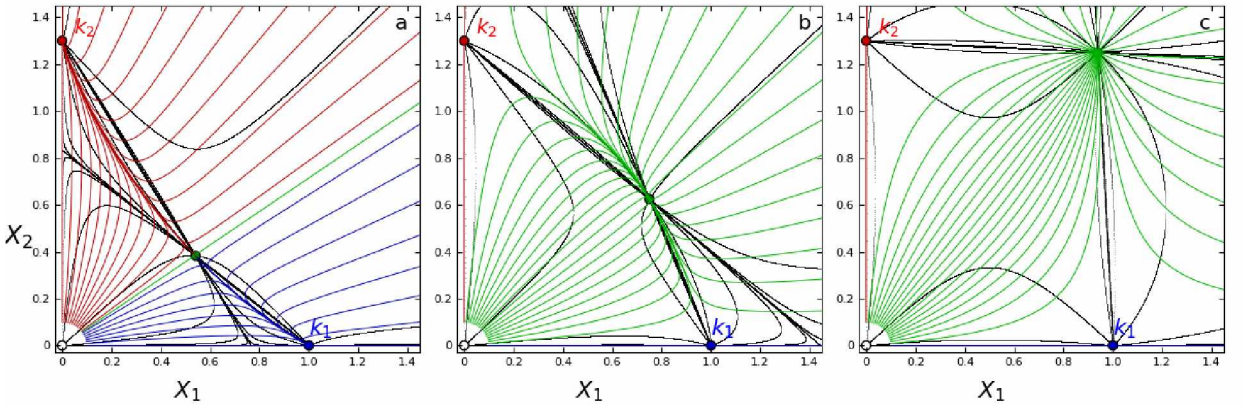

Figure 1.5: Isocline diagram and phase portraits with the saddle point (a) and stable node cases for moderate disassociation (b) and largely disassociated with $a_1, a_2 \ll 1$ (c). Isoclines are black with slope constants $\pm\{1000, 100, 10, 1, 0.1, 0.01, 0.001\}$ and the two nullclines are thickened. The trajectories are colored depending on which fixed point they are attracted to. Initial conditions of trajectories include 20 points at a radius of 0.1 from the origin and 20 points at a radius 2 from the origin.

If $a_1 a_2 \neq 1$ then a fourth nontrivial fixed point exists. If that fixed point is in the negative space, competitive exclusion still occurs. If the fourth fixed point is in the first quadrant of the state space and $a_1 a_2 > 1$, then it is a saddle point, Fig 1.5a. This may describe a system in which both species operate from some mechanisms in which an adversary's presence is

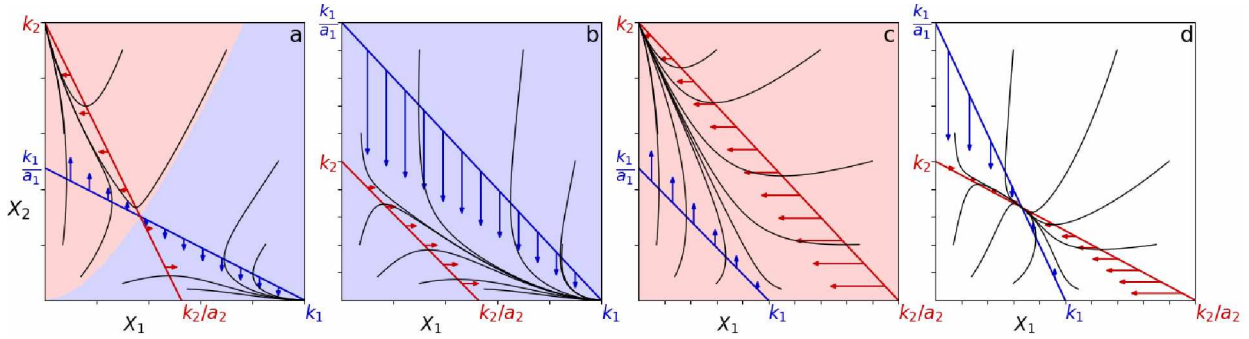

Figure 1.6: Phase portraits of competition model featuring trajectories in black, X_1-nullcline in blue, X_2-nullcline in red, and shading of the domains of attraction for different fixed points. The blue shading covers the initial conditions attracted to the point (k_1,0), the red shading covers the initial conditions attracted to the point (0,k_2), and white covers the initial conditions attracted to the nontrivial fixed point. The arrows on the nullclines depict the flow at those points. a) The nontrivial fixed point, at the intersection of the nullclines, is a saddle point, b) X_1 out-competes and eradicates X_2, c) X_2 out-competes and eradicates X_1, d) The nontrivial fixed point is a stable node and both species coexist.

more inhibiting to growth than the presence of a member of its own tribe. Either species has a chance of monopolizing the system. If an invader wishes to overtake a system already populated by a native species, the non-native species must invade with large enough numbers otherwise the native species will overcome the threat and take back full control.

If the fourth fixed point is in the first quadrant of the state space and $a_1 a_2 < 1$, then it is a stable node and both species will co-inhabit the system, Fig 1.5 b and c. This may describe a system in which the non-native species supplements its food with an alternative source that the native species has less preference for or less access to. The more they disassociate, the larger the populations get at steady state until they have no shared resource and become uncoupled at $a_1 = a_2 = 0$; both species populations approach their respective carrying capacities.

Geometric analysis of the nullclines, Fig. 1.6, reveals regions in the parameter space characterized by different dynamics. Analyzing the sign of the velocities on the nullclines allows a convenient way to visualize the qualitative flow. Figure 1.6a has the fourth fixed point in the first quadrant but the local flow is directed away from it and trajectories approach either the (0,k_2) or (k_1,0) fixed point depending on initial conditions. If the nontrivial fixed point does not exist in the first quadrant, then one species will out-compete the other and the system will come to rest at the carrying capacity of the winner; referred to as competitive exclusion, Fig. 1.6b and c. If it is stable, then both species coexist. The flow is directed toward the nontrivial fixed point when both conditions,

$$k_i < k_j/a_j \tag{1.20}$$

for $i, j \in \{1, 2\} | i \neq j$, are true. Then the nullcline intersection is in the first quadrant and both species persists for all time, Fig. 1.6d. Compactly written

$$k_i < \frac{k_j}{a_j} < \frac{k_i}{a_i a_j}. \tag{1.21}$$

1.3.2 Conventional Nondimensionalization

A traditional approach defines the nondimensional variables

$$\chi_i \equiv \frac{X_i}{k_i} \tag{1.22}$$

and the equations of motion become

$$\dot{\chi}_i = r_i \chi_i (1 - \chi_i - \eta_i \chi_j), \tag{1.23}$$

where $\eta_i = a_i k_j / k_i$. The nontrivial steady state is given by

$$\chi_i^* = 1 - \eta_i \chi_j^* = \frac{1 - \eta_i}{1 - \eta_i \eta_j}, \tag{1.24}$$

and is positive in biological systems. The Jacobian in the steady state is

$$J = - \begin{pmatrix} r_1 & 0 \\ 0 & r_2 \end{pmatrix} \begin{pmatrix} \chi_1^* & \eta_1 \chi_1^* \\ \eta_2 \chi_2^* & \chi_2^* \end{pmatrix}. \tag{1.25}$$

The characteristic equation is quadratic in λ with roots equal to the eigenvalues of J,

$$(\lambda - \lambda_1)(\lambda - \lambda_2) = 0 \tag{1.26}$$

$$\lambda^2 - (\lambda_1 + \lambda_2)\lambda + \lambda_1 \lambda_2 = 0 \tag{1.27}$$

$$\lambda^2 - \tau \lambda + \Delta = 0 \tag{1.28}$$

where τ is the trace of J and also the sum of the eigenvalues of a square matrix, and Δ is its determinant (product of eigenvalues),

$$\tau = -(r_1 \chi_1^* + r_2 \chi_2^*), \quad \Delta = r_1 r_2 (1 - \eta_1 \eta_2) \chi_1^* \chi_2^*. \tag{1.29}$$

A zero-eigenvalue bifurcation occurs when one of the eigenvalues is zero, i.e. $\Delta = 0$. Therefore, the bifurcation points have $\eta_1\eta_2 = 1$, Fig. 1.7a. The nontrivial fixed point is stable when $\eta_1\eta_2 < 1$ and it is a saddle point otherwise.

Conventional nondimensionalization reduces the number of parameters and finds higher order, effective parameters η_i that divide the parameter space into different dynamical regions.

1.3.3 Normalizing Nondimensionalization

For the familiarization with generalized modeling, a similar analytic is done for the specific model, but instead with the trademark transformation of generalized modeling. Assume $X_i^* \neq 0$ and consider the nondimensional variable

$$x_i = \frac{X_i}{X_i^*} \tag{1.30}$$

which normalizes the state variables to the nontrivial fixed point. With this transformation, X_i^* may be treated as unknown yet $x_i^* = 1$. The equations of motion, Eqs. (1.15) and (1.16), become

$$\dot{x_i} = \frac{r_i x_i}{k_i}(k_i - X_i^* x_i - a_i X_j^* x_j). \tag{1.31}$$

Define four parameters $\mu_i \equiv X_i^*/k_i$ and $\tilde{\mu}_i \equiv a_i X_j^*/k_i$ for $i, j \in \{1, 2\} | i \neq j$ and rewrite Eq. (1.31),

$$\dot{x_i} = r_i(x_i - \mu_i x_i^2 - \tilde{\mu}_i x_i x_j). \tag{1.32}$$

In the steady state, total in-flow equals total out-flow, hence $\mu_i + \tilde{\mu}_i = 1$. The Jacobian has its diagonal elements $\partial\dot{x}_i/\partial x_i = r_i(1 - 2\mu_i - \tilde{\mu}_i) = -r_i\mu_i$, and the matrix becomes

$$J = -\begin{pmatrix} r_1 & 0 \\ 0 & r_2 \end{pmatrix}\begin{pmatrix} \mu_1 & \tilde{\mu}_1 \\ \tilde{\mu}_2 & \mu_2 \end{pmatrix} \tag{1.33}$$

with determinant $\Delta = r_1 r_2(\mu_1\mu_2 - \tilde{\mu}_1\tilde{\mu}_2) = r_1 r_2(\mu_1 + \mu_2 - 1)$ and a negative trace for positive μ_1 and μ_2. The zero-eigenvalue bifurcation points have $\mu_1 = 1 - \mu_2$, Fig. 1.7b. The fixed points are stable when

$$\mu_1 > 1 - \mu_2 \tag{1.34}$$

or compactly

$$\mu_i > \tilde{\mu}_j, \tag{1.35}$$

and saddle points otherwise. Equation (1.35) can be rewritten into Eq. (1.20). This approach compacts the entire set of nontrivial, positive fixed points into the space defined by $\mu_i \in [0, 1]$.

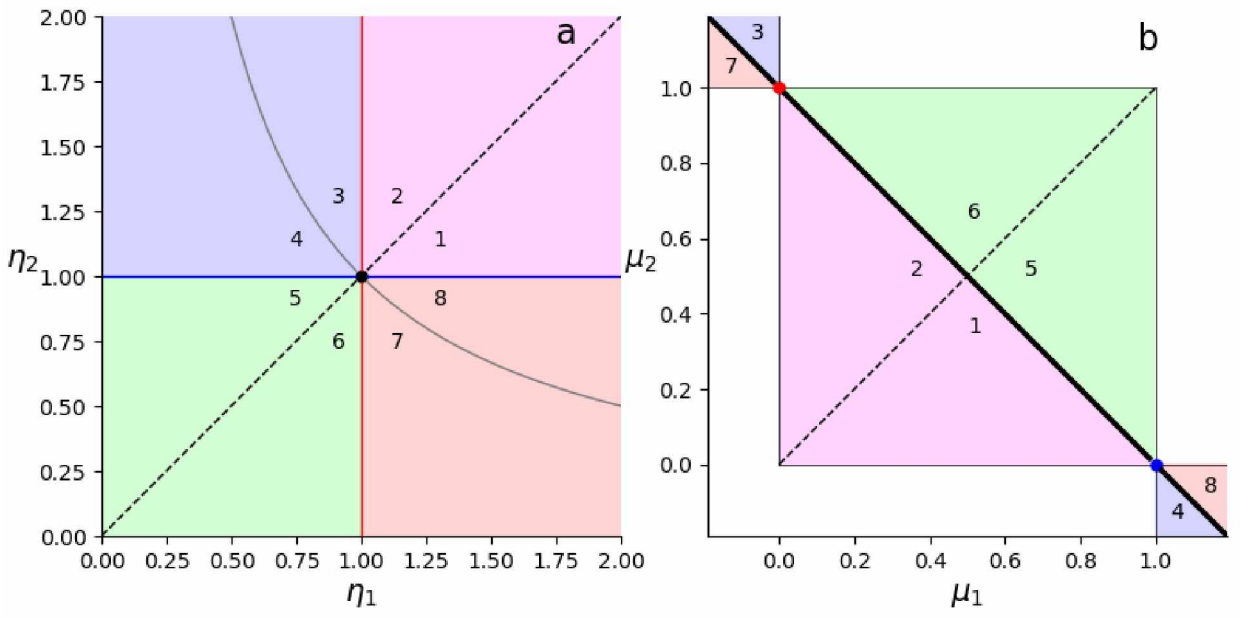

Figure 1.7: Bifurcation diagrams of conventional and normalizing nondimensionalization. Saddle points are exhibited in regions 1 and 2, species X_1 has a monopoly in 3 and 4, nontrivial stable nodes are found in 5 and 6, and species X_2 has a monopoly in 7 and 8. a) Conventional nondimensionalization: The bifurcation line is gray and the black dot is the bifurcation point for direct transitions between saddle point and stable node. b) Normalized nondimensionalization: The zero bifurcation line is the thick black line, the red dot is the boundaries between regions 2 and 3 or regions 6 and 7, and the blue dot is the boundaries between regions 4 and 5 or regions 8 and 1.

1.3.4 Generalized Model

In a generalized modeling context, we expand the system to the general class of equations of the structure

$$\dot{X}_1 = S_1(X_1) - M_1(X_1) - L_1(X_1, X_2) \tag{1.36}$$

$$\dot{X}_2 = S_2(X_2) - M_2(X_2) - L_2(X_1, X_2), \tag{1.37}$$

with gain S_i, intraspecific loss M_i, and interspecific loss L_i. The gain and loss terms are unspecified, therefore the fixed points are unknown. Assuming there is a nontrivial fixed point, we consider the transformation of the state variables normalized to the fixed point

$$x_i = \frac{X_i}{X_i^*}, \tag{1.38}$$

and write the system in terms of the normalized functions,

$$g_i(x_i) = \frac{G_i(X_i^* x_i)}{G_i(X_i^*)} = \frac{G_i(X_i^* x_i)}{G_i^*}, \tag{1.39}$$

to get the system in the form

$$\dot{x}_i = \frac{S_i^*}{X_i^*} s_i(x_i) - \frac{M_i^*}{X_i^*} m_i(x_i) - \frac{L_i^*}{X_i^*} l_i(x_1, x_2) \tag{1.40}$$

with $i \in \{1, 2\}$. The unknown steady state is now located at the point $(x_1^*, x_2^*) = (1, 1)$. The normalized functions at the steady are also known, $s_i^* = m_i^* = l_i^* = 1$.

At the steady state, the sum of the gain terms equals the sum of the loss terms. Use this to define the characteristic timescales

$$\alpha_i = \frac{S_i^*}{X_i^*} = \frac{M_i^* + L_i^*}{X_i^*}. \tag{1.41}$$

These are the turnover rates. If the currency of the system is abundance, then α_i is the per capita birth and death rates or the reciprocal of the average lifetime of an individual. If the currency is biomass, then the turnover rate corresponds to species' metabolic rates typically following allometric scaling laws. We factor out the timescale parameters and consequently the weighting of the flows is made explicit. The system is now in the form

$$\dot{x}_i = \alpha_i(\sigma_i s_i(x_i) - \mu_i m_i(x_i) - \tilde{\mu}_i l_i(x_1, x_2)) \tag{1.42}$$

where

$$\mu_i = \frac{M_i^*}{M_i^* + L_i^*} = \frac{M_i^*}{\alpha_i X_i^*}, \qquad \tilde{\mu}_i = 1 - \mu_i = \frac{L_i^*}{M_i^* + L_i^*} = \frac{L_i^*}{\alpha_i X_i^*}. \tag{1.43}$$

$\sigma_i = 1$ since it is the only gain term. μ_i is the proportion of total loss that is due to intraspecific competition, and $\tilde{\mu}_i$ is the proportion from interspecific competition.

After rescaling time, Eq. (1.42), $\tau = \alpha_1 t$, and defining $\alpha = \alpha_2/\alpha_1$, we can reduce the parameter space by one. The Jacobian evaluated at the steady state has elements $\frac{\partial \dot{x}_i}{\partial x_j}\Big|_{\boldsymbol{x}^*}$

$$J^* = \begin{pmatrix} 1 & 0 \\ 0 & \alpha \end{pmatrix} \begin{pmatrix} s_1^{(x_1)} - \mu_1 m_1^{(x_1)} - \tilde{\mu}_1 l_1^{(x_1)} & -\tilde{\mu}_1 l_1^{(x_2)} \\ -\tilde{\mu}_2 l_2^{(x_1)} & s_2^{(x_2)} - \mu_2 m_2^{(x_2)} - \tilde{\mu}_2 l_2^{(x_2)} \end{pmatrix}. \tag{1.44}$$

The nonlinearity parameters are

$$s_i^{(x_i)} = \frac{\partial}{\partial x_i} s_i(x_i)\bigg|_{\boldsymbol{x}^*}, \quad m_i^{(x_i)} = \frac{\partial}{\partial x_i} m_i(x_i)\bigg|_{\boldsymbol{x}^*}, \quad l_i^{(x_j)} = \frac{\partial}{\partial x_j} l_i(x_1, x_2)\bigg|_{\boldsymbol{x}^*} = \frac{\partial}{\partial x_j} l_i(\boldsymbol{x})\bigg|_{\boldsymbol{x}^*}. \tag{1.45}$$

The Jacobian is parameterized by only the proportional flows (scale parameters) and the nonlinearity parameters that are determined from a suitable range from biologically motivated functional forms. The exact details of the functional forms do not enter.

1.3.5 Connecting the Generalized Model to the Specific Model

The feature that sets generalized modeling apart from other abstract analyses is that the set of generalized parameters can be made less abstract by assuming specific functional forms thus reducing the model to any degree of specificity. The entire set of generalized parameters can be completely determined for a specific model if so desired. The specific model of Eqs. (1.15) and (1.16) have

$$S_i(X_i) = r_i X_i, \quad M_i(X_i) = \frac{r_i X_i^2}{k_i}, \quad L_i(\boldsymbol{X}) = \frac{r_i a_i X_i X_j}{k_i} \tag{1.46}$$

with $i, j \in \{1, 2\} | i \neq j$. The normalized functions, Eq. (1.39), give

$$s_i(x_i) = x_i, \quad m_i(x_i) = x_i^2, \quad l_i(\boldsymbol{x}) = x_i x_j, \tag{1.47}$$

and nonlinearity parameters, Eq. (1.45), yield

$$s_i^{(x_i)} = 1, \quad m_i^{(x_i)} = 2, \quad l_i^{(x_i)} = 1, \quad l_i^{(x_j)} = 1. \tag{1.48}$$

Note, the coefficients, r_i, k_i, a_i, do not appear in the normalized functions. The nonlinearity parameters of generalized modeling are the derivatives of these functions evaluated at the steady state and become the exponents of power laws; hence, they are sometimes called exponent parameters.

The timescale parameters, Eq. (1.41), are

$$\alpha_i = r_i = \frac{r_i}{k_i}(X_i^* + a_i X_j^*) \tag{1.49}$$

which implies $X_i^* + a_i X_j^* = k_i$. The other scale parameters, Eq. (2.10), that describe the relative weighting of interspecific and intraspecific competition out-flows to the total out-flow

are

$$\mu_i = \frac{X_i^*}{k_i}, \quad \tilde{\mu}_i = 1 - \mu_i = \frac{a_i X_j^*}{k_i}, \tag{1.50}$$

respectively. Entering these parameters into Eq. (1.42), we regain the nondimensionalized equations of motion, Eq. (1.32), and the corresponding Jacobian, Eq. (1.33).

1.4 A Different View of the System: Combining Processes

In generalized modeling (GM), identifying the gain and loss terms is a fundamental component to interpreting generalized parameters and tracking details on the relative flow magnitudes for each process. For instance, consider the Lotka-Volterra (LV) competition model, Eqs. (1.15) and (1.16). The growth flow increases linearly as the quantity of the species increases. Two flows are contributing to the total loss of the species. The scale parameters are the relative weighting between the loss due to intraspecific competition and the loss due to interspecific competition. Increasing the size of a system increases the number of generalized parameters. Considering more complex functional forms, the nonlinearity parameters cover a range of possible values. Exploring the parameter space becomes more of a statistical problem. A number of assumptions can be made to reduce the parameter space for more tractable analyses. For example, assuming some causes of loss about a single species are orders of magnitudes greater than other causes permits the negation of some scale parameters, or assuming symmetry in the system such that many species share the same sensitivity to a common process. In effect, these assumptions narrow the dimensionality of the parameter space expediting physical inferences.

Another way to combat the size of the parameter space is to combine related terms from the original structure of the differential equations. For instance, combining processes of a population that are independent of any other population (uncoupled parts). The uncoupled parts of the previous example, Eqs. (1.15) and (1.16), are grouped into the logistic function, Eq. (1.4). The logistic function combines the linear gain term from exponential growth and the quadratic loss term from intraspecific competition into a single gain term that we call production. In general, it is good practice to avoid combining gain and loss terms since the combined function may become zero or flip sign which creates singularities in the parameter space. However, with caution to restrict the study within defined parameter regions, the model remains valid. Doing this to the competition example restructures the general class of equations into

$$\dot{X}_i = P_i(X_i) - L_i(X_i, X_j). \tag{1.51}$$

Each species has a positive gain term that represents its own production and a loss term

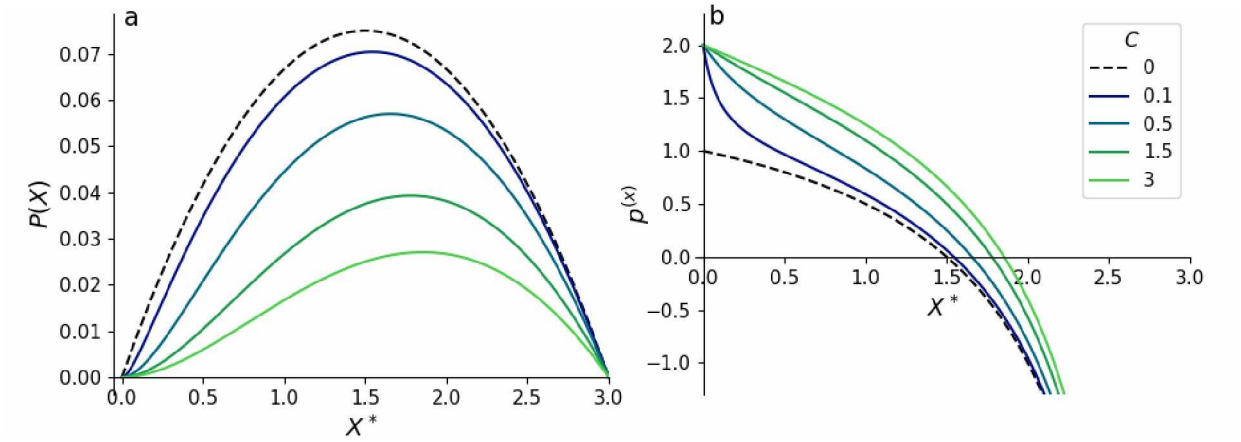

Figure 1.8: Production flow and exponent parameter functions. a) Production growth, Eq. (1.54), and b) corresponding exponent parameter of production, Eq. (1.55), for $k = 3$, $r = 1$, and varying c.

that captures the detrimental effects from the presence of its competition. The normalized nondimensionalized form is

$$\dot{x}_i = \alpha_i(p_i(x_i) - l_i(x_i, x_j)), \tag{1.52}$$

with a Jacobian

$$J^* = \begin{pmatrix} 1 & 0 \\ 0 & \alpha \end{pmatrix} \begin{pmatrix} p_1^{(x_1)} - l_1^{(x_1)} & -l_1^{(x_2)} \\ -l_2^{(x_1)} & p_2^{(x_2)} - l_2^{(x_2)} \end{pmatrix}, \tag{1.53}$$

where $\alpha = \alpha_2/\alpha_1$. $P_i(X_i)$ could be any specific functional form. For instance, suppose both species face additional challenges to grow when populations are small. There are many mechanisms that can cause this effect: Cooperation in changing an environment to make for more suitable living conditions, safety in numbers from predation, difficulty finding mates in under-crowded environments, overall fitness decreased from inbreeding, etc. These are some examples that can give an Allele effect. A typical form that simulates an Allele effect (Wang et al.; 2020) is

$$P_i(X_i) = r_i X_i \left(1 - \frac{X_i}{k_i}\right)\left(\frac{X_i}{X_i + c_i}\right), \tag{1.54}$$

where $c_i \geq 0$, Fig. 1.8a. The exponent parameter for the production term with Allele effect is

$$p_i^{(x_i)} = 2 - \frac{X_i^*}{k_i - X_i^*} - \frac{X_i^*}{X_i^* + c_i}, \tag{1.55}$$

Fig. 1.8b.

Additionally, suppose species 1 is so much more efficient at depleting the shared resource than species 2 that the amount of shared resources depleted by species 2 is negligible compared to the amount depleted by species 1. However, species 2 is still a cause of loss for

species 1. Suppose species 2 is so much bigger than species 1 that species 2 is destructive for species 1 through trampling. Thus species 2 must have an encounter with species 1 to contribute to the loss of species 1. The number of encounters per-capita species 2 is directly related to the quantity of species 1. Thus, the nonlinearity of interspecific competitive loss of species 1 with respect to species 1 is one when species 1 is in low quantities. However, the foot size of species 2 is only so big, thus only a finite quantity of species 1 can fit under the feet of species 2. When the population of species 1 is very large, species 2 will be trampling as much as possible and further increase in species 1 population will not change how many individuals species 2 is trampling. In this extreme case, the loss of species 1 will have saturated and is no longer dependent on the quantity of species 1. This scenario results in a zero nonlinearity. It will be assumed that the nonlinearity of loss of species 1 with respect to itself, $l_1^{(x_1)}$, can be anywhere from zero to one.

The rest of the processes are taken to be consistent with Lotka-Volterra competition. I.e., the loss of species 2 due to interspecific competition with species 1 is linear in X_1 and linear in X_2, $l_2^{(x_1)} = l_2^{(x_2)} = 1$. The loss of species 1 due to species 2 is linear in X_2 as the number of encounters is directly related to quantity X_2, $l_1^{(x_2)} = 1$. After these assumptions, the Jacobian at steady state becomes

$$J^* = \begin{pmatrix} 1 & 0 \\ 0 & \alpha \end{pmatrix} \begin{pmatrix} p_1^{(x_1)} - l_1^{(x_1)} & -1 \\ -1 & p_2^{(x_2)} - 1 \end{pmatrix}. \tag{1.56}$$

Determining when the determinant is zero, gives solutions of a zero eigenvalue; then a zero-eigenvalue bifurcation surface is at

$$p_1^{(x_1)} = \frac{1}{p_2^{(x_2)} - 1} + l_1^{(x_1)}. \tag{1.57}$$

Figure 1.9 displays the zero-eigenvalue bifurcation surfaces. The vanishing of the trace can lead to Hopf surfaces; but in this case, it does not since the determinant remains negative, indicating a symmetric pair of real numbers. The plane described by $l_1^{(x_1)} = 1$ and $p_1^{(x_1)}, p_2^{(x_2)} \leq 1$ represents fixed points for the LV competition model, Eqs. (1.15) and (1.16), by varying a_i and k_i such that there is a fourth fixed point in the first quadrant of the state space.

When both species are in low quantities they have a nonlinearity of production, $p_i^{(x_i)}$, bigger than one and as large as two. If the Allele effect is strong on species 1, then their population can get bigger and still have a large $p_1^{(x_1)}$. In such a scenario, there could be a nontrivial unstable node, a dynamic situation unreachable by the LV competition model. Built into this bifurcation diagram is any specific model that has these nonlinearities. That

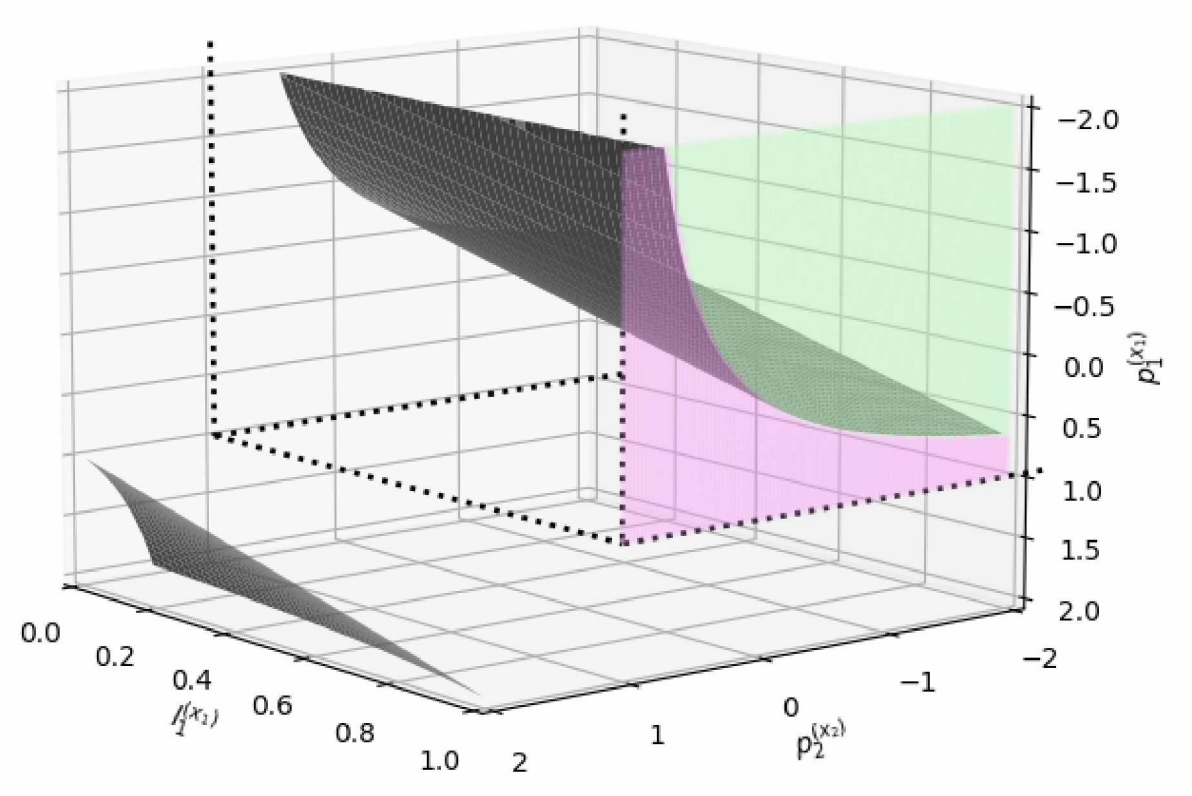

Figure 1.9: Bifurcation surfaces of a two-species competition system. Zero-eigenvalue bifurcation surfaces (black) of competition between two species in which species 2 must actively disrupt the activities of species 1, otherwise there is no competitive effect from 2 on 1. The fixed points are stable nodes above the upper bifurcation surface, saddle points between the bifurcation surfaces in the middle region, and unstable nodes below the lower bifurcation surface. Points outside the region outlined by dotted edges are points potentially accessible if the species are subject to an Allele effect. Points inside the dotted region are points found in models with logistic growth or Allele affected growth. The planes depict stable nodes (green) and saddle points (purple) from the LV competition model.

includes logistic growth models, Allele effect models, other forms of production such as those in Chapter 3, linear competition terms as in LV competition, or other forms of competition that have nonlinearities less than one.

1.5 Synopsis

This thesis focuses on ecological networks as mathematical constructs called generalized models. Generalized models are a transformation of a system of differential equations for which the exact functional forms of the various processes need not be fully specified or parameterized, yet the local dynamics around fixed points is obtainable for any specific system that fits the overall class of equations.

In Chapter 2*, a food-web structuring algorithm is developed that uses the size of the network and boundaries of feeding ranges for each species as inputs. An ensemble of abstract webs is gathered that consists of web sizes from two to sixty species and an organized range of topologies is constructed from varying feeding ranges. A generalized model is created for each web and the stability of fixed points is determined for a wide range of dynamically possible conditions. The resulting bifurcation diagrams are used to explore overarching structural features that strongly correlate to average stability, implications for when systems become enriched with a limiting resource, and impacts from small changes to topology from single-link additions.

Chapter 3† is designed to elucidate the relationship between generalized models and specific models on small food webs. Using a variety of specific production terms and two topologies, the fixed points of the specific models are transferred into a generalized modeling context. Those results are used to vet the validity of common assumptions made on purely generalized ecological networks and to discuss the limitations and strengths of a generalized modeling approach.

Chapter 4 is on realistic ecological networks derived from Arctic marine ecosystems in the Southern Beaufort Sea (SBS). From thirty carefully selected species thought to be of the most ecologically significant to the SBS ecosystem, thousands of food webs are probabilistically constructed based on body-mass ratios. Initially, the webs are constructed from the body-mass ratios based on a crude estimate observed in real food webs that predators often feed on prey within a similar relative body-size range. Overarching stability properties are tracked as more realistic features are applied to the models, namely the incorporation of specialized foraging traits, habitat constraints, and predator preference. Additionally, because of concerns that Arctic warming causes ecosystem restructuring, especially due to changes in species composition, the stability properties are followed as vulnerable species are removed and interloping candidates take their place. As a final piece to the SBS ecosystem models, communities are made to reside inside the larger ecosystem to reveal the stability effects of a perturbation on the primary web from a weakly-interacting ecological network that subsumes the primary web.

1.6 References

Awender, S., Wackerbauer, R. and Breed, G. A. (2021). Stability of generalized ecological-network models, *Chaos* **31**(2): 023106.

*Chapter 2 is published in Chaos (Awender et al.; 2021)

†Chapter 3 is published in Chaos (Awender et al.; 2023)

Awender, S., Wackerbauer, R. and Breed, G. A. (2023). Combining generalized modeling and specific modeling in the analysis of ecological networks, *Chaos* **33**(3): 033130.

Basu, S. and Mackey, K. R. (2018). Phytoplankton as key mediators of the biological carbon pump: Their responses to a changing climate, *Sustainability* **10**(3): 869.

Boenigk, J., Wodniok, S. and Glücksman, E. (2015). *Biodiversity and earth history*, Springer.

Borges, A. and Abril, G. (2011). Carbon dioxide and methane dynamics in estuaries, *Estuar. Coast. Shelf Sci.* **5**: 119.

Coale, K. H., Johnson, K. S., Fitzwater, S. E., Gordon, R. M., Tanner, S., Chavez, F. P., Ferioli, L., Sakamoto, C., Rogers, P., Millero, F. et al. (1996). A massive phytoplankton bloom induced by an ecosystem-scale iron fertilization experiment in the equatorial Pacific Ocean, *Nature* **383**(6600): 495.

Costanza, R., d'Arge, R., De Groot, R., Farber, S., Grasso, M., Hannon, B., Limburg, K., Naeem, S., O'neill, R. V., Paruelo, J. et al. (1997). The value of the world's ecosystem services and natural capital, *Nature* **387**(6630): 253.

De Ruiter, P. C., Wolters, V. and Moore, J. C. (2005). *Dynamic food webs: Multispecies assemblages, ecosystem development and environmental change*, Elsevier.

Drew, K. L., Buck, C. L., Barnes, B. M., Christian, S. L., Rasley, B. T. and Harris, M. B. (2007). Central nervous system regulation of mammalian hibernation: Implications for metabolic suppression and ischemia tolerance, *J. Neurochem.* **102**(6): 1713.

Elmgren, R. and Hill, C. (1997). Ecosystem function at low biodiversity—the Baltic example, *Mar. Biodivers.* p. 319.

Gaichas, S. K. and Francis, R. C. (2008). Network models for ecosystem-based fishery analysis: A review of concepts and application to the Gulf of Alaska marine food web, *Can. J. Fish. Aquat. Sci.* **65**(9): 1965.

Gause, G. F. (2019). *The struggle for existence: A classic of mathematical biology and ecology*, Courier Dover Publications.

Groß, T. (2004). *Population dynamics: General results from local analysis*, PhD thesis, Universität Oldenburg.

Gross, T. and Feudel, U. (2006). Generalized models as a universal approach to the analysis of nonlinear dynamical systems, *Phys. Rev. E* **73**(1): 016205.

Gross, T., Rudolf, L., Levin, S. A. and Dieckmann, U. (2009). Generalized models reveal stabilizing factors in food webs, *Science* **325**(5941): 747.

Guill, C., Drossel, B., Just, W. and Carmack, E. (2011). A three-species model explaining cyclic dominance of Pacific salmon, *J. Theor. Biol.* **276**(1): 16.

Hazen, W. E. (1975). *Readings in population and community ecology*, W. B. Saunders.

Hop, H. and Gjøsæter, H. (2013). Polar cod (Boreogadus saida) and capelin (Mallotus villosus) as key species in marine food webs of the Arctic and the Barents Sea, *Mar. Biol. Res.* **9**(9): 878.

Jorgensen, S. E. (2009). *Ecosystem ecology*, Academic press.

Karam, A. P., Parker, M. S. and Lyons, L. T. (2012). Ecological comparison between three artificial refuges and the natural habitat for Devils Hole pupfish, *N. Am. J. Fish. Manag.* **32**(2): 224.

Koon, W. S., Lo, M. W., Marsden, J. E. and Ross, S. D. (2000). Dynamical systems, the three-body problem and space mission design, *Equadiff 99: (In 2 Volumes)*, World Scientific, p. 1167.

Kuznetsov, Y. A. (1998). *Elements of applied bifurcation theory*, Vol. 112, Springer.

Lotka, A. J. (1932). The growth of mixed populations: Two species competing for a common food supply, *J. Wash. Acad. Sci.* **22**(16, 17): 461.

Marmottant, P., Ponomarenko, A. and Bienaimé, D. (2013). The walk and jump of Equisetum spores, *P. Roy. Soc. B-Biol. Sci.* **280**(1770): 20131465.

Pascual, M., Dunne, J. A., Dunne, J. A. et al. (2006). *Ecological networks: Linking structure to dynamics in food webs*, Oxford University Press.

Polimene, L., Sailley, S., Clark, D., Mitra, A. and Allen, J. I. (2017). Biological or microbial carbon pump? The role of phytoplankton stoichiometry in ocean carbon sequestration, *J. Plankton Res.* **39**(2): 180.

Polis, G. A. and Winemiller, K. O. (2013). *Food webs: Integration of patterns & dynamics*, Springer Science & Business Media.

Ripple, W. J. and Beschta, R. L. (2012). Trophic cascades in Yellowstone: The first 15 years after wolf reintroduction, *Biol. Conserv.* **145**(1): 205.

Strogatz, S. H. (2018). *Nonlinear dynamics and chaos: With applications to physics, biology, chemistry, and engineering*, CRC press.

Volterra, V. (1926). Fluctuations in the abundance of a species considered mathematically, *Nature* **118**(2972): 558.

Wang, S., Yu, H., Dai, C. and Zhao, M. (2020). The dynamical behavior of a predator-prey system with Holling type II functional response and allee effect, *Appl. Math.* **11**(5): 407.

Winemiller, K. O. and Polis, G. A. (1996). Food webs: What can they tell us about the world?, *Food Webs*, Springer, p. 1.

Chapter 2 Stability of Generalized Ecological Network Models

2.1 Abstract

The stability of ecological networks of varying topologies and predator-prey relationships is explored by applying the concept of generalized modeling. The effects of omnivory, complexity, enrichment, number of top predators, and predatory response are discussed. The degree of omnivory plays a large role in governing web stability at steady state. Complexity as measured from connectance and network size is not a perfect indicator of stability; large, highly connected webs can be just as stable as smaller, less connected ones. Learning behavior as expressed in a Holling's type III predatory response is stabilizing for food webs and provides exceptions to the paradox of enrichment for some topologies.

2.2 Abstract Extension

Factors that control stability, instability and reorganization of real and model food webs are little understood. Food webs are described as ecological networks where the vertices represent species and the edges represent predator-prey relationships and encode dynamical equations of biomass. Specific functions and biomass initial conditions are largely unknown, but are required for conventional food web models to solve for trajectories. Generalized modeling requires less information and provides a powerful approach for understanding network stability in poorly characterized systems. A series of generalized models are developed to investigate how different factors like omnivory, network complexity, and types of predator-prey relationships either stabilize or destabilize a food web's steady state. Consequences of individual factors are not always unique across networks. E.g., while adding omnivory to a short food chain with three or four species has a stabilizing effect, omnivory destabilizes steady states in longer food chains.

2.3 Introduction

Ecological food webs can be represented as networks, and such representations are a central idea in ecology (Winemiller and Polis; 1996; Newman; 2018). Ecological networks may include sink nodes (top predators), source nodes (basal species), and relay nodes (intermediate species). Basal species can represent autotrophic primary producers or heterotrophic herbivores while intermediate and top nodes represent different types of predators. Food webs show intermediary types of mixing by body-size (Williams and Martinez; 2000; Rohr

et al.; 2010). A predator usually eats prey that is one to four orders of magnitude smaller than itself (Woodward et al.; 2005). Larger prey are difficult to kill and smaller prey are not worth the effort. This results in body-size stratification of the network.

Ecosystem network models are typically described as a dynamical system using a set of ordinary differential equations that govern biomass flows throughout the network (Drossel and McKane; 2003; Stouffer and Bascompte; 2010; Fussmann and Heber; 2002). Modelers vary parameters or functional forms of the governing differential equations to explore different regimes of dynamical behavior such as steady state or oscillatory motion.

It is generally not possible to empirically determine complete descriptions of the processes and parameters controlling biomass flows between network nodes. Linear inverse modeling (LIM) is one common approach to deal with under-determined ecosystem models, which uses mass-balancing and biological constraints at an assumed steady state to estimate the unknown flows (Niquil et al.; 2011). In marine ecosystems, the most well-known implementation of LIM is Ecopath (Christensen and Pauly; 1992), a software suite mostly used to evaluate ecosystem impact from fisheries (Pauly et al.; 2000). Although this approach does generate plausible networks and dynamics, results from inverse modeling techniques are highly uncertain (Stukel et al.; 2012).

Generalized modeling approaches, by contrast, have been developed to analyze network dynamics without the need to make specific assumptions about all the processes (Gross and Feudel; 2004, 2006; Kuehn et al.; 2013). They explore system dynamics across all biologically plausible behavior and weighting in the network and are efficient enough to handle large network sizes (Gross et al.; 2009; Yeakel et al.; 2014). Generalized modeling does not require that interactions between the nodes be well characterized; only the structure of the governing equations is presumed. The approach does not presume information about population sizes, initial conditions, or detailed functional forms for biomass flows, yet it can compute local asymptotic stability properties of steady states and provide a means for evaluating dynamics using high-dimensional bifurcation analysis (Gross and Feudel; 2004; Kuehn et al.; 2013).

A perennial issue in real and modeled food webs is understanding how "complexity" affects "stability" (Pascual and Dunne; 2006; Elton; 1958; May; 1972). In most cases, "complexity" is meant as structural complexity and usually quantified as NC, the size N of the network (species richness) times the connectance C (proportion of possible connections that actually occur). "Stability" on the other hand is much more ambiguously defined. A noninclusive list of interpretations of ecosystem stability is: local asymptotic stability, resilience, invasibility, persistence, reactivity, and robustness (Pascual and Dunne; 2006). Here, stability describes the linear growth or decay of a perturbation from a steady state in phase space. Most observational evidence indicates that increased complexity increases stability,

yet most mathematical models show that complexity destabilizes webs (Gross et al.; 2009; Allesina et al.; 2015).

This paper discusses impacts of topology and predator-prey relationships on the stability of ecological networks in a steady state. Section 2.4 introduces food web topology, food web dynamics, and the corresponding generalized models. The sensitivity of network stability to connectance is explored in Sec. 2.5 by changing prey body-size limits or adding one-link at a time. Changes to feeding dynamics (predatory response) affect stability (Sec. 2.6) and offer exemptions to the paradox of enrichment (Sec. 2.7). Impacts of the degree of omnivory in different sized food webs are discussed in Sec. 2.8. The ratio of intermediate to top predators is introduced as a defining property for the complexity-stability relationship, Sec. 2.9.

2.4 Model

2.4.1 Food Web Topology

A food web of N species (network nodes) is constructed by giving each species a unique rank, i, based on its body-size relative to all other network members. $i = 0$ represents the smallest body-size and $i = N - 1$ the largest. The prey body-size upper limit, U, defines the largest prey $(i-U)$ that species i consumes, and the prey body-size lower limit, L, defines the smallest prey $(i - L)$ that species i consumes, with $i - U$ and $i - L$ non-negative. Figure 2.1 (a) shows an example for $U = 3$ and $L = 5$. Together, U and L describe the feeding range of a species. Species i is a predator (consumer) to species j, if their rank difference $r_{ij} = i - j$ is greater than or equal to U and less than or equal to L. The linking probability between species i and j is given by

$$P_{ij}(r_{ij}, U, L) = \begin{cases} 1, & U \leq r_{ij} \leq L \\ 0, & r_{ij} \text{ otherwise} \end{cases}$$

with the condition that $U \leq L$.

For $U = L = 1$, the nodes are linked as a chain; species i consumes only the next smallest species in the network and is consumed only by the next largest species. This linking rule holds across all members in the network, making it a food chain. For $L > U$, more than one prey is available for predatory species, and the connectivity in the network increases. More prey species become available as U and L become increasingly different. The upper limit U sets both the number of top predators and the number of basal species [Fig. 2.1 (a)], which are the same. The ratio $N/U = (2U + I)/U = 2 + I/U$ determines the ratio of intermediate species I to top predators U, a common measurement in food web studies (Briand and Cohen; 1984). Increasing the lower limit, L, increases the connectance and the

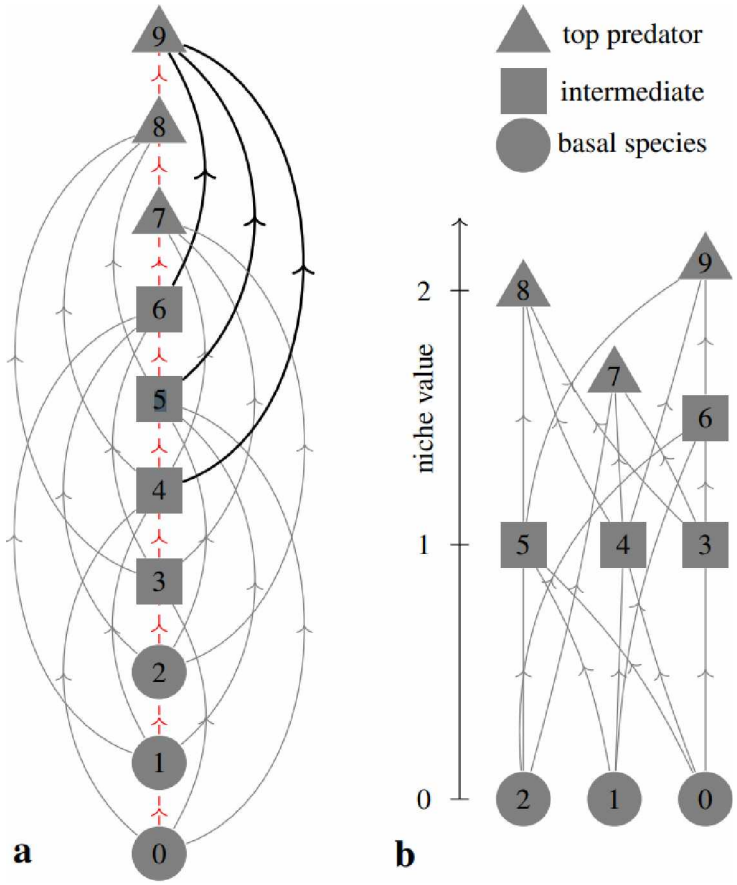

Figure 2.1: Network diagram of a food web of $N = 10$ species, a prey body-size upper limit $U = 3$, and a prey body-size lower limit $L = 5$, (a) plotted by rank and (b) plotted by niche value. The number inside a node represents the rank of the species, a link represents a predator-prey interaction, and the different symbols mark the type of species: top predator, intermediate species, and basal species. The special case of a 10-trophic food chain, $U = L = 1$, is superimposed in (a) using the dashed, red links.

degree of omnivory in the system.

The niche value, n_i, of species i measures the various paths and their lengths through which a species is connected to the bottom of a food web (Brinck; 2014). Basal species are defined to have niche values of zero. The niche value of a predator is the average of the niche values plus one of all its prey: $n_i = \sum_j (n_j + 1)/k_i^{\text{in}}$, where k_i^{in} is the in-degree or number of prey items for species i, and j is in the set of species ranks that are prey to species i. If the 10-species food web from Fig. 2.1(a) is graphed instead for niche values, Fig. 2.1(b), the first two trophic levels and the niche value distribution can be visualized. Increasing the prey body-size lower limit, L, shifts the niche distribution to lower values as omnivory increases.

2.4.2 Food Web Dynamics

In a food web of N species, the state variable X_i represents the biomass of species i, and $i \in \{0, 1, ..., N-1\}$. The change in biomass is governed by a growth from production $\mathscr{S}$ and predation $\mathscr{F}$ and a loss from mortality $\mathscr{M}$ and predation $\mathscr{L}$,

$$\dot{X}_i(t) = \mathscr{S}_i(X_i) + \eta_i \mathscr{F}_i(T_i, X_i) - \mathscr{M}_i(X_i) - \sum_{j=0}^{N-1} \mathscr{L}_{ij}(\boldsymbol{X}). \tag{2.1}$$

The state vector $\boldsymbol{X} = (X_0, ..., X_{N-1})$ represents the biomass of each species and η is the assimilation coefficient. Only functional forms are discussed in the following, since generalized modeling does not require information on initial conditions or other model parameters.

The total resource T_i available to species i is given by

$$T_i(\boldsymbol{X}) = \sum_k C_{ik}(X_k), \tag{2.2}$$

where C_{ik} is the contribution of species k to the available resources for species i. This study assumes no self predation, setting $C_{ii} = 0$. The functional form of $C_{ik}(X_k)$ depends on the preference of the predator for specific prey and on the success rate of attacks (Gross and Feudel; 2006). If species i has no preference in prey types (passive prey switching), the contribution of species k is proportional to its population size X_k. Active prey switching or when predators must also learn to be more successful hunters introduces another proportionality to X_k.

The production growth rate $\mathscr{S}_i$ is constant when resources are limited and grows linearly with the number of producers X_i when resources are not limited (Gross and Feudel; 2006). The mortality $\mathscr{M}_i$ is usually modeled as a linear function (Lotka-Volterra predator-prey model) (Strogatz; 2018), a quadratic function (Lotka-Volterra model of competition) (Strogatz; 2018), or somewhere in between (Edwards and Bees; 2001).

The predatory growth rate is modeled as

$$\mathscr{F}_i(T_i, X_i) = H_t(T_i) X_i, \tag{2.3}$$

with $H_t(T_i)$ one of the Holling's type functional responses to prey abundance T_i (Fig. 2.2, Table 2.1). Predators that continuously search for prey (e.g. filter feeders) follow a Holling's type I functional response; $H_1(T)$ goes linear with prey abundance T. Predators that require additional handling time (e.g. for killing, eating, digesting) follow a Holling's type II functional response; $H_2(T)$ grows linearly at low prey abundance and smoothly saturates at high

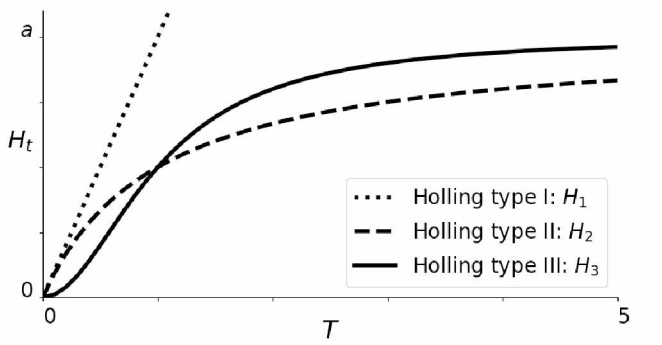

Figure 2.2: Illustration of Holling's type functional responses $H_1(T)$, $H_2(T)$, and $H_3(T)$ to prey abundance T, Table 2.1.

prey abundance. Holling's type III functional response exhibits an S-shaped curve that saturates for high prey abundance; it applies in situations where predators learn to hunt more successfully with more practice or where predators have difficulty getting the remaining prey at good hiding spots (Rosenzweig; 1971; Dawes and Souza; 2013). The predatory growth term $\mathscr{F}_i$ is linear in the predator population X_i, which assumes no intraspecific competition (Gross and Feudel; 2006).

The predation loss $\mathscr{L}_{ij}$ of prey item i is proportional to the predation growth $\mathscr{F}_j(T_j, X_j)$ of predator j and the fraction with which prey i contributes to the resources for predator j, (Gross and Feudel; 2006)

$$\mathscr{L}_{ij}(\boldsymbol{X}) = \frac{C_{ji}(X_i)}{T_j(\boldsymbol{X})}\mathscr{F}_j(T_j, X_j). \tag{2.4}$$

2.4.3 Generalized Modeling

Generalized modeling (Gross and Feudel; 2006; Gross et al.; 2009) assumes that the specific mathematical expressions for $\mathscr{S}$, $\mathscr{F}$, $\mathscr{M}$, and $\mathscr{L}$ are unknown except for general functional forms. For a nontrivial fixed point $\boldsymbol{X}^*$ of Eq. (4.2), i.e. $X_i \neq 0$ for any species i, the state vector is normalized to its fixed point by

$$x_i = \frac{X_i}{X_i^*}. \tag{2.5}$$

This maps the unknown fixed point $\boldsymbol{X}^*$ of Eq. (4.2) to the known fixed point $\boldsymbol{x}^* = (1, 1, \ldots, 1)$ of the rescaled system,

$$\dot{x}_i = \frac{\mathscr{S}_i^*}{X_i^*} s_i(x_i) + \frac{\eta_i \mathscr{F}_i^*}{X_i^*} f_i(\boldsymbol{x}) - \frac{\mathscr{M}_i^*}{X_i^*} m_i(x_i) - \sum_{j=1}^{N} \frac{\mathscr{L}_{ij}^*}{X_i^*} l_{ij}(\boldsymbol{x}), \tag{2.6}$$

with the rescaled functions,

$$\begin{aligned}
s_i(x_i) &= \frac{\mathscr{S}_i(X_i)}{\mathscr{S}_i(X_i^*)} = \frac{\mathscr{S}_i(X_i^* x_i)}{\mathscr{S}_i^*}, \\
m_i(x_i) &= \frac{\mathscr{M}_i(X_i^* x_i)}{\mathscr{M}_i^*}, \\
t_i(\boldsymbol{x}) &= \frac{T_i}{T_i^*} = \sum_k \frac{C_{ik}^*}{T_i^*} c_{ik}(x_k), \\
f_i(\boldsymbol{x}) &\equiv f_i(t_i(\boldsymbol{x}), x_i) = \frac{\mathscr{F}_i(T_i^* t_i, X_i^* x_i)}{\mathscr{F}_i^*}, \\
l_{ij}(\boldsymbol{x}) &= \frac{C_{ji}(X_i)\mathscr{F}_j(T_j, X_j)}{T_j(\boldsymbol{X})} \frac{T_j^*}{C_{ji}^* \mathscr{F}_j^*} = \frac{c_{ji}(x_i)}{t_j(\boldsymbol{x})} f_j(t_j, x_j).
\end{aligned} \tag{2.7}$$

These rescaled functions are normalized to themselves at the fixed point $\boldsymbol{x}^* = (1, 1, \ldots, 1)$, i.e., $x_i^* = s_i^* = f_i^* = m_i^* = l_{ij}^* = t_i^* = c_{ji}^* = 1$. The total influx (growth) is equivalent to the total outflux (loss) at the fixed point [Eq. (2.6)]. This defines the characteristic time scale parameter α_i,

$$\alpha_i = \frac{\mathscr{S}_i^* + \eta_i \mathscr{F}_i^*}{X_i^*} = \frac{\mathscr{M}_i^* + \sum_j \mathscr{L}_{ij}^*}{X_i^*}, \tag{2.8}$$

which has dimensionality of inverse time. This quantity can be thought of as the per capita birth or death rate, or the inverse of an individual's life expectancy. Pulling out the characteristic time scale from Eq. (2.6) yields

$$\dot{x}_i = \alpha_i \Big(\sigma_i s_i(x_i) + \phi_i f_i(\boldsymbol{x}) - \mu_i m_i(x_i) - \lambda_i \sum_j \beta_{ij} l_{ij}(\boldsymbol{x}) \Big),$$

and after inserting $l_{ij}(\boldsymbol{x})$ becomes the working equation of motion in its "non-dimensionalized form",

$$\dot{x}_i = \alpha_i \Bigg(\sigma_i s_i(x_i) + \phi_i f_i(t_i, x_i) - \mu_i m_i(x_i) - \lambda_i \sum_j \beta_{ij} \frac{c_{ji}(x_i)}{\sum_k \gamma_{jk} c_{jk}(x_k)} f_j(t_j, x_j) \Bigg), \tag{2.9}$$

with $\sigma_i, \phi_i, \mu_i, \lambda_i, \beta_{ij}, \gamma_{ij}$ representing proportions of biomass flow, and α_i the only dimensional term defining the time scale of the system.

The links in the web are weighted by the *scale parameters*,

$$\sigma_i = \frac{\mathscr{S}_i^*}{\alpha_i X_i^*}, \quad \phi_i = \frac{\eta_i \mathscr{F}_i^*}{\alpha_i X_i^*}, \quad \mu_i = \frac{\mathscr{M}_i^*}{\alpha_i X_i^*}, \quad \lambda_i = \frac{\sum_j \mathscr{L}_{ij}^*}{\alpha_i X_i^*} \tag{2.10}$$
$$\beta_{ij} = \frac{\mathscr{L}_{ij}^*}{\sum_k \mathscr{L}_{ik}^*}, \quad \gamma_{ij} = \frac{C_{ij}^*}{T_i^*}.$$

σ_i is the relative weight of the source (production) growth to total growth of species i, and ϕ_i is the relative weight of predatory growth to total growth of species i. μ_i is the relative weight of natural mortality to total loss of species i, and λ_i is the relative weight of predatory loss to total loss of species i. γ_{ij} is the relative weight of predatory gain from species j to the total predatory gain of species i. β_{ij} is the relative weight of predatory loss from species j to the total predatory loss of species i. Each scale parameter is the scalar coefficient of some convex combination, i.e., a linear combination where non-negative coefficients sum to one. The coefficient sets of the convex combinations are $\{\sigma_i, \phi_i\}$, $\{\mu_i, \lambda_i\}$, $\{\beta_{i,1}, ..., \beta_{i,N}\}$, $\{\gamma_{i,1}, ..., \gamma_{i,N}\}$.

The stability of an equilibrium of the food web in Eq. (2.9) is determined by the sign of the real part of the eigenvalues of the Jacobian matrix evaluated at the fixed point $\boldsymbol{x}^*$. For the case of no cannibalism ($c_{ii} = \beta_{ii} = \gamma_{ii} = 0$), the diagonal elements of the Jacobian at the steady state are

$$J_{ii}|_* = \alpha_i \Bigg[\sigma_i s_i^{(x_i)} + \phi_i f_i^{(x_i)} - \mu_i m_i^{(x_i)} - \lambda_i \sum_k \beta_{ik} c_{ki}^{(x_i)} (1 + \gamma_{ki} (f_k^{(t_k)} - 1)) \Bigg], \tag{2.11}$$

and the off-diagonal elements are

$$J_{ij}|_* = \alpha_i \Bigg[\phi_i f_i^{(t_i)} \gamma_{ij} c_{ij}^{(x_j)} - \lambda_i \beta_{ij} f_j^{(x_j)} - \lambda_i \sum_k \beta_{ik} c_{kj}^{(x_j)} \gamma_{kj} (f_k^{(t_k)} - 1) \Bigg]. \tag{2.12}$$

The five *exponent parameters* $s_i^{(x_i)}, f_i^{(x_i)}, m_i^{(x_i)}, c_{ki}^{(x_i)}$, and $f_i^{(t_i)}$ are generally defined as

$$g^{(\xi)} \equiv \left. \frac{\partial g(\boldsymbol{x})}{\partial \xi} \right|_{\boldsymbol{x}=\boldsymbol{x}^*}, \tag{2.13}$$

with $\xi \in \{x_i, t_i\}$. They describe the nonlinearity of process $\mathscr{G}(\boldsymbol{X})$ with respect to ξ, where $g(\boldsymbol{x}) = \mathscr{G}(\boldsymbol{X}^*\boldsymbol{x})/\mathscr{G}^*$ analogous to Eq. (2.7). As an example for deriving an exponent parameter, consider a growth term $\mathscr{G}(X, Y) = aYX^3$. Then the rescaled function [Eq. (2.7)], $g(x, y) = \mathscr{G}(X, Y)/\mathscr{G}(X^*, Y^*) = yx^3$, yields the exponent parameters $g^{(x)} = 3$ and $g^{(y)} = 1$ from Eq. (2.13). Further examples are given in Table 2.1.

Table 2.1: Examples of functions $\mathscr{G}(X)$ and their corresponding exponent parameters $g^{(x)}$.

Function	$\mathscr{G}(X)$	$g^{(x)}$
power	aX^p	p
exponential	ae^{bX^p}	pbX^{*p}
Holling's type I, H_1	aX	1
Holling's type II, H_2	$\frac{aX}{k+X}$	$\frac{k}{k+X^*}$
Holling's type III, H_3	$\frac{aX^p}{k^q+X^p}$	$\frac{p}{1+X^{*p}/k^q}$

§ Generalized Parameters: Assumptions and Interpretation

The stability of the steady state of the food web [Eqs. (2.11) and (2.12)] depends only on the time scale parameter α_i [Eq. (2.8)], the scaling parameters [Eq. (2.10)], the exponent parameters [Eq. (2.13)], and the topology of the web. Therefore, making assumptions on body-size distribution, proportion of biomass flows, nonlinearities of functional forms, and connectance of species determines this stability without the need for initial conditions or specific forms.

The characteristic timescale α_i is the inverse of an organism's life expectancy, which is expected to increase with body-size m_i. An exponential dependence, $\alpha_i = \alpha_s^{m_i}$ and $\alpha_s = 0.008$, is commonly applied (Gross et al.; 2009). The body sizes are chosen such that their histogram fits a beta distribution $B(a = 0.5, b = 2)$.

The scale parameters [Eq. (2.10)] quantify the proportions of biomass fluxes at the steady state. The following assumptions are made: The biomass of basal species grows only from production (σ=1) and decreases only from predation (λ=1); growth from predation is absent (ϕ=0) and natural mortality is neglected in comparison to predation (μ=0). Populations of intermediate species grow from predation (ϕ=1) and decline from predation (λ=1). A top predator population grows only from predation (ϕ=1) and decreases only from natural mortality (μ=1). Hence the proportions for σ, ϕ, μ, and λ are either ones or zeros [Table 2.2]. β_{ij} (γ_{ij}) represents the proportion of the jth species contribution to the predative loss (gain) of species i. Each predator (prey) species is assumed to contribute the same amount as its competitors to predative loss (gain). As an example, if X_1 has 4 predators, each predator contributes 25% to the total predative loss of X_1. Similarly, if X_4 consumes X_3, X_2, and X_1, then $\gamma_{43} = \gamma_{42} = \gamma_{41} = 1/3$. In other words, β_{ij} represents the inverse of the in-degree of node i, and γ_{ij} represents the inverse of the out-degree of node i. The scale parameters are summarized in Table 2.2.

Table 2.2: Summary of the assumptions for the scale parameters for top, intermediate, and basal species. k_i^{in} is the in-degree of node i, and k_i^{out} is its out-degree. $\beta_{ij} = 0 = \gamma_{ij}$ in the absence of a link between i and j.

Parameter	Value	Node Type	Proportion of Flux			
			σ_i	ϕ_i	μ_i	λ_i
α_i	0.008^{m_i}	Top	0	1	1	0
β_{ij}^{-1}	k_i^{out}	Intermediate	0	1	0	1
γ_{ij}^{-1}	k_i^{in}	Basal	1	0	0	1

The exponent parameter, $S \equiv s_i^{(x_i)}$, describes the nonlinearity of the production rate $\mathscr{S}_i(X_i)$ of basal species (Gross and Feudel; 2006). When production is limited by resources or nutrients, the production rate is constant with respect to the population of the basal species, $S = 0$. When resources are plentiful, production goes linear, $S = 1$. In this study, S takes on values between zero and one, $S \in [0, 1]$.

The nonlinearity of natural mortality, $M \equiv m_i^{(x_i)}$, in top predators is often referred to as the exponent of closure (Edwards and Bees; 2001). Linear to quadratic mortality functions have been shown to describe biological systems (Edwards and Bees; 2001; Lan and Li; 2008). This corresponds to values for M between one and two, $M \in [1, 2]$.

The predatory growth term $\mathscr{F}_i(T_i, X_i)$ [Eq. (2.3)] depends on the available prey T_i and on the predator itself X_i. Since $\mathscr{F}_i$ is linear in X_i, the nonlinearity of predation with respect to the predator itself, $f_i^{(x_i)}$, is equal to one. The prey dependence is of Holling's types and the nonlinearity of predation with respect to prey, $f_i^{(t_i)}$, follows from Table 2.1. The nonlinearity range of $H_3(T)$ with $p = 2$ varies between two, when prey is scarce, and zero,

as prey becomes very abundant, $F \in [0, 2]$. Analogously, the nonlinearity range of $H_2(T)$ is given by $F \in [0, 1]$, and $F = 1$ for $H_1(T)$.

The nonlinearity of predator preference for prey, $c_{ik}^{(x_k)}$, is one for passive prey switching and two for active prey switching. Here, $c_{ik}^{(x_k)} = 1$ is used. The exponent parameters are summarized in Table 2.3.

Table 2.3: Summary of exponent parameters and their range of nonlinearities.

Exponent Parameter Parameter	Alias	Nonlinearity of	Range
$s_i^{(x_i)}$	S	basal growth	[0,1]
$f_i^{(x_i)}$	-	predation w.r.t. predator itself	1
$f_i^{(t_i)}$	F	predation w.r.t prey	[0,2]
$m_i^{(x_i)}$	M	mortality (top species)	[1,2]
$c_{ik}^{(x_k)}$	-	prey switching	1

§ Stability Profiles

Throughout this paper, steady states of a food web are discussed as a function of three main nonlinearity (exponent) parameters, basal growth (production) S, feeding (predation) gain F, and mortality of the top predator M. The stability profile color-codes the stability of the steady states as a function of two or more of these parameters for a given network topology [Fig. 2.3]. Since the dependence of the stability profiles on the mortality M is generally low compared to the dependence on the production S and feeding gain F parameters [Fig. 2.3 (a)], a superimposition of two-dimensional profiles in S and F for several M values is used for the analysis [Fig. 2.3 (b)]. In some stability profiles M is fixed. The *proportion of stable equilibria* P of a particular food web topology is the number of stable equilibria divided by the total number of sample points.

2.5 Sensitivity to Topology

This section provides an overview of stability profiles as connectivity in the network changes by varying the prey body-size upper and lower limit (U, L). Small changes to topology can have a dramatic impact on a stability profile. A network that has no stable steady state (for all combinations of exponent parameters S, F, and M, Table 2.3) can switch to a network with a large portion (e.g., 50%) or an intermediate portion (e.g., 10%) of stable steady states by changing the prey body-size lower limit L by one. This sensitivity to L is visible from the proportion of stable equilibria P in Fig. 2.4(a) or from the stability

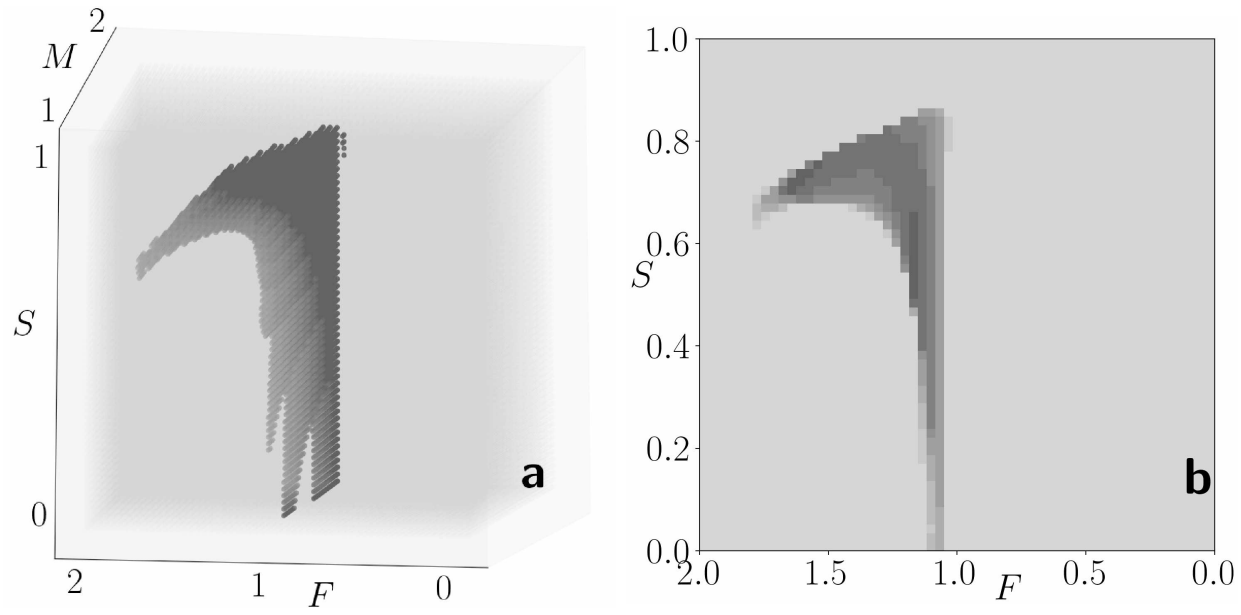

Figure 2.3: Stability profile for equilibrium states as a function of the nonlinearity parameters, basal growth S, feeding gain F, and mortality M for a network of $N = 30$ species, prey body-size upper limit $U = 5$, and prey body-size lower limit $L = 12$. Unstable (stable) equilibria are marked in light gray (dark gray). The three-dimensional plot (a) is simplified to a two-dimensional superimposition (b) of ten equidistant slices from (a) parallel to the $S - F$ plane. Prey availability increases to the right on F-axis, and production increases upwards on S-axis.

profiles in Figs. 2.4(b)-(d). Some regularities in the fluctuations of stability exist. For the lower range of L-values, the peaks in the proportion of stable steady states P occur with a periodicity of (about) U; this is why the stability profiles in Figs. 2.4(b)-(e) are arranged with the number of columns equal to U. For some intermediate L-values there is no stable steady state. As L increases further until it approaches its upper bound of $N - 1$, a certain proportion of stable steady states is regained.

Networks with more than one top predator (basal species), $U > 1$, have large portions of stable steady states for L-values near their upper and lower bounds (e.g., Fig. 2.4(b)). As the number of top predators (and basal species) U increases, larger portions of stable steady states appear for more intermediate L [Figs. 2.4(c) - (d)], until a large portion of stable steady states is reached for all L at (or near) the upper bound on U [Fig. 2.4(e)]. The upper bound on U is $N/2$ (truncated to integer value; otherwise the network is disjoint). For even N, the webs are comprised of top predators and basal species, and no intermediate species. Depending on the prey body-size lower limit L, a top predator consumes one or more basal species. For such webs the stability profiles are no longer sensitive to L, are (nearly) identical to that of a 2-trophic food chain, and have the largest portions of stable steady states among

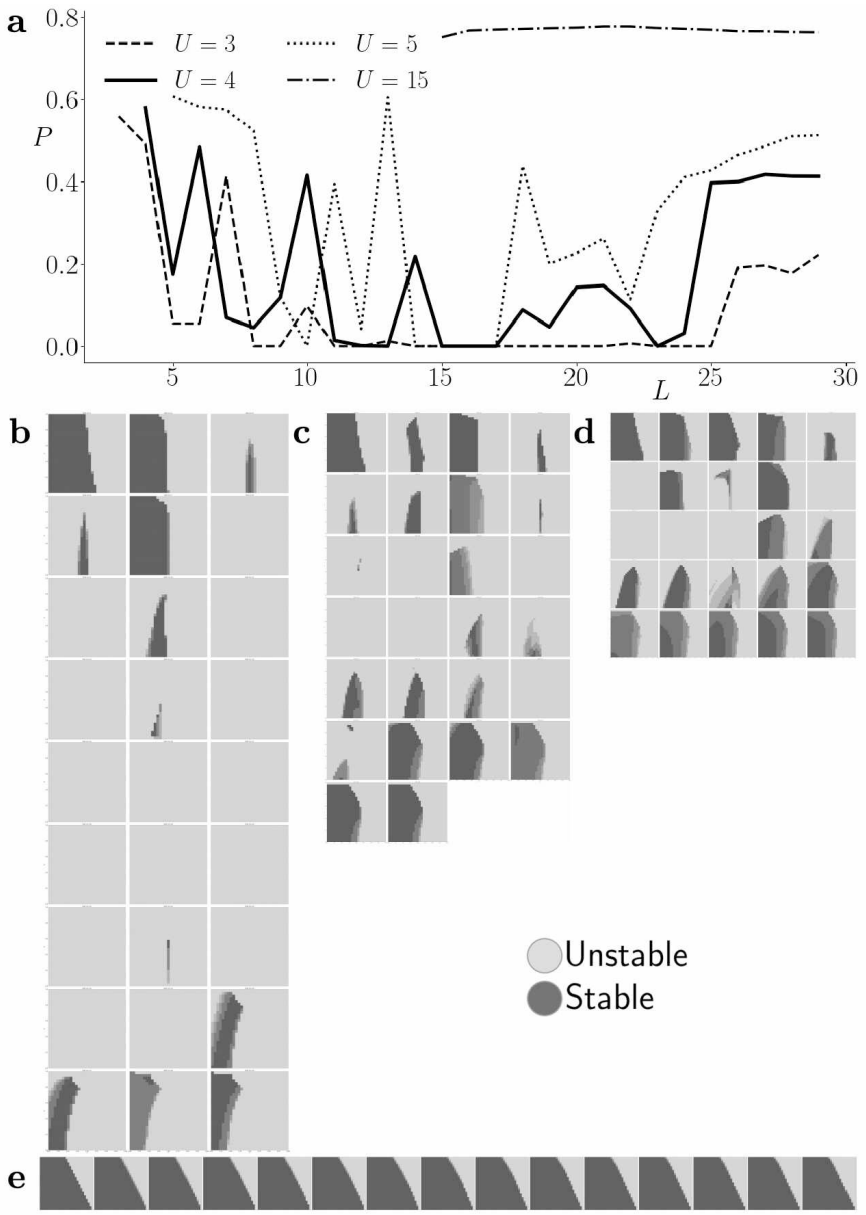

Figure 2.4: (a) Proportion of stable equilibria P for a network of $N = 30$ species and different topologies, defined by the prey body-size lower limit L, $U \leq L \leq N-1$, and the prey body-size upper limit U. P is measured over the biological range of nonlinearities of the gain and loss mechanisms, (S, F, and M) from Table 2.3. Stability profiles for the webs from (a) for $U = 3$ (b), $U = 4$ (c), $U = 5$ (d), and $U = 15$ (e). The number of columns in each subfigure is U. L increases from left-to-right and top-to-bottom, following script directionality. For axes and color information see Fig. 2.3(b).

the webs explored in this research [Fig. 2.4(e)].

An increase of the prey body-size lower limit by just one, from L to $L+1$ adds $N-(L+1)$ links to the network, which can substantially change the connectance for large N and small

L. If L is close to N, few links are added, and Figs. 2.4(b)-(e) demonstrate that the change in stability is small in these cases. Changing L by one, occasionally results in dramatic fluctuations in the stability profiles (discussed above) that are accompanied by larger changes in connectance. In the following, the topology is changed gradually (one link at a time) to test whether the proportion of stable steady states P changes gradually as well. From the numerous permutations to sequentially add a set of links to a network, two orders are considered [Fig. 2.5]. Either starting with the largest species and going sequentially down the ranks to add predatory links, or, starting with the predator that is ranked $L+1$ near the bottom of the web and going sequentially up the ranks to add predatory links.

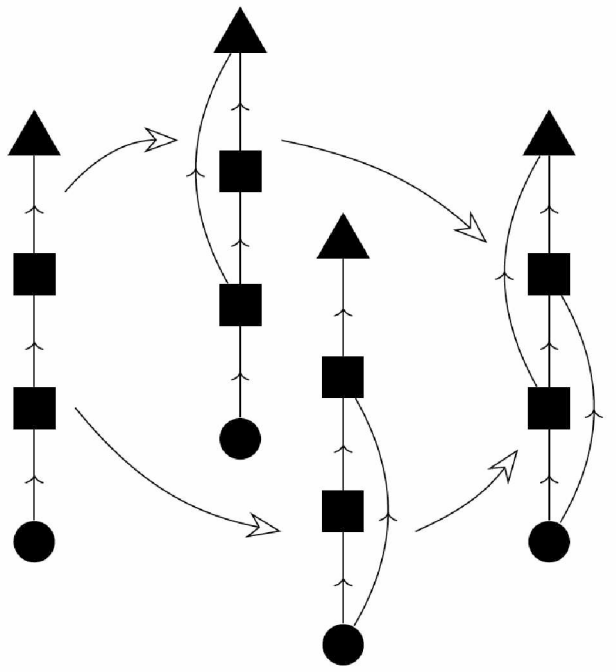

Figure 2.5: Two options to add links one at a time: The network $(N, U, L) = (4, 1, 1)$ (left) evolves into the network $(N, U, L) = (4, 1, 2)$ (right) by adding links from the top down (upper path) or from the bottom up (lower path).

Changing the network topology one link at a time can show smooth changes in P but also dramatic change. Figure 2.6 shows an example for a dramatic increase in stable steady states, from $P = 0$ to $P \approx 0.5$ when the network topology changes from $(N, U, L) = (30, 5, 17)$ to $(30, 5, 18)$. If the twelve links are added one at a time and from the top down, the entire change in stability occurs with the very last link addition [Fig. 2.6(a)]. If these links are added from the bottom up, the first link produces already measurable stability and the second link results in a profile that is qualitatively similar to the final profile [Fig. 2.6(b)]. The first link of the bottom up order and the last link of the top down order represent the same link, which indicates that this particular link is crucial for stability. Figure 2.7(a) shows an

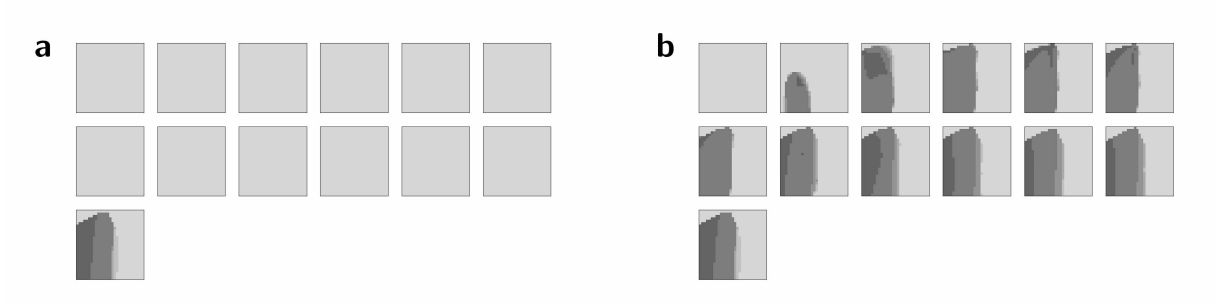

Figure 2.6: Sequence of stability profiles for a network change from $(N, U, L) = (30, 5, 17)$ to $(30, 5, 18)$. (Twelve) links are added one at a time (a) from the top down and (b) from the bottom up. For axes and color information see Fig. 2.3(b).

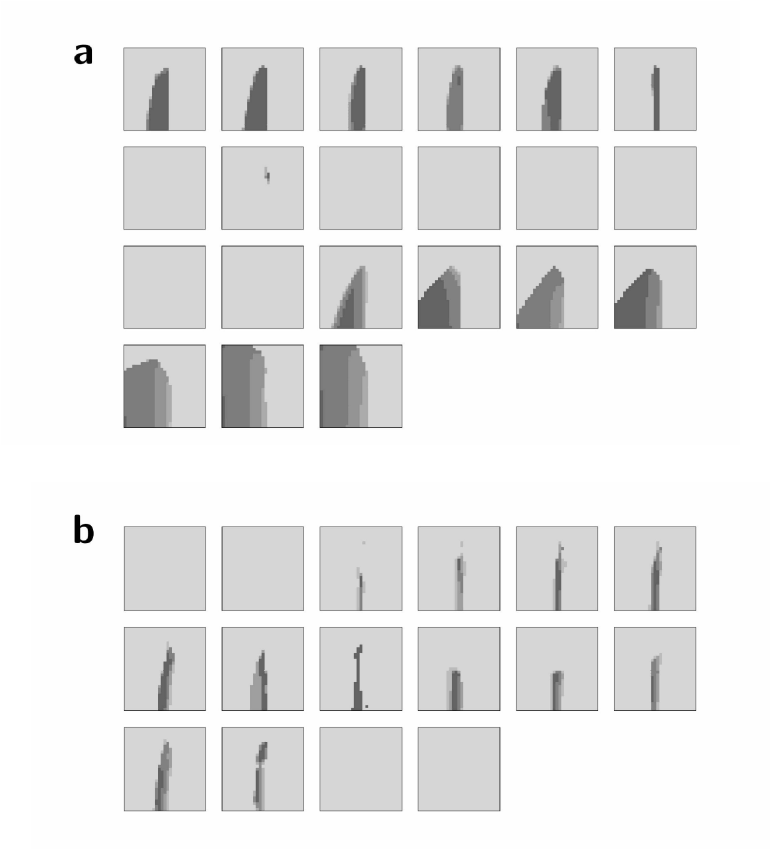

Figure 2.7: Sequence of stability profiles when links are added one by one from the top down. The network topology changes (a) from $(N, U, L) = (30, 4, 9)$ to $(30, 4, 10)$ and (b) from $(N, U, L) = (30, 5, 14)$ to $(30, 5, 15)$. For axes and color information see Fig. 2.3(b).

example where the proportion of stable steady states approximately triples with a topology change from $(N, U, L) = (30, 4, 9)$ to $(30, 4, 10)$. Adding the twenty links sequentially reveals a hidden and profound dip in stability after a few links are added. Figure 2.7(b) shows an example where the proportion of stable steady states is zero and stays zero when the topology

is changed from $(N, U, L) = (30, 5, 14)$ to $(30, 5, 15)$. Adding the fifteen links sequentially reveals a hidden spike in stability over a large portion of the sequence.

2.6 Predatory Response and Stability

Stability profiles with the most occurrences amongst the different topologies are categorized by shape: "50/50 block" [Fig. 2.8(a)], "cantilever" [Fig. 2.8(b)], "3/4 block" [Fig. 2.9(a)], "tongue" (Fig. 2.7, top left), and "completely unstable profile" (Fig. 2.7, second row).

"50/50 blocks" [Fig. 2.8(a)] are characterized by stable steady states for greater than linear feeding responses F, which are accessible for a Holling's type III predatory response in low prey abundance (Fig. 2.2). Steady states are unstable for large prey abundance ($F < 1$ in Holling's types III). If the predatory response in the network is modeled with a Holling's type II function where $F \in [0, 1]$, steady states are unstable for both, low and high prey abundance. "50/50 blocks" and similar patterns show up throughout topologies and network sizes; they are typical for long food chains.

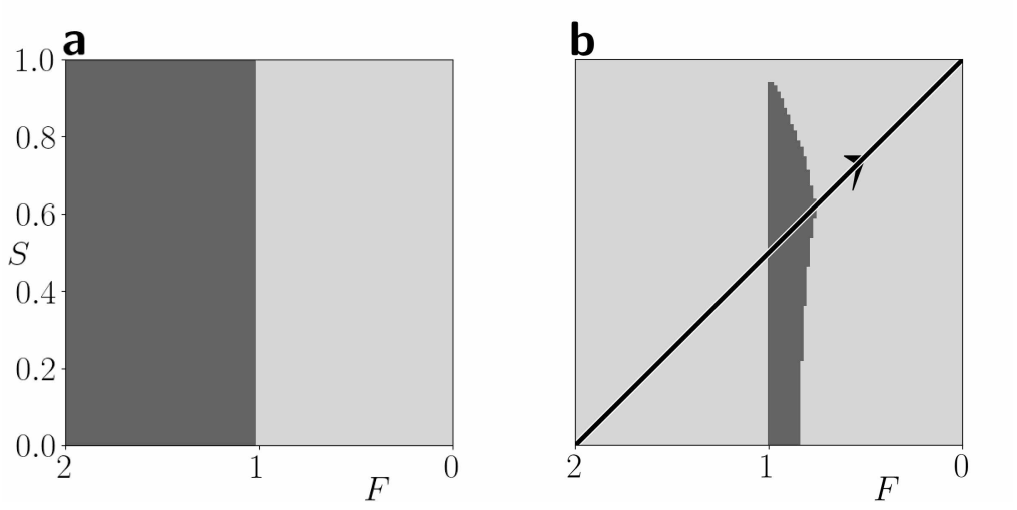

Figure 2.8: Typical stability profiles: (a) "50/50 block", $(N, U, L) = (5, 1, 2)$, and (b) "cantilever", $(N, U, L) = (30, 6, 9)$. A path of enrichment (Sec. 2.7) is highlighted. Mortality is quadratic, $M = 2$.

"Cantilevers" [Fig. 2.8(b)] are stability profiles with stable steady states only near $F = 1$ over a range of production nonlinearities S; they represent food web topologies with a stable steady state only for a linear predatory response to prey (e.g., H_1, filter feeders) and limited or somewhat limited production. "Tongues" (Fig. 2.7, top left) are fatter "cantilevers" that typically exist in the neighborhood of $F = 1$; in some cases the tongue is located in the range $F > 1$, which is accessible via a Holling's type III functional response. A "tongue" pattern has unstable fixed points for $F = 2$, to distinguish it from "50/50 block"

like patterns. A "completely unstable profile" is defined by $P = 0$. "Cantilevers", "tongues", and "completely unstable profiles" are found in the more realistic web topologies which have intermediate values of U and L.

A "3/4 block" [Fig. 2.9(a)] has the largest proportion of stable equilibria, $P \approx 0.75$ for a Holling's type III predatory response. "3/4 blocks" and similar stability profiles are obtained from short chains and webs with few to no intermediate species ($U \approx N/2$). For a Holling's type II functional response, the stability diagram is restricted to $F \in [0, 1]$, and exhibits stable steady states for prey and production limited food webs.

2.7 Paradox of Enrichment

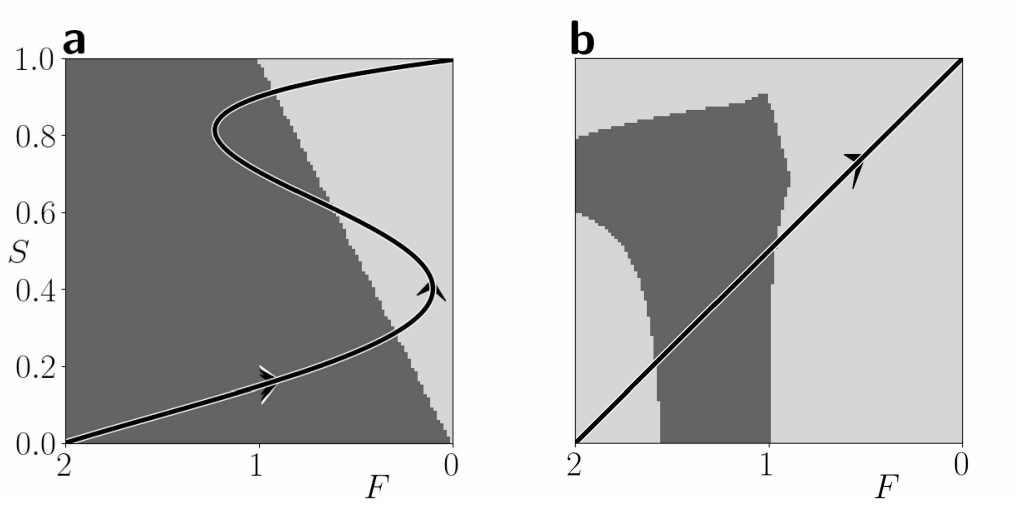

Figure 2.9: Stability profiles: (a) "3/4 block", $(N, U, L) = (2, 1, 1)$, and (b) a special profile, $(N, U, L) = (30, 6, 8)$. Paths of enrichment (Sec. 2.7) are highlighted. Mortality is linear, $M = 1$.

Rosenzweig (1971) demonstrated that increasing yield to the exploiting predator, by increasing nutrients or carrying capacity of the prey, destabilizes the system in six two-species ecosystem models. He called this the "Paradox of Enrichment." In experimental systems, enrichment has been demonstrated to destabilize, stabilize, or neither (Roy and Chattopadhyay; 2007). Mathematical models have generally demonstrated that enrichment destabilizes large realistic food webs (Yeakel et al.; 2014). Various authors have presented exceptions to the apparent paradox (Abrams and Walters; 1996; Genkai-Kato and Yamamura; 1999; Jansen; 1995; Mougi and Nishimura; 2007; Gross et al.; 2004). One important study used generalized modeling to demonstrate stabilizing impacts of enrichment for special predatory responses (Gross et al.; 2004).

A system that is being enriched traces out a path in the parameter space of nonlinearity of production (S) and nonlinearity of predation (F) such that basal production and prey availability increases (Fig. 2.9). As nutrients increase in a production-limited system ($S = 0$) the basal population increases and consequentially so do the prey populations. For typical Holling's type predatory responses (H_2, H_3) more abundant prey and a growth of predator populations from predation is expressed in a decrease of the nonlinearity parameter for predatory gain F, Fig. 2.9(b). For a different and hypothetical predatory response (Gross et al.; 2004) an "S-shaped" enrichment path is shown in Fig. 2.9(a); note that the increase of F with increasing S would not be consistent with enrichment for a Holling's type predatory response.

Stability profiles with a "cantilever" [Fig. 2.8(b)] or "tongue" pattern, or with the special pattern in Fig. 2.9(b) provide an exception to the paradox of enrichment in the case of a Holling's type III predatory response. A path of enrichment passes through a parameter regime with limited production and limited prey for which the stability of the web's steady state switches from unstable to stable. Such stabilization through enrichment exists for F-values larger than one, a parameter regime that is accessible for a Holling's type III response. In contrast, the enrichment path reaches unstable steady states in ecosystems with plenty of prey and production, consistent with the paradox of enrichment, and accessible for both Holling's type II and III predatory responses (where $F \leq 1$)). The stable region of the cantilever pattern along the path of enrichment [Fig. 2.8(b)] is bounded on the left by a zero-eigenvalue bifurcation and bounded on the right by a Hopf bifurcation [Fig. 2.10(a)]. Crossing the zero-eigenvalue bifurcation as the system is enriched turns the fixed point stable. The stable region for the stability profile in Fig. 2.9(b) is bounded by Hopf bifurcations along the path of enrichment, Fig. 2.10(b).

The superimposition of stability profiles from over 4000 webs (Fig. 2.11) shows that the ratio of intermediate to top predators influences stabilization through enrichment. For low ratios ($I/U < 2$) overall stability P is high, and a stable steady state likely becomes unstable as enrichment takes place [Fig. 2.11(a)], consistent with the paradox of enrichment. For higher ratios, topologies provide exceptions to the paradox since a steady state becomes stable with enrichment for superlinear feeding characteristics [Fig. 2.11(b)], i.e. for H_3 in low prey abundance ($F > 1$). As for the region encompassing the H_2 functional response ($F \in [0, 1]$), enrichment causes a rapid decrease in the percentage of stable fixed points to yield only unstable fixed points for highly enriched systems, consistent with the paradox. Different functional responses would need to be postulated, as the hypothetical curve in Fig. 2.9(a), to construct an exception to the paradox in this F-regime.

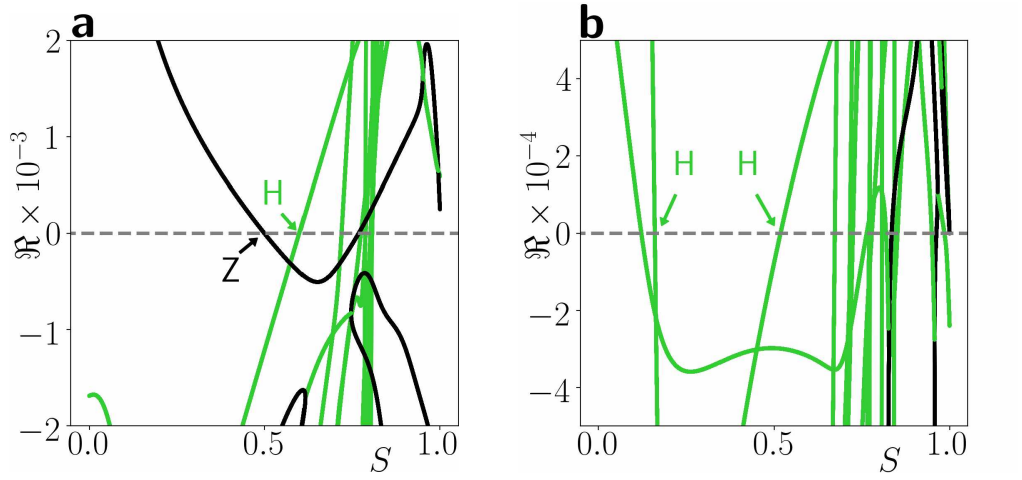

Figure 2.10: $\Re$ (real part of complex eigenvalues (green); real eigenvalues (black)) along the diagonal path of enrichment: (a) for path in Fig. 2.8(b) and (b) for path in Fig. 2.9(b). The label "Z" marks a zero-eigenvalue bifurcation while "H" marks a Hopf bifurcation. Between "Z" and "H" as well as between "H" and "H", $\Re$ is negative for all eigenvalues outside of the plotting range.

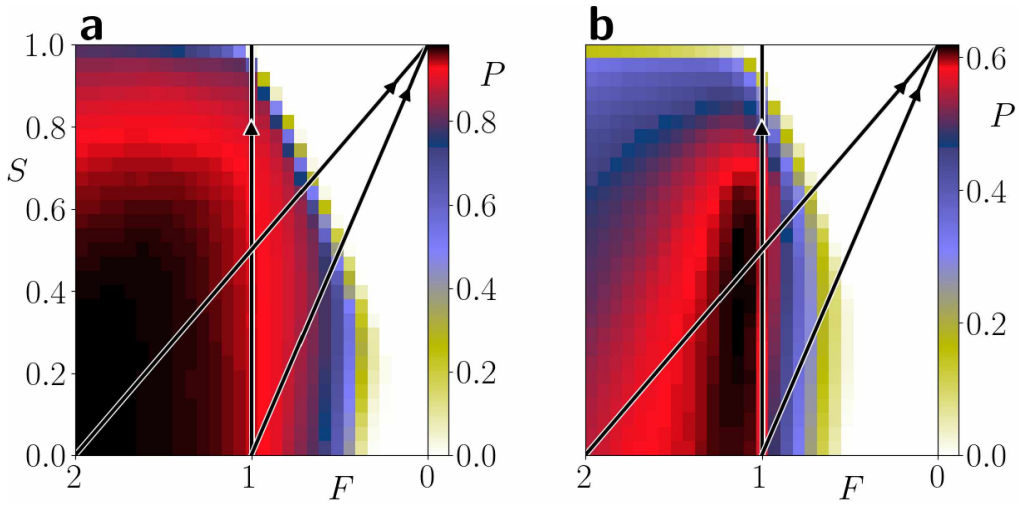

Figure 2.11: Proportion of stable equilibria (P) versus nonlinearity of basal growth (S) and nonlinearity of predation growth (F), calculated from a superimposition of stability diagrams from webs of sizes $N = 2, 3, ..., 19, 20, 25, ..., 55, 60$, with upper limits $1 < U \leq N/2$ and lower limits $U < L < N$. The ratio of intermediate predators to top predators is (a) $I/U < 2$ resulting in 2726 webs, and (b) $2 \leq I/U < 6$ resulting in 1745 webs. The vertical line represents the path of enrichment for H_1 ($F = 1$). The two diagonal lines represent paths of enrichment for H_3 ($F \in [0, 2]$) and H_2 ($F \in [0, 1]$). Topologies with $U = 1$ and $U = L$ are excluded; networks with $U = L \neq 1$ are disjoint, and networks with $U = 1$ have a long predatory pathway of length $N - 1$ for large N (Williams and Martinez; 2004).

2.8 Omnivory: Food Chains to Food Webs

Omnivory allows species in a trophic network to feed on resources from multiple trophic levels (e.g., Fig. 2.12); its role in stabilization and destabilization of trophic webs is an important area of research (Vandermeer; 2006; Holyoak and Sachdev; 1998; Namba et al.; 2008). For example, in a real invertebrate food web, Fagan found that abundant spider omnivores made the web more robust to perturbation (Fagan; 1997). In theoretical networks, ominvory is the intermediate topology between any three-species networks organized as chain, polyphagy (generalist predator) or competition (Vandermeer; 2006); networks transition through omnivory to move between any of these network types. Computer models of these three-species webs offer strong evidence that increased omnivory can have either a stabilizing or destabilizing impact (Vandermeer; 2006; McCann and Hastings; 1997; Gellner and McCann; 2011). Given the equivocal evidence, the role of omnivory to the stability is unclear.

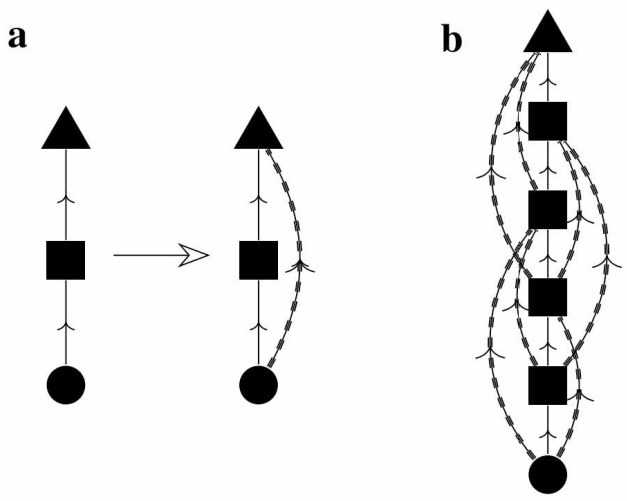

Figure 2.12: (a) Tri-trophic chain transition to omnivory, $(N, U, L) = (3, 1, 1) \rightarrow (3, 1, 2)$. (b) Six-trophic chain transition to omnivory, $(N, U, L) = (6, 1, 1) \rightarrow (6, 1, 3)$. The segmented arrows are the added links.

A comparison of the stability profiles of a three-species chain to a three-species omnivorous web is shown in Fig. 2.13. In the omnivorous web steady states flip from unstable to stable over a range of basal production S and feeding gain F nonlinearities. Large increases in the real part of the largest eigenvalue are seen for most of the production-limited region ($S \approx 0$) although this region remained stable, Fig. 2.13(b). Stability profiles for larger food chains and various degrees of omnivory are presented in Fig. 2.14. Adding omnivory (with prey body-size lower limit $L = 2$) to a food chain of four species yields a similar increase in stable steady states to the 3 species system [Fig. 2.14(a)], except that the region of high

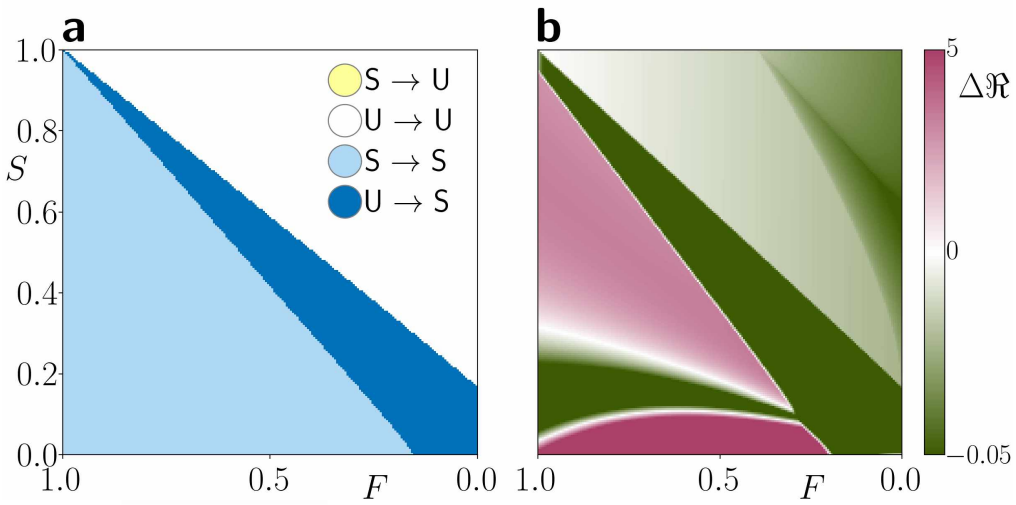

Figure 2.13: (a) Difference in stability of steady state and (b) difference in real part of the largest eigenvalue $\Re$ for a change in topology [Fig. 2.12(a)] from a tri-trophic chain to omnivory, $(N, U, L) = (3, 1, 1) \to (3, 1, 2)$. S (U) denote a stable (unstable) steady state. Positive and negative changes in $\Re$ are scaled differently. The nonlinearity of feeding gain is restricted to $F \in [0, 1]$, since no change of stability occurred on $[1, 2]$. Quadratic mortality is used, $M = 2$.

prey abundance is unstable. In a five-species chain, Fig. 2.14(b), creating omnivores ($L = 2$) completely destabilizes all fixed points on this F-range, leading to a "50/50" block over the full Holling's type III range, $F \in [0, 2]$. Creating omnivores with $L = 2$ in a six-species chain, Fig. 2.14(b), results in a similar destabilization of fixed points to that of the five species case; however, making the omnivores more omnivorous by increasing the lower limit to $L = 3$ re-stabilizes the fixed points for low prey abundance ($F \approx 1$ for H_2), Fig. 2.14(d). The trend that creating omnivores destabilizes longer food chains continues but to a lesser degree as N gets large.

Figure 2.15 shows the proportion of stable steady states P for networks with up to sixty species and a variety of topologies, ranging from a chain ($L = 1$) to the maximum degree of omnivory ($L = N - 1$), and assuming a Holling's type III predatory response. Short chains have the highest number of stable steady states and their stability profiles are similar to a "3/4 block" ($P \approx 0.75$); as chain length increases, steady states loose stability and the profiles asymptotically approach a "50/50 block", ($P \approx 0.5$). Adding various degrees of omnivory to a chain generally destabilizes (a portion of the) steady states. For essentially all longer chains than four, creating omnivores ($L = 2$) makes networks with about a "50/50" stability profile, Fig. 2.15(a). As the degree of omnivory increases by increasing the prey body-size lower limit L, the portion of stable steady states P generally continues to decline, Fig. 2.15(b). For networks of more than twenty species, this decline reaches $P = 0$, where

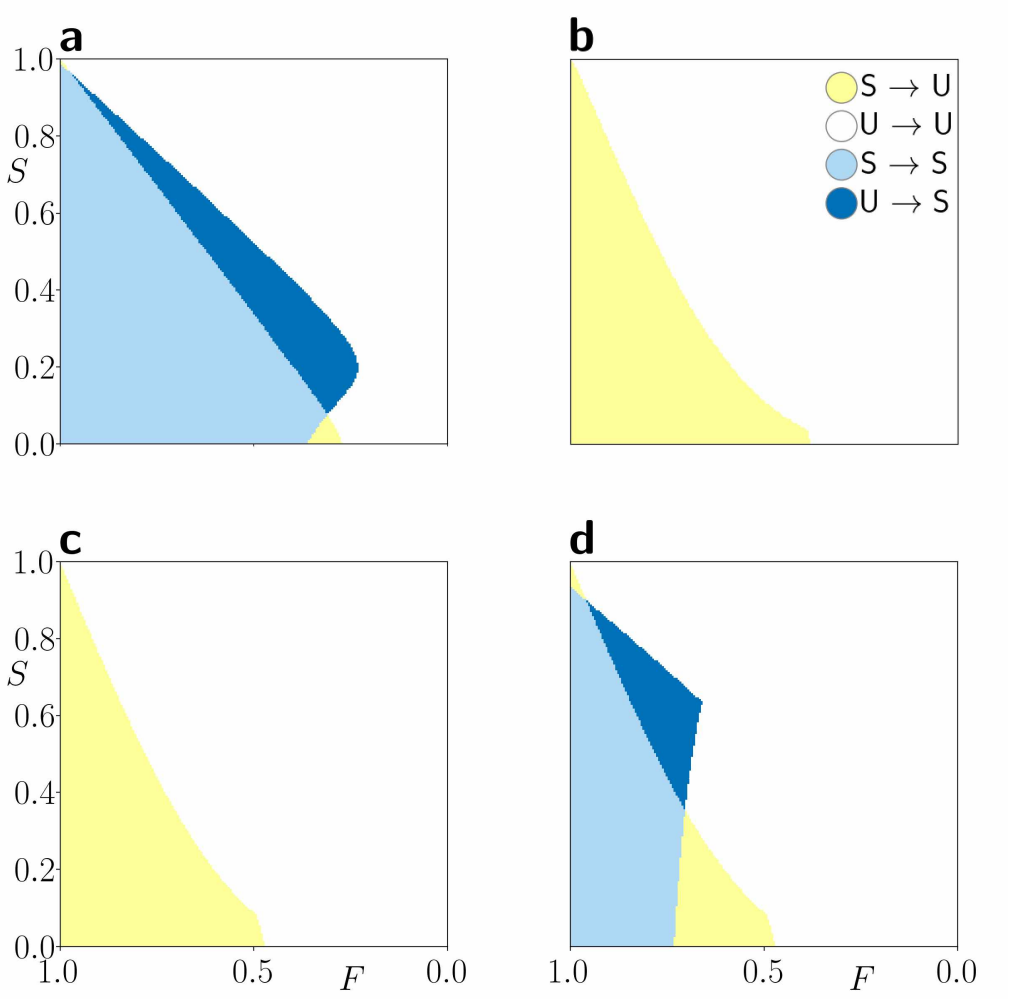

Figure 2.14: Stability flipping for topology change from chain to omnivory, (a) $(N, U, L) = (4, 1, 1) \rightarrow (4, 1, 2)$, (b) $(5, 1, 1) \rightarrow (5, 1, 2)$, (c) $(6, 1, 1) \rightarrow (6, 1, 2)$, (d) $(6, 1, 1) \rightarrow (6, 1, 3)$. Quadratic mortality is used, $M = 2$. The color coding (b) is the same in all panels.

all steady states are unstable. If the prey body-size upper limit U is changed, the trend to fewer stable steady states as L increases continues.

2.9 Complexity-Stability Debate and the Ratio of Intermediate to Top Predators

"Ecosystem complexity increases stability" was considered a core ecological principle (Pimm; 1984), where complexity is quantified with species richness N and connectance C. Still today, most observational evidence indicates that increased complexity increases stability, yet most mathematical models show that complexity destabilizes webs (Gross et al.; 2009; Allesina et al.; 2015). Law and Blackford (1992) argue that a more connected network has more reassembly pathways that allow it to persist. Some theoretical studies show that

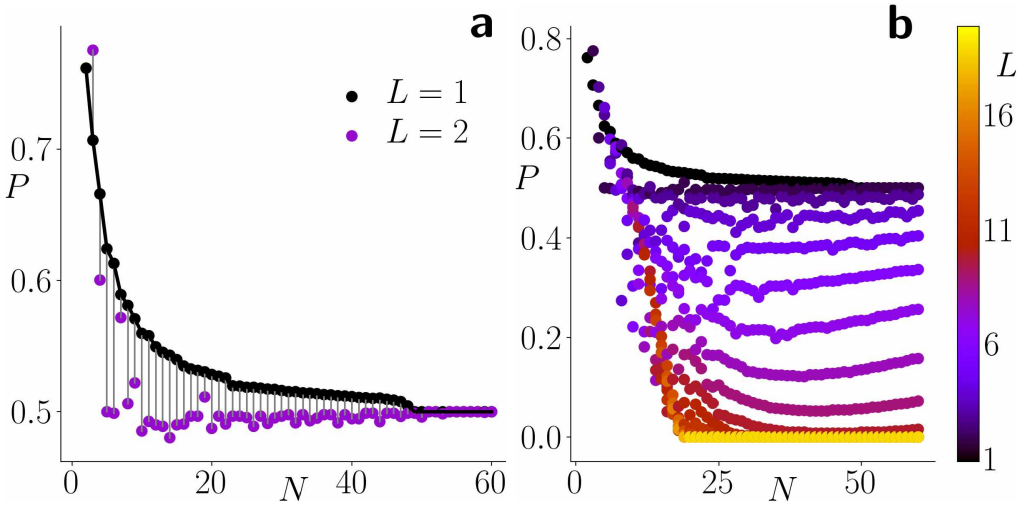

Figure 2.15: Proportion of stable equilibria P versus network size N for topologies with prey body-size upper limit $U = 1$ and varying prey body-size lower limits L: (a) $L = 1, 2$, and (b) $L \in [1, N-1]$ (color coded). Black dots represent food chains, $U = L = 1$. Sample points for P are based on $F \in [0, 2]$, $S \in [0, 1]$ and $M \in [1, 2]$.

large connectance or high polyphagy reduces population fluctuations and allow diminishing prey populations to recover when predators switch to more abundant prey (Polis; 1998). In niche-modeled food webs with large prey abundance, generalized modeling reveals an increase of stability for larger networks and larger connectance (Plitzko et al.; 2012).

Figure 2.15 shows that more connectance (larger L) decreases the proportion of stable steady states for networks with prey body-size upper limit $U = 1$. This trend is consistent with results for the niche model (Gross et al.; 2009). In contrast, networks with larger prey body-size upper limit, $U > 1$, don't follow a consistent trend (Fig. 2.16). Networks with a large proportion of stable steady states P are interspersed with cases of low P over a range of complexities; the size of the web N and its connectance C cannot solely be used to predict its stability P. For a Holling's type II predatory response, Fig. 2.16(a), networks with large NC complexity have predominantly lower portions of stable steady states P. A Holling's type III predatory response leads to predominantly high values of P for a range of NC complexities, Fig. 2.16(b). A trend that maximum values of P decline linearly with increasing complexity persists for higher complexities, but is less pronounced than in food webs with Holling's type II predatory response. Large networks with intermediate NC complexity can have the stability of a di-trophic chain, the most stable configuration in these models.

A non-monotonic relation between stability and connectance consistently occurs throughout this study, Figs. 2.4(b)-(d) and Fig. 2.17, for large webs ($N > 15$) and intermediate values of U. As connectance increases with increasing prey body-size lower limit L, the stability profiles show a decrease in the proportion of stable steady states P to (or to almost) "com-

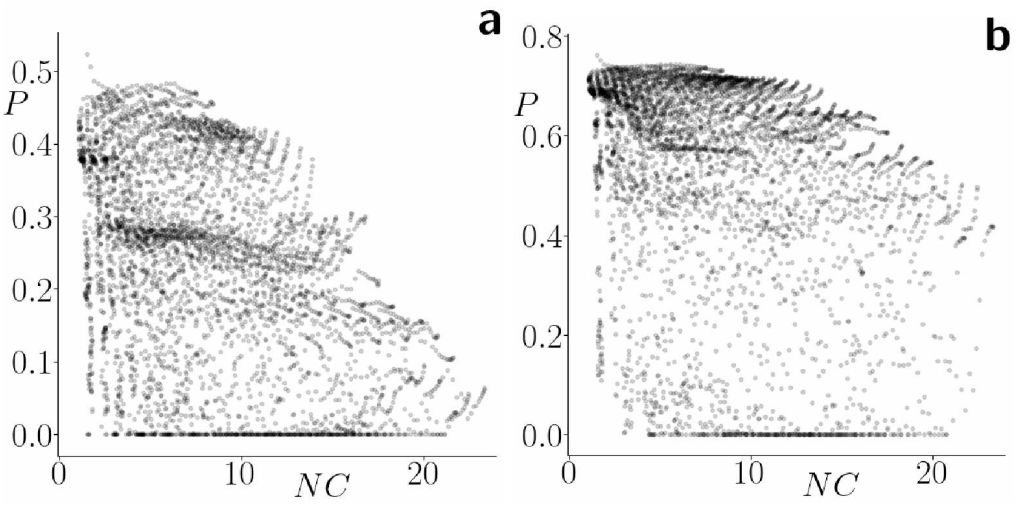

Figure 2.16: Proportion of stable equilibria (P) versus NC complexity for a Holling's type II (a) and III (b) predatory response. All networks from Fig. 2.11 with a ratio of intermediate predators to top predators, $0 \leq I/U < 6$, are used. Connectance describes the ratio of actual links to possible links in the network, $C = \sum_{k=U}^{L}(N-k)/(N(N-1))$. Each point has an opacity of 0.2.

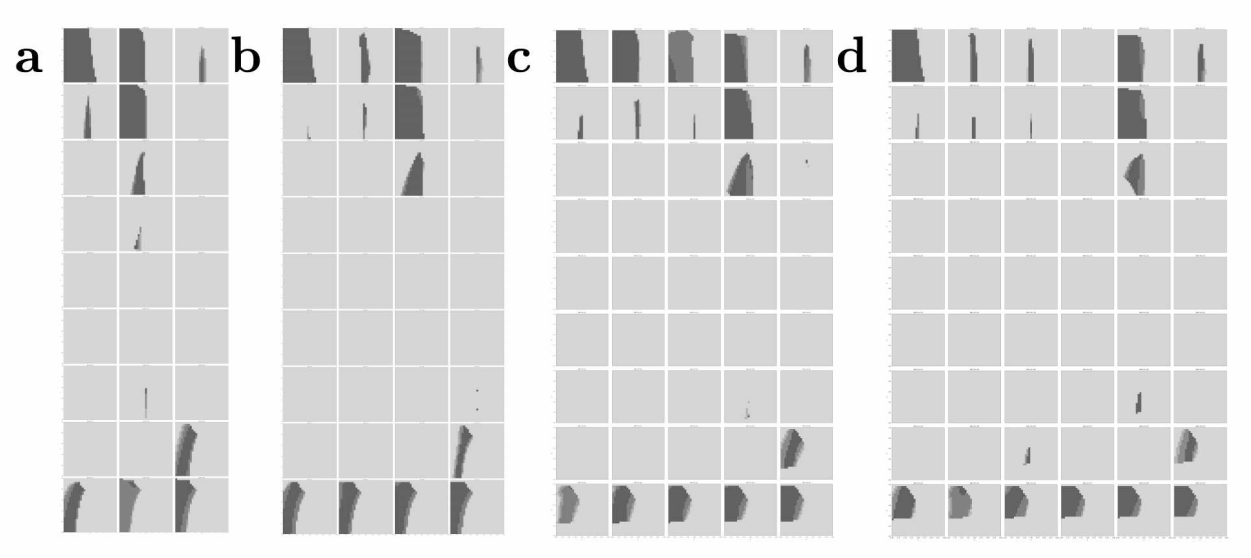

Figure 2.17: Consistency in stability profiles for same N/U ratios, (a) $(N, U) = (30, 3)$, (b) (40, 4), (c) (50, 5), and (d) (60, 6). L increases from U to $N-1$ from top to bottom. Choosing U columns in each set of profiles demonstrates their similarity. For axes and color information see Fig. 2.3(b).

pletely unstable profiles" at intermediate values of L; continuing the increase of L leads to stability returning. Figure 2.17 shows this trend across four different sizes of webs. This figure also demonstrates that the ratio of N/U predicts the entire set of profiles as L is varied.

A good indicator for stability is the ratio of intermediate predators to top predators. The ratio N/U is the ratio of intermediate predators to top predators I/U plus two (Sec. 2.4.1). Smaller ratios N/U correspond to webs (stability profiles) that have on average a larger portion of stable steady states, Figs. 2.4(b)-(d). If this ratio is minimized to two, i.e. no intermediate species exists, di-trophic webs are formed, where top predators consume one or more basal species depending on the value of L. The stability profiles have the largest portion of stable steady states, and look the same for all values of L, Fig. 2.4(e). This study confirms that, even for webs of sixty species, a di-trophic web has the same stability profile as a food chain with two species as claimed by Gross in 2004 (Groß; 2004). While he studied webs where every species in a trophic level is connected to every species in the trophic levels above and below, this study shows that stability profiles are preserved for all values of L, Fig. 2.4(e). And more general, if the ratio of intermediate to top species is the same, then there is a similar web with the smallest amount of species such that N/U is constant.

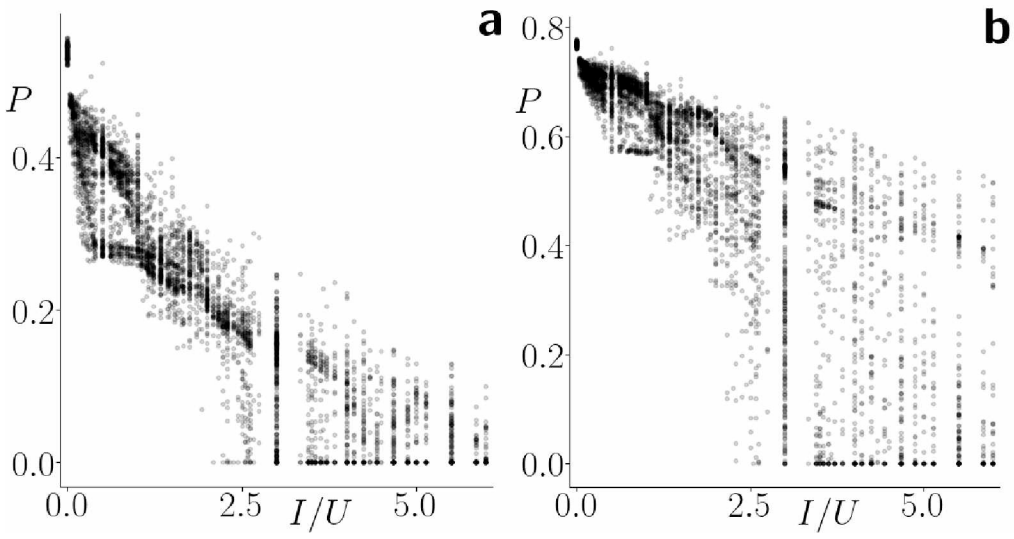

Figure 2.18: Proportion of stable equilibria (P) versus ratio of intermediate to top predators (I/U) for a Holling's type II (a) and III (b) predatory response. All networks from Fig. 2.11 with a ratio of intermediate predators to top predators, $0 \leq I/U < 6$, are used. Each point has an opacity of 0.2.

Figure 2.18 shows the relation of complexity and stability when complexity is measured by the ratio of intermediate predators to top predators I/U, in analogy to NC complexity in Fig. 2.16. For small ratios I/U (below about 2.5) only networks with larger proportions of stable steady states exist while mixing of large and small values of P prevails for increasing ratios of intermediate to top predators. This finding holds for both, Holling's type II and III predatory responses. A trend that maximum values of P decline linearly with increasing complexity persists, but is less pronounced for the Holling's type III predatory response.

2.10 Conclusion

A series of generalized ecological network models is developed and implemented to investigate how topology, particularly omnivory and complexity, and functional dynamics (predatory responses) stabilize and destabilize a steady state across a wide range of network shapes and sizes. The webs are generated in a way derived from the niche model (Williams and Martinez; 2000), but without the randomness. Each predator has a feeding range that is defined by a prey body-size upper and lower limit.

Holling's type predatory responses affect stability. Some webs have stable steady states only when predatory behavior is governed by a Holling's type I predatory response. A type II functional response yields stable steady states when the food web is prey and nutrient (production) limited, and a type III response yields stable steady states predominantly when predators are prey limited. In general, when systems become more nutrient limited, they tend to become more stable across all Holling response types. Thus, the paradox of enrichment (Rosenzweig; 1971) generally holds for each predatory response when both top down and bottom up forces are acting.

Some topologies, in which predators are governed by a type III predatory response, provide exceptions to the paradox of enrichment when steady states switch from unstable to stable as the system is enriched. They often have stability profiles that look like "tongues" or "cantilevers". They have a relatively small set of stable steady states, but nonetheless, these profiles belong to a considerable number of networks.

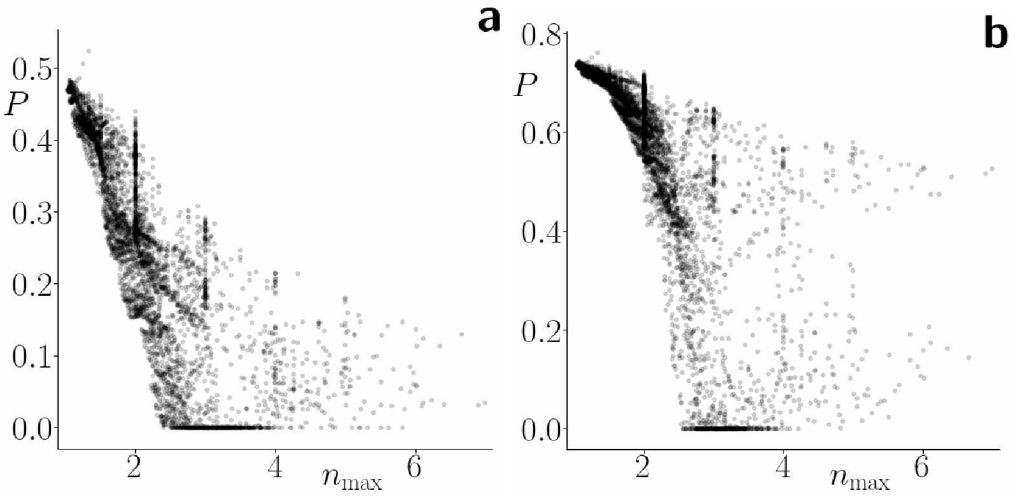

Figure 2.19: Proportion of stable equilibria (P) versus maximum niche value (n_{max}) for a Holling's type II (a) and III (b) predatory response. All networks from Fig. 2.11 with a ratio of intermediate predators to top predators, $0 \leq I/U < 6$, are used. Basal species in this paper are defined to have a niche value of zero, not one. Each point has an opacity of 0.2.

The degree of omnivory plays a large role in governing web stability at steady state. Adding omnivory to short food chains with three or four species has a stabilizing effect. For longer food chains, increasing omnivory is destabilizing. For intermediate values of predators' prey body-size upper limit, increasing omnivory is destabilizing at first and then restabilizing. As predators' prey body-size lower limit increases, the degree of omnivory increases, which in turn decreases the average niche value. Lower average niche values usually have a stabilizing effect on steady states. Figure 2.19 exhibits a sharp increase in the proportion of stable steady states as the maximum niche value drops below a certain value (2.75). This increase is more pronounced for a Holling's type III predatory response.

Other papers have used generalized modeling to investigate ecosystem complexity. They have found that increasing structural complexity, with either network size or connectance (Landi et al.; 2018), decreases stability (Gross et al.; 2009). However, increasing complexity is stabilizing in prey limited systems when body-mass and intraspecific competition are incorporated (Plitzko et al.; 2012). We find that size and connectance cannot solely be used to determine stability, which is particularly obvious when a broader range of generalized parameters is considered that includes Holling's type III predatory responses. A strong indicator for stability turns out to be the ratio of intermediate predators to top predators. Increasing this ratio decreases the height of the web or maximum niche value and keeping this ratio constant results in a similar dependence of stability diagrams on omnivory.

2.11 References

Abrams, P. A. and Walters, C. J. (1996). Invulnerable prey and the paradox of enrichment, *Ecology* **77**(4): 1125.

Allesina, S., Grilli, J., Barabás, G., Tang, S., Aljadeff, J. and Maritan, A. (2015). Predicting the stability of large structured food webs, *Nat. Commun.* **6**: 7842.

Briand, F. and Cohen, J. E. (1984). Community food webs have scale-invariant structure, *Nature* **307**(5948): 264.

Brinck, K. (2014). *Information entropy and ecological energetics: Predicting and analysing structure and energy flow in ecological networks applying the concept of MaxEnt*, Master's thesis, Umeå University.

Christensen, V. and Pauly, D. (1992). Ecopath II—a software for balancing steady-state ecosystem models and calculating network characteristics, *Ecol. Model.* **61**(3-4): 169.

Dawes, J. and Souza, M. (2013). A derivation of Holling's type I, II and III functional responses in predator–prey systems, *J. Theor. Biol.* **327**: 11.

Drossel, B. and McKane, A. J. (2003). Modelling food webs, *Handbook of graphs and networks: From the genome to the internet*, Wiley-VCH Verlag GmbH & Co. KGaA, Weinheim, p. 218.

Edwards, A. M. and Bees, M. A. (2001). Generic dynamics of a simple plankton population model with a non-integer exponent of closure, *Chaos Solitons Fractals* **12**(2): 289.

Elton, C. S. (1958). *The ecology of invasions by plants and animals*, Methuen.

Fagan, W. F. (1997). Omnivory as a stabilizing feature of natural communities, *Am. Nat.* **150**(5): 554.

Fussmann, G. F. and Heber, G. (2002). Food web complexity and chaotic population dynamics, *Ecol. Lett.* **5**(3): 394.

Gellner, G. and McCann, K. (2011). Reconciling the omnivory-stability debate, *Am. Nat.* **179**(1): 22.

Genkai-Kato, M. and Yamamura, N. (1999). Unpalatable prey resolves the paradox of enrichment, *P. Roy. Soc. B-Biol. Sci.* **266**(1425): 1215.

Groß, T. (2004). *Population dynamics: General results from local analysis*, PhD thesis, Universität Oldenburg.

Gross, T., Ebenhöh, W. and Feudel, U. (2004). Enrichment and foodchain stability: The impact of different forms of predator–prey interaction, *J. Theor. Biol.* **227**(3): 349.

Gross, T. and Feudel, U. (2004). Analytical search for bifurcation surfaces in parameter space, *Physica D* **195**(3-4): 292.

Gross, T. and Feudel, U. (2006). Generalized models as a universal approach to the analysis of nonlinear dynamical systems, *Phys. Rev. E* **73**(1): 016205.

Gross, T., Rudolf, L., Levin, S. A. and Dieckmann, U. (2009). Generalized models reveal stabilizing factors in food webs, *Science* **325**(5941): 747.

Holyoak, M. and Sachdev, S. (1998). Omnivory and the stability of simple food webs, *Oecologia* **117**(3): 413.

Jansen, V. A. (1995). Regulation of predator-prey systems through spatial interactions: A possible solution to the paradox of enrichment, *Oikos* **74**(3): 384.

Kuehn, C., Siegmund, S. and Gross, T. (2013). Dynamical analysis of evolution equations in generalized models, *IMA J. Appl. Math.* **78**(5): 1051.

Lan, Y. and Li, Q.-G. (2008). Control of Hopf bifurcation in a simple plankton population model with a non-integer exponent of closure, *Appl. Math. Comput.* **200**(1): 220.

Landi, P., Minoarivelo, H. O., Brännström, Å., Hui, C. and Dieckmann, U. (2018). Complexity and stability of ecological networks: A review of the theory, *Popul. Ecol.* **60**(4): 319.

Law, R. and Blackford, J. C. (1992). Self-assembling food webs: A global viewpoint of coexistence of species in Lotka-Volterra communities, *Ecology* **73**(2): 567.

May, R. M. (1972). Will a large complex system be stable?, *Nature* **238**(5364): 413.

McCann, K. and Hastings, A. (1997). Re–evaluating the omnivory–stability relationship in food webs, *P. Roy. Soc. B-Biol. Sci.* **264**(1385): 1249.

Mougi, A. and Nishimura, K. (2007). A resolution of the paradox of enrichment, *J. Theor. Biol.* **248**(1): 194.

Namba, T., Tanabe, K. and Maeda, N. (2008). Omnivory and stability of food webs, *Ecol. Complex.* **5**(2): 73.

Newman, M. (2018). *Networks*, Oxford University Press.

Niquil, N., Saint-Béat, B., Johnson, G., Soetaert, K., Van Oevelen, D., Bacher, C. and Vézina, A. (2011). Inverse modeling in modern ecology and application to coastal ecosystems, *T. Estuar. Coast. Sci.* p. 115.

Pascual, M. and Dunne, J. A. (2006). From small to large ecological networks in a dynamic world, *Ecological networks: Linking structure to dynamics in food webs*, Oxford University Press, p. 3.

Pauly, D., Christensen, V. and Walters, C. (2000). Ecopath, Ecosim, and Ecospace as tools for evaluating ecosystem impact of fisheries, *ICES J. Mar. Sci.* **57**(3): 697.

Pimm, S. L. (1984). The complexity and stability of ecosystems, *Nature* **307**(5949): 321.

Plitzko, S. J., Drossel, B. and Guill, C. (2012). Complexity–stability relations in generalized food-web models with realistic parameters, *J. Theor. Biol.* **306**: 7.

Polis, G. A. (1998). Ecology: Stability is woven by complex webs, *Nature* **395**(6704): 744.

Rohr, R. P., Scherer, H., Kehrli, P., Mazza, C. and Bersier, L.-F. (2010). Modeling food webs: Exploring unexplained structure using latent traits, *Am. Nat.* **176**(2): 170.

Rosenzweig, M. L. (1971). Paradox of enrichment: Destabilization of exploitation ecosystems in ecological time, *Science* **171**(3969): 385.

Roy, S. and Chattopadhyay, J. (2007). The stability of ecosystems: A brief overview of the paradox of enrichment, *J. Biosci.* **32**(2): 421.

Stouffer, D. B. and Bascompte, J. (2010). Understanding food-web persistence from local to global scales, *Ecol. Lett.* **13**(2): 154.

Strogatz, S. H. (2018). *Nonlinear dynamics and chaos: With applications to physics, biology, chemistry, and engineering*, CRC Press.

Stukel, M. R., Landry, M. R., Ohman, M. D., Goericke, R., Samo, T. and Benitez-Nelson, C. R. (2012). Do inverse ecosystem models accurately reconstruct plankton trophic flows? Comparing two solution methods using field data from the California Current, *J. Marine Syst.* **91**(1): 20.

Vandermeer, J. (2006). Omnivory and the stability of food webs, *J. Theor. Biol.* **238**(3): 497.

Williams, R. J. and Martinez, N. D. (2000). Simple rules yield complex food webs, *Nature* **404**(6774): 180.

Williams, R. J. and Martinez, N. D. (2004). Limits to trophic levels and omnivory in complex food webs: Theory and data, *Am. Nat.* **163**(3): 458.

Winemiller, K. O. and Polis, G. A. (1996). Food webs: What can they tell us about the world?, *Food Webs*, Springer, p. 1.

Woodward, G., Ebenman, B., Emmerson, M., Montoya, J. M., Olesen, J. M., Valido, A. and Warren, P. H. (2005). Body-size determinants of the structure and dynamics of ecological networks, *Dynamic food webs : Multispecies assemblages, ecosystem development and environmental change*, Academic Press, p. 179.

Yeakel, J. D., Pires, M. M., Rudolf, L., Dominy, N. J., Koch, P. L., Guimarães, P. R. and Gross, T. (2014). Collapse of an ecological network in Ancient Egypt, *PNAS* **111**(40): 14472.

Chapter 3 Combining Generalized Modeling and Specific Modeling in the Analysis of Ecological Networks

3.1 Abstract

The complexity of real food webs involves uncertainty in data and in underlying ecological processes, and modeling approaches deal with these challenges differently. Generalized modeling provides a linear stability analysis without narrow specification of all processes, and conventional dynamical systems models approximate functional forms to discuss trajectories in phase space. This study compares results and ecological interpretations from both methods in four-species ecological networks at steady state. We find that a specific (dynamical systems) model only provides a subset of the stability data from the generalized model, which spans many plausible dynamic scenarios, allowing for conflicting results. Nevertheless, both approaches reveal that fixed points become stable when nutrient flows to predators are fettered and even more when the basal growth rate approaches a maximum. The specific model identifies a distinct ecosystem response to bottom-up forcing, the enrichment of lower trophic levels. Enrichment stabilizes a fixed point when basal species are in a resource-deprived environment but destabilizes it if resources become more abundant. The generalized model provides less specific information since the infinitely many paths of enrichment are hypothetical. Nevertheless, generalized modeling of ecological systems is a powerful technique that enables a meta analysis of these uncertain complex systems.

3.2 Abstract Extension

Food webs describe biomass flow in an ecological system that is based on biological growth and loss processes like predator-prey interactions, primary production, or natural mortality. Complete empirical descriptions of the processes and parameters controlling biomass flows are unknown and mathematical models require abstraction and approximation. Factors that control stability of real and model food webs are not fully understood. Generalized modeling presents a powerful mathematical framework to analyze network stability without the need for detailed assumptions about processes and initial conditions. Only the structure of the governing equations is presumed to explore the stability of steady states for infinitely many biologically plausible behaviors. Results and ecological interpretations from generalized modeling are compared to those from a deterministic dynamical system of coupled ordinary differential equations (specific model), where detailed functional forms need to be

assumed. One result shows that enrichment through the increase of carrying capacity can stabilize a system when basal species are in a resource-deprived environment but destabilizes a system if resources become more abundant.

3.3 Introduction

The complexity of real systems, like the climate system or ecological systems, provides challenges in data acquisition and modeling. Precision in data is affected, among others, by the resolution of time/spatial scales and limited access to the (sometimes huge number of) system players. The need to abstract and approximate in modeling is evident. Hierarchical modeling is necessary to gain insight into complex processes on different scales and from different dynamical aspects. Food web models describe biomass flow into and within a network of species, accounting for biological processes such as predator-prey interactions, primary production, parasitism, natural mortality, and respiration (Drossel and McKane; 2003; Stouffer and Bascompte; 2010; Fussmann and Heber; 2002). But, ecological systems like food webs (Winemiller and Polis; 1996; Newman; 2018) are so big and dispersed that empirical observation of population sizes, rates of processes, and interaction characteristics induce an uncertainty in the data.

Progress can be made without precision in data and by avoiding narrow specification of all processes if generalized modeling approaches (Gross and Feudel; 2004; Gross et al.; 2005; Stiefs et al.; 2008; Gross et al.; 2009; Gross and Feudel; 2009; Kuehn et al.; 2013; Kuehn and Gross; 2013; Lade and Niiranen; 2017; Plitzko et al.; 2012; Stiefs et al.; 2009; Stiefs; 2009; Yeakel et al.; 2011, 2014; Awender et al.; 2021) or random matrix models (May; 1972; Allesina and Tang; 2012) are used. Generalized models explore system dynamics across all biologically plausible behavior and are efficient enough to handle large network sizes; one study uses over a hundred million different network topologies (Gross et al.; 2009). Generalized modeling only presumes the structure of the governing equations, grouping processes into unspecified gain and loss terms that represent biomass flows into and within the network. The approach does not presume information about population sizes, initial conditions, or detailed functional forms for biomass flows, yet it can compute local stability of steady states and extract (higher co-dimension) bifurcation information that is based on steady states. Although the steady states per se are unknown, the dynamics can still be formally linearized around them after a normalizing coordinate transformation. This yields a parameterization of the model in the Jacobian matrices. Whether a fixed point is stable or not depends on these generalized parameters and the network properties. Previous generalized modeling studies have explored how stability is affected by various attributes, including en-

richment, omnivory, specialization, predator-prey number ratios, niche-value distribution, and complexity in terms of network size, connectance, and link-strength variability (Gross et al.; 2009; Plitzko et al.; 2012; Awender et al.; 2021).

Specific food web models typically describe biomass flow throughout the network by a set of ordinary differential equations (Drossel and McKane; 2003; Stouffer and Bascompte; 2010; Fussmann and Heber; 2002) and require the explicit reconstruction of a mathematical expression for each of the interactions or processes. Modelers vary initial conditions, parameters or functional forms of these governing equations to explore trajectories, the stability of steady states, and ecosystem persistence in terms of periodic and chaotic attractors. When trajectories exhibit large biomass fluctuations, they can orbit into dangerously low population levels to make the species susceptible to stochastic extinctions; at small populations, a tiny perturbation can induce the extinction of species. Such complex behaviors as well as coexistence of fixed points and attractors can be assessed in a specific model in contrast to generalized modeling.

A perennial issue in real and modeled food webs is understanding the implications of bottom-up forcing, the enrichment of lower trophic levels, on ecosystem functioning. First gaining traction after a study by Rosenzweig (1971) that shows increasing the limiting nutrient in order to increase the yield of an exploitable species - somewhat counterintuitively - destabilizes simple predator-prey models. Upon enrichment, a Hopf bifurcation changes the dynamics from stable steady state to oscillatory. Further enrichment increases the amplitude of the oscillations until species extinction occurs. Since then, the "paradox of enrichment" is widely studied (Gross et al.; 2004; Mougi and Nishimura; 2007; Jansen; 1995; Genkai-Kato and Yamamura; 1999; Abrams and Walters; 1996; Yeakel et al.; 2014). One review article supports the particularly relevant inference that destabilization is suppressed by inhibition of predatory growth (Roy and Chattopadhyay; 2007). Destabilization by enrichment has generally been predicted in mathematical models, but rarely been observed in real systems. This might be because the complexity of real biological processes is not fully captured in mathematical models or empirical observations cover only parts of the dynamical complexity theoretically possible.

This paper compares local food web stability derived from generalized modeling and specific modeling to assess implications on ecological interpretations. Section 3.4 introduces generalized and specific ecological network models that are analyzed in Sec. 3.5 for four-species food webs with varying topologies, feeding constraints and basal production processes. The stability of steady states is discussed for equal feeding nonlinearities across trophic levels (Sec. 3.6), a common assumption in generalized models, and for differing basal production terms (Sec. 3.7). The abundance of resources is shown to determine whether enrichment

stabilizes or destabilizes (Sec. 3.8), offering exceptions to the paradox of enrichment. The stabilizing effect of adding an omnivorous link to a food chain is discussed in Sec. 3.9. Coexistence of fixed points is explored in Sec. 3.10. The impact of differing production forms on the distribution of feeding nonlinearities is explored in Sec. 3.11, and the weighting of links in steady states is presented in Sec. 3.12. Section 3.13 summarizes the main outcomes of the paper.

3.4 Model

The state of an ecological network with N species is $\boldsymbol{x} \in \mathbb{R}^N$, with x_i representing the biomass of species i and $x_i \geq 0$. The state evolves (Gross et al.; 2009; Awender et al.; 2021) by a growth rate from production $\mathscr{S}$ and predation $\mathscr{F}$, and a loss rate from predation $\mathscr{L}$ and other mortality $\mathscr{M}$,

$$\dot{x}_i(t) = \mathscr{S}_i(x_i) + \ \eta_i \mathscr{F}_i(T_i, x_i) \ - \ \mathscr{M}_i(x_i) \ - \ \sum_j \mathscr{L}_{ij}(\boldsymbol{x}). \tag{3.1}$$

η_i is an assimilation coefficient. The total predatory resource T_i available to species i is given by

$$T_i(\boldsymbol{x}) = \sum_k C_{ik}(x_k), \tag{3.2}$$

where C_{ik} is the contribution from x_k to the diet of x_i. The predatory loss $\mathscr{L}_{ij}$ of prey i from predator j is proportional to the predatory growth of the predator $\mathscr{F}_j$ and the fraction with which prey i contributes to the resources of predator j,

$$\mathscr{L}_{ij}(\boldsymbol{x}) = \Lambda_{ij} \frac{C_{ji}(x_i)}{T_j(\boldsymbol{x})} \mathscr{F}_j(T_j, x_j). \tag{3.3}$$

Λ_{ij} is a constant. Only a fraction of the killed biomass from prey, x_i, is incorporated into the predator biomass, x_j.

3.4.1 Generalized Model

Generalized modeling (Gross et al.; 2009) does not restrict the processes $\mathscr{S}$, $\mathscr{F}$, $\mathscr{M}$, and $\mathscr{L}$ in Eq. (3.1) to specific mathematical expressions. Normalizing the state vector to an unknown, nontrivial fixed point $\boldsymbol{x}^*$, and each unknown process of the form $\mathscr{G}$ to its value at

the fixed point $\mathscr{G}^* \equiv \mathscr{G}(\boldsymbol{x}^*)$, gives following rescaled variables and functions,

$$\chi_i = \frac{x_i}{x_i^*}, \qquad t_i = \frac{T_i}{T_i^*} = \sum_k \gamma_{ik} c_{ik}(\chi_k), \qquad g(\boldsymbol{\chi}) = \frac{\mathscr{G}(\mathbb{X}^* \boldsymbol{\chi})}{\mathscr{G}^*}, \tag{3.4}$$

where $\gamma_{ij} = C_{ij}^*/T_i^*$ and $\mathbb{X}^*$ is a diagonal matrix, $\mathbb{X}_{ij}^* = \boldsymbol{x}_i^* \delta_{ij}$. This normalization maps the unknown fixed point $\boldsymbol{x}^*$ to a known fixed point $\boldsymbol{\chi}^* = (1, 1, \ldots, 1)$, and the unknown process to a known process value at the fixed point, $g(\boldsymbol{\chi}^*) = 1$ in the rescaled system,

$$\begin{aligned} \dot{\chi}_i = \alpha_i \Bigg(& \sigma_i s_i(\chi_i) + \phi_i f_i(t_i, \chi_i) - \mu_i m_i(\chi_i) \\ & - \lambda_i \sum_j \beta_{ij} \frac{c_{ji}(\chi_i)}{\sum_k \gamma_{jk} c_{jk}(\chi_k)} f_j(t_j, \chi_j) \Bigg). \end{aligned} \tag{3.5}$$

The time scale parameter (turnover rate) α_i is determined from the steady state, where the total influx (growth) is equal to the total outflux (loss),

$$\alpha_i = \frac{\mathscr{S}_i^* + \eta_i \mathscr{F}_i^*}{x_i^*} = \frac{\mathscr{M}_i^* + \sum_j \mathscr{L}_{ij}^*}{x_i^*}. \tag{3.6}$$

The scale parameters that describe the weighting of the flows of the network at the steady state are

$$\begin{gathered} \sigma_i = \frac{\mathscr{S}_i^*}{\alpha_i x_i^*}, \qquad \phi_i = \frac{\eta_i \mathscr{F}_i^*}{\alpha_i x_i^*}, \qquad \mu_i = \frac{\mathscr{M}_i^*}{\alpha_i x_i^*}, \qquad \lambda_i = \frac{\sum_j \mathscr{L}_{ij}^*}{\alpha_i x_i^*} \\ \beta_{ij} = \frac{\mathscr{L}_{ij}^*}{\sum_k \mathscr{L}_{ik}^*}, \qquad \gamma_{ij} = \frac{C_{ij}^*}{T_i^*}. \end{gathered} \tag{3.7}$$

The local dynamics near the fixed point is governed by the Jacobian matrix $\mathbb{J}^*$ evaluated at the fixed point. The diagonal elements are

$$\begin{aligned} J_{ii}|_* = \alpha_i \Big[& \sigma_i s_i^{(\chi_i)} + \phi_i (f_i^{(t_i)} \gamma_{ii} c_{ii}^{(\chi_i)} + f_i^{(\chi_i)}) - \mu_i m_i^{(\chi_i)} \\ & - \lambda_i \beta_{ii} f_i^{(\chi_i)} - \lambda_i \sum_k \beta_{ik} c_{ki}^{(\chi_i)} (1 + \gamma_{ki} (f_k^{(t_k)} - 1)) \Big], \end{aligned} \tag{3.8}$$

and the off-diagonal elements are

$$J_{ij}|_* = \alpha_i \Bigg[\phi_i f_i^{(t_i)} \gamma_{ij} c_{ij}^{(\chi_j)} - \lambda_i \beta_{ij} f_j^{(\chi_j)} - \lambda_i \sum_k \beta_{ik} c_{kj}^{(\chi_j)} \gamma_{kj} (f_k^{(t_k)} - 1) \Bigg]. \tag{3.9}$$

The exponent parameters of the form $g^{(\xi)}$ in the Jacobian are defined as

$$g^{(\xi)} \equiv \left. \frac{\partial g(\boldsymbol{\chi})}{\partial \xi} \right|_{\boldsymbol{\chi}=\boldsymbol{\chi}^*}, \tag{3.10}$$

with $\xi \in \{\chi_i, t_i\}$. They describe the nonlinearity of process $\mathscr{G}(\boldsymbol{x})$ in Eq. (3.1) with respect to ξ. What is remnant of the unspecified functions $\mathscr{S}, \mathscr{M}, \mathscr{F}, or \mathscr{L}$ in the Jacobian is their nonlinearity parameters $s_i^{(\chi_i)}$, $m_i^{(\chi_i)}$, $f_i^{(\chi_i)}$, and $f_i^{(t_i)}$. In generalized modeling, these nonlinearity parameters are varied in a range of values to represent many different specific functions simultaneously.

3.4.2 Specific Models

To construct a specific model, a functional form for each process in Eq. (3.1) must be specified. The production term $\mathscr{S}$ is a growth term that allows matter to enter the system. It is linear near population sizes of zero, and it peaks when the population is big enough for intraspecific competition for limited resources to dominate. Five different functional forms are chosen [Fig. 3.1(a)]:

$$\mathscr{S}_i(x_i) = D_i x_i \begin{cases} (K - x_i) & \text{logistic equation} & \text{(3.11a)} \\ (e^{R(K-x_i)} - 1) & \text{exponential eq.} & \text{(3.11b)} \\ (\dfrac{2K^b}{K^b + x_i^b} - 1) & \text{Bellow's eq.} & \text{(3.11c)} \\ e^{R(K-x_i)} & \text{exponential map} & \text{(3.11d)} \\ 1/(K^b + x_i^b) & \text{Bellow's map,} & \text{(3.11e)} \end{cases}$$

with rate constant D_i and constants b and R. All five production functions retain the same basic shape [Fig. 3.1(a)] featured by a root at zero population, a maximum productivity at an intermediate population size, and a monotonic decrease for the remainder of the domain. They differ, as a carrying capacity K is defined for the logistic, exponential, and Bellow's equations, while the carrying capacity is undefined (is at infinity) for the exponential map (Cook; 1965; Sinha and Sinha; 2005) and Bellow's map (Bellows; 1981). The production

forms [Eqs. (3.11d, e)] are included to test a larger range of functional forms, although they are typically used in discrete time population models. The exponential equation is derived from the exponential map in the continuous limit, and Bellow's equation is inspired from Bellow's map.

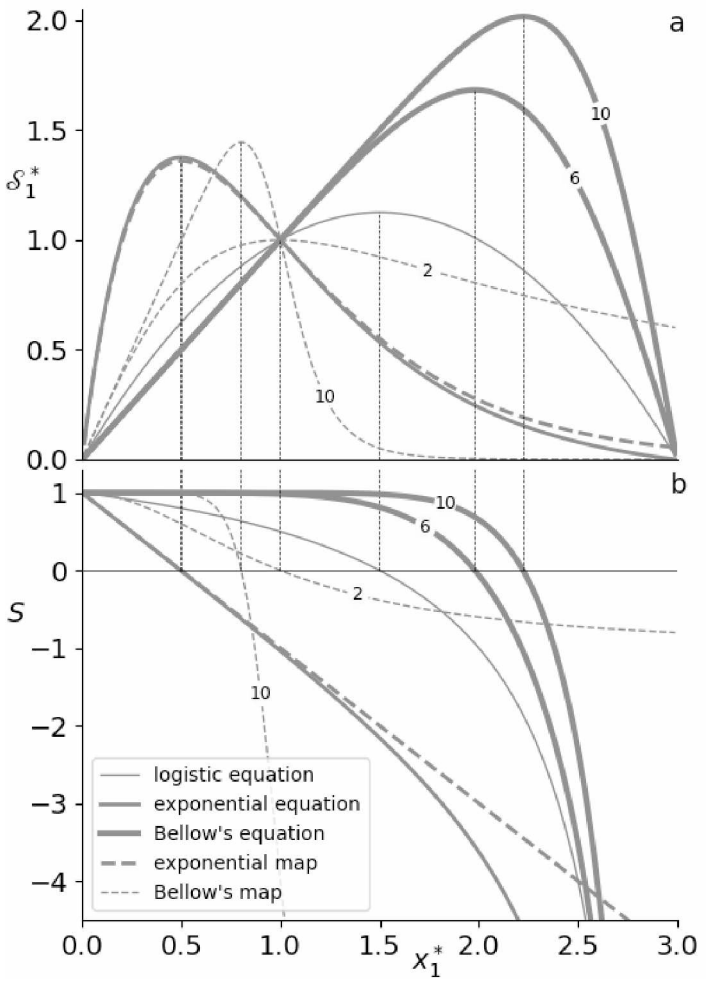

Figure 3.1: Basal production growth [$\mathscr{S}_1^*$, Eq. (3.11), upper panel] and nonlinearity of production [S, Eq. (3.23), bottom panel] as a function of basal population at the fixed point (x_1^*). Maximal growth corresponds to a nonlinearity of zero (vertical dashed lines). The parameters are $K = 3$, $D = 1/(K-1)$ (logistic equation); $K = 3$, $R = 2$, $D = [\exp(R(K-1))-1]^{-1}$ (exponential equation); $K = 3$, $b =$ (6 and 10), $D = (K^b+1)/(K^b-1)$ (Bellow's equation); $K = 1$, $R = 2$, $D = \exp(-R(K-1))$ (exponential map); and $K = 1$, $b =$ (2 and 10), $D = K^b + 1$ (Bellow's map). The choice of D ensures that $\mathscr{S}_1(1) = 1$.

Predatory growth rate is modeled in the form of Holling's type II functional response,

$$\mathscr{F}_i(T_i, x_i) = \frac{A_i T_i x_i}{H_i + T_i}. \tag{3.12}$$

A_i is the reciprocal of the handling time. H_i is the half saturation constant (Mulder and Hendriks; 2014), which describes the prey population size for which the per capita predatory growth is half its maximum. T_i represents the total resources available to predator i, $T_i = \sum_k a_{ik} x_k$ with $\sum_k a_{ik} = 1$. Holling's type II predatory growth is linear at low prey abundance and smoothly saturates as prey abundance increases. It describes predators that experience limitations of growth from handling time (e.g. for killing, eating, digesting) when prey are abundant and no additional limitations when prey are scarce.

Natural mortality and respiration describe the matter that leaves x_i due to processes other than predation, taken to be a simple power law,

$$\mathscr{M}_i(x_i) = \Omega_i x_i^p, \tag{3.13}$$

with constants Ω_i and p. No detritivores are modeled hence resources leaving x_i from mortality also leave the system.

Predatory loss of prey i depends on the predatory growth $\mathscr{F}_j$ of predator j [Eq. (3.3)],

$$\mathscr{L}_{ij}(\boldsymbol{x}) = \eta_i \frac{C_{ji}(x_i)}{T_j(\boldsymbol{x})} \mathscr{F}_j(T_j, x_j), \tag{3.14}$$

with $\Lambda_{ij} = \eta_i = r^{i-1}$ assuming a hierarchy of relative time scales, and $r \in [0, 1]$ the base of the assimilation coefficient (Groß; 2004). If a predator j attacks prey i with a niche or trophic level difference of $j - i$, then r^{j-i} is the proportion of killed biomass from prey x_i that remains in the network locked in x_j.

3.5 Four-species food web and analysis

A four-species food web, consisting of top and intermediate predators and a basal species, is built with gradient control between a food chain and an omnivorous web by adding a link of intraguild predation (Fig. 3.2). More generally, such species can be interpreted as trophospecies that combine species with similar ecological function into one unit to represent larger and more complex networks. Although there are reports of long chain lengths in observed webs (Lafferty et al.; 2006), chain lengths above four are considered uncommon from aggregated data of over hundred real food webs (Cohen et al.; 1986; Pimm et al.; 1991). Intraguild predation with a chain length of three has been explored using generalized models (Yeakel et al.; 2011).

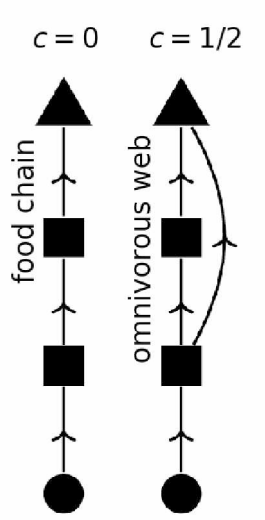

Figure 3.2: Four-species food web topologies with top predator (triangle), intermediate predators (square), and basal species (circle). The link-strength c is used to switch between a food chain and an omnivorous web. This study considers $c = 0$ and $c = 1/2$.

3.5.1 Specific Model and Steady States

The four-species network model, consistent with the topologies in Fig. 3.2, is derived from the specific model in Sec. 3.4.2. For these topologies, the prey available to the top predator (biomass x_4) is $T_4 = cx_2 + (1-c)x_3$, while the intermediate predators only feed on one prey species, $T_i = x_{i-1}$ for $i = 2, 3$. $c \in [0, 1)$ controls the proportionate link strength of x_4 with x_2 and x_3. This study considers $c = 0$ and $c = 1/2$. At $c = 0$, the system describes a food chain. At $c = 1/2$, species 4 is a balanced omnivore that feeds on x_2 and x_3 with same preference. It is assumed that only basal species show growth from production, $D_i = D\delta_{1i}$ [Eq. (3.11)], and only top predators show loss from mortality, $\Omega_i = \Omega\delta_{4i}$ [Eq. (3.13)]. After setting the half-saturation constants equal for each species, $H_i = H$, and the rate constants D_i, A_i, and Ω_i to

$$\begin{pmatrix} \boldsymbol{D}^\intercal \\ \boldsymbol{A}^\intercal \\ \boldsymbol{\Omega}^\intercal \end{pmatrix} = \begin{pmatrix} D & 0 & 0 & 0 \\ 0 & A & A(1-c) & A \\ 0 & 0 & 0 & r^3 \end{pmatrix},$$

equations (3.1) and (3.11-3.14) result in following equations of motion,

$$\dot{x}_1 = \mathscr{S}_1(x_1) - A\frac{x_1 x_2}{H + x_1}, \tag{3.15}$$

$$\dot{x}_2 = rA\left(\frac{x_1 x_2}{H + x_1} - (1-c)\frac{x_2 x_3}{H + x_2} - c\frac{x_2 x_4}{H + T_4}\right), \tag{3.16}$$

$$\dot{x}_3 = r^2 A\left((1-c)\frac{x_2 x_3}{H + x_2} - (1-c)\frac{x_3 x_4}{H + T_4}\right), \tag{3.17}$$

$$\dot{x}_4 = r^3 A\left(\frac{T_4 x_4}{H + T_4} - \frac{x_4^p}{A}\right), \tag{3.18}$$

with $\mathscr{S}_1(1) = 1$ [Eq. (3.11), Fig. 3.1] and $T_4 = cx_2 + (1-c)x_3$.

The nontrivial fixed points ($x_i^* \neq 0$) of the food web can be determined fast and convenient due to the symmetry of Eqs. (3.15) - (3.18), not requiring a convergence algorithm such as Newton's method. Summing up these equations at the steady state, gives

$$x_4^* = \mathscr{S}_1^{*1/p}, \tag{3.19}$$

and Eq. (3.15), Eqs. (3.16) and (3.17), and Eq. (3.18) yield

$$x_2^* = \frac{H + x_1^*}{A x_1^*}\mathscr{S}_1^*, \tag{3.20}$$

$$x_3^* = \frac{(H + x_2^*)x_1^*}{(1-c)(H + x_1^*)} - \frac{c x_2^*}{1-c}, \tag{3.21}$$

$$x_4^* = \left(\frac{A T_4^*}{H + T_4^*}\right)^{\frac{1}{p-1}}, \tag{3.22}$$

respectively. An intersection of the two resulting curves, x_4^* versus x_1^*, determines x_1^* and subsequently all coordinates of the fixed point. Trivial fixed points exist at $\boldsymbol{x}^* = (0,0,0,0)$, $(0, x_2^*, 0, 0)$, $(0, 0, x_3^*, 0)$, and also at $(K, 0, 0, 0)$ and $(K, 0, x_3^*, 0)$ when a carrying capacity is defined. They describe steady states with one or more species extinctions. These fixed points are not stable in the parameter regime under study and are not considered further, since generalized modeling does not define trivial fixed points.

3.5.2 Generalized Parameters

To compare steady states in the specific and the generalized four-species food web model, the generalized parameters are calculated for the specific model. The nonlinearity of production, $S \equiv s_1^{(\chi_1)}$, for the different functional production forms in Eq. (3.11) is determined

from Eq. (3.10),

$$S = \begin{cases} \dfrac{K - 2x_1^*}{K - x_1^*} & \text{logistic equation} \quad (3.23a) \\ \dfrac{(1 - Rx_1^*)e^{R(K-x_1^*)} - 1}{e^{R(K-x_1^*)} - 1} & \text{exponential equation} \quad (3.23b) \\ 1 - \dfrac{2bK^b x_1^{*b}}{K^{2b} - x_1^{*2b}} & \text{Bellow's equation} \quad (3.23c) \\ 1 - Rx_1^* & \text{exponential map} \quad (3.23d) \\ \dfrac{K^b + (1-b)x_1^{*b}}{K^b + x_1^{*b}} & \text{Bellow's map,} \quad (3.23e) \end{cases}$$

and plotted in Fig. 3.1(b). The nonlinearity of production S is one at zero population size and monotonically decreases as population size increases. S becomes infinitely more negative as population size approaches the end of the domain, except for the Bellow's map, where $S \to (1 - b)$ as $x_1^* \to \infty$.

The nonlinearity of predation F_i with respect to prey (nonlinearity of feeding) for Holling's type II predatory response [Eq. (3.12)] is

$$F_i = f_i^{(t_i)} = \frac{H}{H + T_i^*}. \tag{3.24}$$

It depends on the half-saturation constant H and prey abundance T_i^*, and ranges from zero at high prey abundance to one at low prey abundance.

The nonlinearity of predation with respect to the predator itself is $f_i^{(\chi_i)} = 1$. The nonlinearity of mortality $m_i^{(\chi_i)}$ is the exponent p of the mortality term [Eq. (3.13)], and the nonlinearity of the contribution $c_{ik}^{(\chi_k)}$ is one, since T_i is linear in x_k.

To complete the mapping from the specific model to generalized coordinates, the scale parameters are determined from Eqs. (3.6) and (3.7),

$$\begin{pmatrix} \boldsymbol{\alpha}^\intercal \\ \boldsymbol{\sigma}^\intercal \\ \boldsymbol{\phi}^\intercal \\ \boldsymbol{\mu}^\intercal \\ \boldsymbol{\lambda}^\intercal \end{pmatrix} = \begin{pmatrix} \frac{\mathscr{I}_1^*}{x_1^*} & \frac{rAx_1^*}{H+x_1^*} & \frac{r^2(1-c)Ax_2^*}{H+x_2^*} & \frac{r^3AT_4^*}{H+T_4^*} \\ 1 & 0 & 0 & 0 \\ 0 & 1 & 1 & 1 \\ 0 & 0 & 0 & 1 \\ 1 & 1 & 1 & 0 \end{pmatrix},$$

$$\boldsymbol{\beta} = \begin{pmatrix} 0 & 1 & 0 & 0 \\ 0 & 0 & (1-c)\frac{(H+x_1^*)x_3^*}{(H+x_2^*)x_1^*} & c\frac{(H+x_1^*)x_4^*}{(H+T_4^*)x_1^*} \\ 0 & 0 & 0 & 1 \\ 0 & 0 & 0 & 0 \end{pmatrix},$$

$$\boldsymbol{\gamma} = \begin{pmatrix} 0 & 0 & 0 & 0 \\ 1 & 0 & 0 & 0 \\ 0 & 1 & 0 & 0 \\ 0 & \frac{cx_2^*}{T_4^*} & \frac{(1-c)x_3^*}{T_4^*} & 0 \end{pmatrix}.$$

Since $\alpha_i x_i^* = \eta_i \mathscr{F}_i^* = \sum_j \mathscr{L}_{ij}^*$ for intermediate predators [Eq. (3.6)], $\beta_{2j} = C_{j2}^* \mathscr{F}_j^* / (T_j^* \mathscr{F}_2^*)$.

3.5.3 Generalized Versus Specific Model: Parameter Scenarios

This study of the generalized model focuses on varying the nonlinearity of production $S = s_1^{(\chi_1)}$ and the nonlinearity of feeding $F_i = f_i^{(t_i)}$. These parameters show up in the Jacobian matrix and influence the stability of the rescaled fixed point, $\chi^* = (1, 1, 1, 1)$. They are not related to any particular functional form but represent infinitely many functional forms. The parameters of the specific model [Eqs. (3.15) - (3.18)] are chosen such that their range of generalized parameters S and F_i mostly spans the dynamically possible range. The nonlinearity of feeding F_i for Holling's type II ranges from 0 to 1 [Eq. (3.12)], which is achieved in the specific model by varying the half-saturation constant $H \in (0.01, 100)$. The base of the assimilation coefficient is $r = 0.3$ and the exponent of the mortality term is $p = 2$ unless noted otherwise. Two types of feeding scenarios are considered for comparing generalized models with specific models: the nonlinearity of feeding for each predator is equal across trophic levels (type 1), and no such restriction (type 2).

§ Feeding Nonlinearities Equal Across Trophic Levels

Generalized ecological models commonly assume equal feeding nonlinearities ($F_i = F$) (Gross and Feudel; 2006, 2009; Plitzko et al.; 2012; Yeakel et al.; 2014; Awender et al.; 2021). In the specific models, equal feeding nonlinearities [Eq. (3.24)] require equal prey abundance ($T_2^* = T_3^* = T_4^*$) at the fixed point. When the reciprocal of the handling time is set to $A = (H + 1)$, $\boldsymbol{x}^* = (1, 1, 1, 1)$ is a fixed point for all parameters that also fulfills $F_i = F$. Other nontrivial fixed points can coexist that have non-identical feeding nonlinearities.

Table 3.1: Color legend for the stability properties of fixed points in Figs. 3.3 to 3.6, using four base colors for the four types of eigenvalues. Positive (negative) real eigenvalues are represented by a "+" ("-") symbol and contribute a dark red (light red) color to the total color, and complex eigenvalues with a positive (negative) real part are represented by "+j" ("-j") and contribute a dark blue (light blue) color. A fixed point with more stable manifolds is represented with a more faint color.

All nontrivial fixed points of Eqs. (3.15) - (3.18) for a given specific model $(H, \mathscr{I}_1)$, and their corresponding nonlinearities of feeding F_i [Eq. (3.24)] and nonlinearity of production S [Eq. (3.23)] are determined. To output the appropriate range of S for the fixed point (1,1,1,1), the production terms are varied: $K \in [1.3, 101]$ for the logistic equation, $K = 3$ and $R \in [0.01, 3]$ for the exponential equation, $K = 1$ and $R \in [0.01, 3]$ for the exponential map, $K = 3$ and $b \in [0.0001, 20]$ for Bellow's equation, and $K = 1$ and $b \in [0.0001, 20]$ for Bellow's map.

§ Feeding Nonlinearities Not Constrained

When feeding nonlinearities are not forced to be equal, the reciprocal of the handling time A is a free parameter. All nontrivial fixed points of Eqs. (3.15) - (3.18) are numerically determined for a given set of parameters (A, H) and a given production term $\mathscr{I}_1$. Each fixed point corresponds to nonlinearities of feeding F_i [Eq. (3.24)] and a nonlinearity of production S [Eq. (3.23)]. A is varied linearly over the empirically determined interval $A \in [0.001, 2(H + 1)]$ to achieve the desired range of production nonlinearities S. Only production terms from Fig. 3.1 are considered in this scenario.

3.6 Interface of Specific and Generalized Model

Fixed point stability of the specific models is displayed in the generalized modeling parameter space to compare both modeling approaches and resulting interpretations. Type

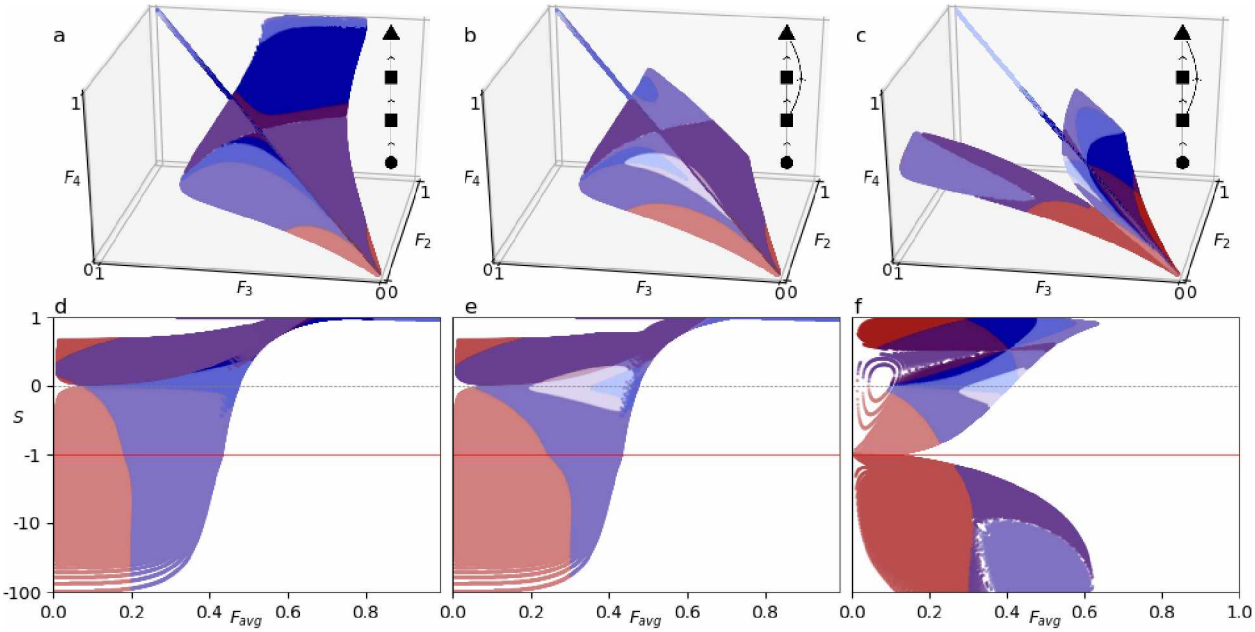

Figure 3.3: Stability of fixed points (color coding in Table 3.1) versus feeding nonlinearities F_i for a type 1 specific model with logistic production (a-c). For each panel, the fixed points off the diagonal are shown in the panel beneath (d-f) positioned by nonlinearity of production (S) and the average nonlinearity of feeding (F_{avg}). The fixed points on the diagonal (panel a, b) are unfolded in Fig. 3.4. The mortality exponent $p \in (1, 2]$ is varied in panel (c) and (f) and $K = 3$. In panels d-f, the vertical axis is scaled linearly above the red line, and logarithmically ($\log_{10}$) below. The horizontal dashed line marks $S = 0$.

1 specific models always have a fixed point, $(1, 1, 1, 1)$, for which all feeding nonlinearities are equal ($F_i = F$) and possibly coexisting, nontrivial fixed points for which the feeding nonlinearities differ across trophic levels. This holds for both topologies, the food chain and the omnivorous web. Fixed point stability is plotted as a function of the three feeding nonlinearities in Fig. 3.3(a) for the food chain and in Fig. 3.3(b) for the omnivorous web in the case of a logistic production of basal species. Much of this feeding nonlinearity space is not accessible to the specific model, while it would be filled for a generalized model with varying feeding nonlinearities. The simulation results don't exhibit stable fixed points that coexist.

Any point off the diagonal represents a coexisting fixed point with unequal feeding nonlinearities F_i. The stability of these coexisting fixed points is delineated in the nonlinearity space of production S and (average) feeding F_{avg}, Figs 3.3(d) and 3.3(e). While there is some overall similarity regarding eigenvalue characteristics, stable coexisting fixed points exist for the omnivorous web and not for the food chain. All of these coexisting fixed points go unexplored in generalized modeling, if the typical assumption (Gross and Feudel; 2006, 2009; Plitzko et al.; 2012; Yeakel et al.; 2014; Awender et al.; 2021) of equal feeding nonlinearities

is made; the corresponding ecological implications are unclear.

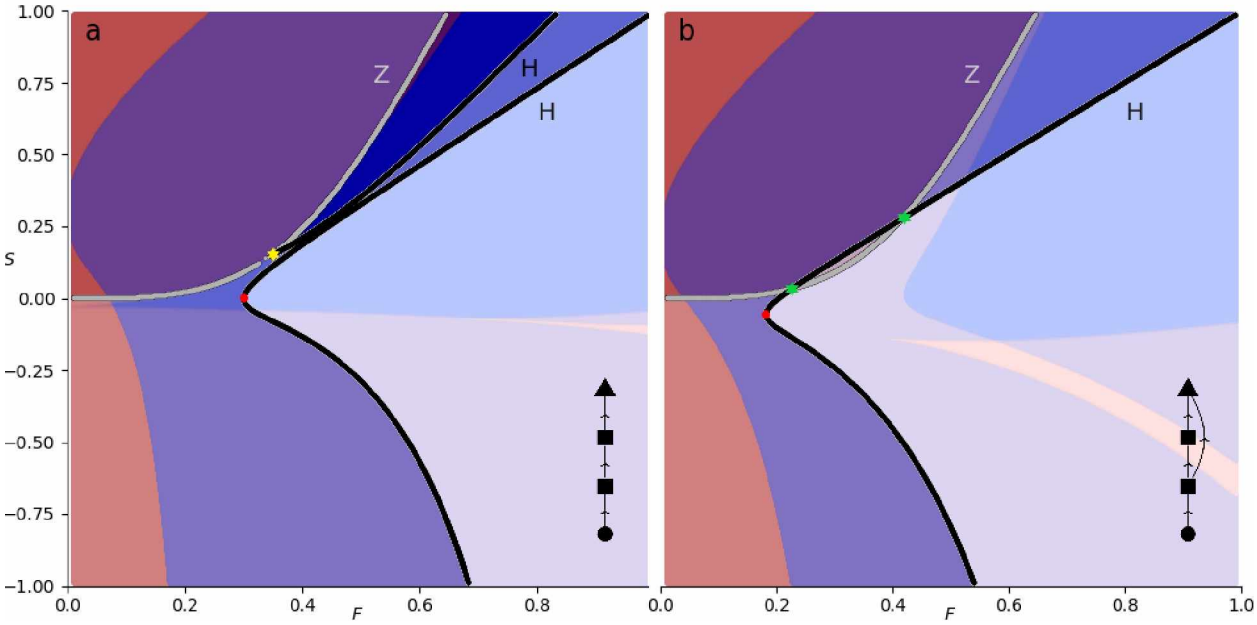

Figure 3.4: Stability of the fixed point (1,1,1,1) as a function of the nonlinearity of production (S) and the nonlinearity of feeding (F) for the food chain (a) and the omnivorous web (b). These data are aligned along the diagonal in Fig. 3.3(a) and 3.3(b), respectively. Hopf bifurcation (H, black) and zero-eigenvalue bifurcation (Z, gray) lines are shown. The higher co-dimension bifurcations include a Takens-Bogdanov bifurcation [(a), yellow star] and two Gavrilov-Guckenheimer bifurcations [(b), green star]. The stable fixed point with the lowest F value (F_{min}) is marked by the red dot. For color coding, see Table 3.1.

Figure 3.4 shows the stability of the fixed point $\mathbf{x}^* = (1, 1, 1, 1)$ in the nonlinearity space of production S and feeding F. This fixed point is characterized by equal feeding nonlinearities and represented by data on the diagonal in Fig. 3.3(a) and 3.3(b), respectively. Stable fixed points exist for larger F values and the boundary separating unstable from stable fixed points shifts to larger F as the absolute value of S increases. The point on the stable/unstable boundary with the smallest F coordinate (red dot in Fig. 3.4) marks the largest range of half-saturation constants H for which the system has a stable fixed point. The omnivorous link increases stability: The stable/unstable boundary shifts to smaller F to increase the percentage of stable fixed points and the number of Hopf-bifurcation lines decreases from two to one. Comparing Fig. 3.4(b) with Fig. 3.3(e) reveals that nonlinearity regimes with stable fixed points correlate well if the (uniform) feeding nonlinearity F is replaced with the average value F_{avg} in the case of unequal feeding nonlinearities across trophic levels. This indicates that ecological implications derived from a reduction of model complexity by assuming equal feeding nonlinearities across trophic levels can be relevant for the more general case.

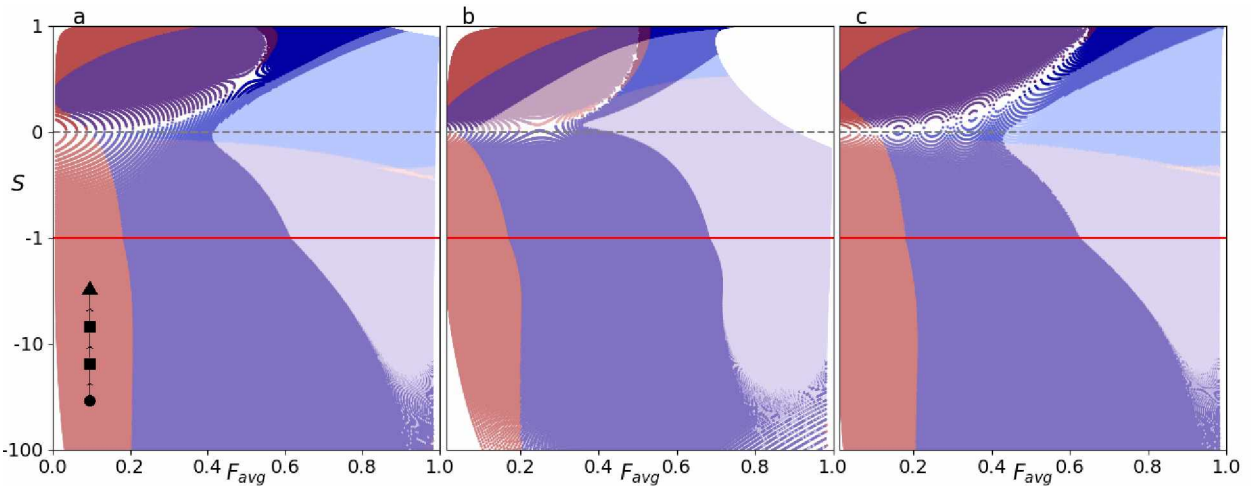

Figure 3.5: Stability of fixed points versus nonlinearity of production S and average nonlinearity of feeding F_{avg} for a type 2 specific food chain model and different production terms: (a) logistic equation, (b) exponential equation, and (c) Bellow's equation, $b = 6$. The vertical axis is scaled linearly above the red line, and logarithmically ($\log_{10}$) below. The horizontal dashed line is at $S = 0$, denoting maximum production rate. For color coding, see Table 3.1.

In Figs. 3.3(c) and 3.3(f) the nonlinearity of production S is varied by keeping the carrying capacity constant and instead varying the mortality exponent p. Varying p means varying the fixed point $\mathbf{x}^*$, which enters S [Eq. (3.23)a] and F_i. The surface in the 3-dimensional F_i space consists of two branches, and stable fixed points exist for equal and unequal feeding nonlinearities across trophic levels. The stable fixed points with unequal feeding nonlinearities coexist with unstable fixed points. Simulations show that these stable fixed points have a small basin of attraction in which all four species stabilize at nonzero biomass values; outside of this basin a three-level food chain persists in stable oscillations.

3.7 Robustness of stability for various basal production

The nontrivial fixed points and the associated nonlinearities of production S and feeding F_i are determined from a range of type 2 specific models. Figure 3.5 shows the stability of fixed points in the food chain model for the three production forms with a defined carrying capacity (logistic, exponential, and Bellow's equation). The stability patterns are qualitatively similar for the three production terms: The stable/unstable boundaries are homologous and the eigenvalue characteristics of the fixed points depends similarly on the nonlinearity parameters S and F_{avg}. For example, along the top boundary of the nonlinearity space (near S=1 in Fig. 3.5), the eigenvalue characteristics follows the sequence, $(+++-) \rightarrow (+j+j+-) \rightarrow (+j+j++) \rightarrow (+j+j+j+j) \rightarrow (+j+j-j-j)$, with increasing F_{avg}. On the other hand, the regime where the bifurcation lines are intersect-

ing is more variable. For the omnivorous web (not shown), the stability patterns are also qualitatively robust when varying the basal production terms.

Stable fixed points appear for larger average feeding nonlinearities, which indicates ecologically that prey populations far from saturation is stabilizing. A larger nonlinearity of feeding results from a smaller prey abundance T_i^* at steady state [Eq. 3.24]. More details in Sec. 3.8.

The similarity of Figs. 3.5 and 3.4(a) supports again that the average feeding nonlinearity parameter F_{avg} plays a similar role for web stability as F in the case of equal feeding nonlinearities across trophic levels, motivating studies of generalized models with equal feeding nonlinearities.

3.8 Enrichment stabilizes and destabilizes

The system is enriched by increasing the amount of limiting nutrients for basal growth, which effectively increases the carrying capacity K. Figure 3.6(a) shows half-saturation contours for the omnivorous web (type 2) with logistic growth [Eq. (3.23)a] in the nonlinearity space of production S and average feeding F_{avg}. Along each contour the carrying capacity K increases in the direction of the arrows, and the system gets enriched. Increasing the carrying capacity predominantly decreases the nonlinearity of production S and the average feeding nonlinearity F_{avg}.

Figures 3.6(b) and 3.6(c) show the steady state basal species population x_1^* and carrying capacity K along these contours. Enriching the system through the increase of carrying capacity K typically increases the exploited species population x_1^* to asymptotically approach $x_1^* = K$ from below. For smaller half-saturation constants, e.g. contour (1) [Fig. 3.6(b)], a coexisting fixed point $x_1^* = 0$ is also asymptotically approached for infinite K. Contours with a smaller half-saturation constant have population sizes x_1^* farther away from K. Stable fixed points arise in a regime of smaller carrying capacity K and smaller basal population size x_1^*.

Five representative contours with qualitatively different changes in stability arise (Fig. 3.6). They describe diverse findings on enrichment and stabilization in the literature (Roy and Chattopadhyay; 2007) in a single model. For the larger half-saturation constants H [contour (5)], a stable fixed point eventually destabilizes via a Hopf bifurcation as the carrying capacity K increases. Lowering H reveals contours along which an unstable fixed point stabilizes and then destabilizes with increasing K [contour (4)]. If H is lowered further, the system exhibits three nontrivial coexisting fixed points for a range of carrying capacities [contours (3) and (2)]. These contours reveal a stable branch where increasing the carrying capacity

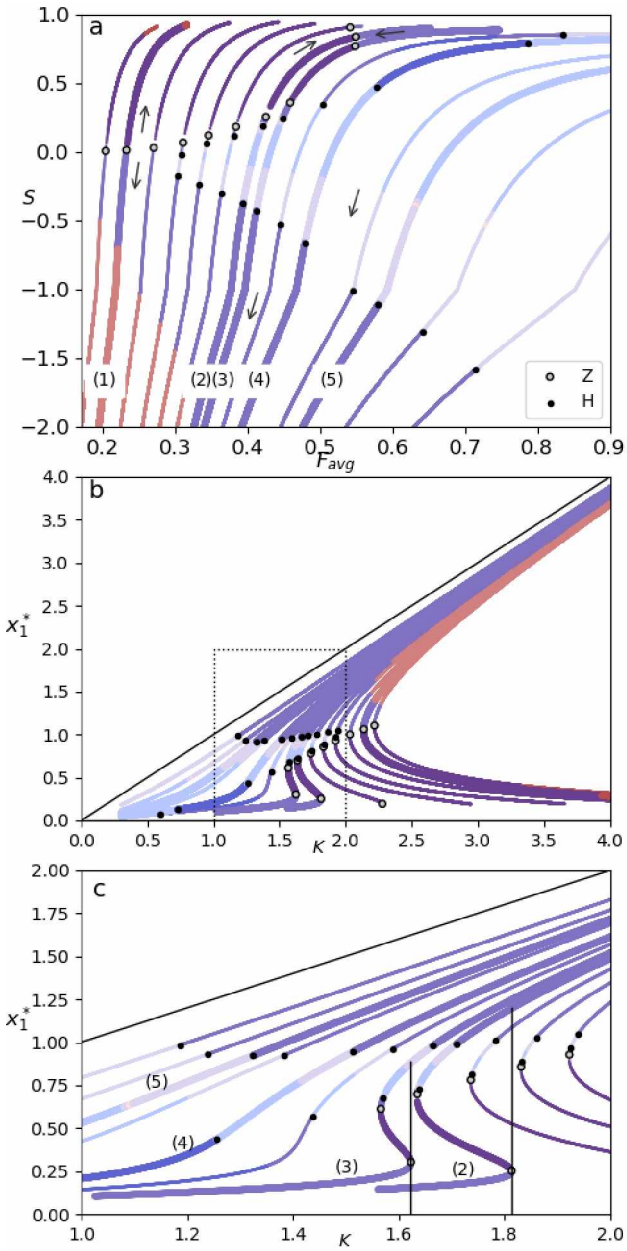

Figure 3.6: Half-saturation contours for steady states of the type 2 omnivorous web with logistic production: a) Contours in the nonlinearity space of production S and average feeding F_{avg} with the carrying capacity K increasing in the direction of the arrows. b) Contours as a function of steady state basal species x_1^* and carrying capacity K, with c) a zoom of b). Representative contours are highlighted in bold and correspond to half-saturation constants $H = 0.25$ (1), $H = 0.449$ (2), $H = 0.476$ (3), $H = 0.585$ (4), and $H = 0.818$ (5). Light colors mark stable equilibria. For color coding, see Table 3.1. Zero eigenvalue bifurcations (Z, open circle) and Hopf bifurcations (H, full circle) are labeled. The two vertical lines mark the saddle node bifurcation for curve (2) and (3), after which only one nontrivial fixed point exists. The diagonal black line in b) and c) shows $x_1^* = K$. Figure a) is analogous to contours for the food chain, Fig. 3.5(a).

first stabilizes a fixed point and then destabilizes it after further enrichment. Simulations of the specific model show that the basin of attraction for the coexisting nontrivial fixed point is small [contour (2) and (3)] and suddenly increases for carrying capacities beyond the saddle node bifurcation, when the stable fixed point is the only nontrivial fixed point of the system [contour (3)]. For small half-saturation constants [contour (1)] the steady states are unstable regardless of carrying capacity.

Destabilizing a fixed point due to enrichment is referred to as the paradox of enrichment (Rosenzweig; 1971; Veilleux; 1979; Gounand et al.; 2014). Previous studies of diverse systems have reported that enrichment either stabilizes or destabilizes a system (Roy and Chattopadhyay; 2007). This omnivorous web [and similarly, the type 2 food chain, Fig. 3.5(a)] exhibits both, behavior that is consistent and that is not consistent with the paradox of enrichment depending on the degree of enrichment. A stable fixed point becomes unstable when the system is relatively enriched and resources are more abundant. An unstable fixed point can be stabilized by increasing the carrying capacity when basal species are in a resource-deprived environment.

While a specific model exhibits a defined path of enrichment, as for example along a contour line, generalized modeling allows for infinitely many hypothetical paths of enrichment that may be consistent or not consistent with the paradox of enrichment. These hypothetical paths might be accessible by a specific model or not. As a consequence, interpretations from the generalized models and specific models might differ.

Increasing the feeding nonlinearity leads to stable fixed points in the generalized models and the specific models, as seen in Figs. 3.4 and 3.5 or from the successive contours in Fig. 3.6(a). For a Holling's type II functional form, the nonlinearity of feeding is controlled by changing the half-saturation constant, which is analogous to controlling the hunting conditions (cost of capturing prey) or nutritional value of prey. If the hunting conditions are hampered (e.g. mobility reduction from more viscous medium (Harrison; 1995)), successful hunting is harder and prey would need to be of higher density to allow predators the same growth. Similarly, if prey are less nutritious (e.g. inedible, unpalatable, invulnerable, defensive prey individuals (Roy and Chattopadhyay; 2007)) a higher prey density would be required. Therefore, impairing hunting conditions or reducing a prey's nutritional value effectively reduces the available prey T_i^* or effectively increases the half-saturation constant. Both of these increase the nonlinearity of feeding F_i, which is stabilizing in the considered specific models.

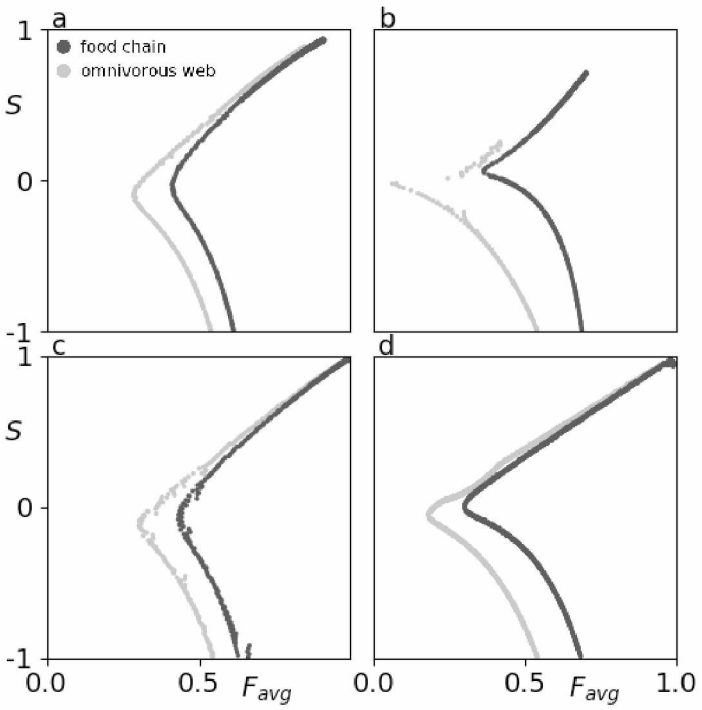

Figure 3.7: Stable/unstable boundary comparison of the food chain (dark grey) to the omnivorous web (grey) for type 2 specific models with (a) logistic, (b) exponential equation, (c) Bellow's equation ($b = 6$) production term and for (d) type 1 specific models (Fig.3.4) for the fixed point (1, 1, 1, 1) and generalized models.

3.9 Adding the omnivorous link stabilizes

Omnivory is predation on multiple trophic levels. Its role in stabilization and destabilization of trophic webs is an ongoing area of research (Vandermeer; 2006; Awender et al.; 2021). Figure 3.7 compares the stable/unstable boundary of food chain and omnivorous web for type 1 and 2 specific models with various basal production terms. Adding the omnivorous link always shifts the stable/unstable boundary toward smaller feeding nonlinearities. This makes the omnivorous webs more stable, since their area of stable fixed points in the nonlinearity space of production and feeding is larger. When feeding nonlinearities are equal across trophic levels, Figure 3.7(d) is identical for all basal production forms in type 1 specific models as well as for generalized models, since the fixed point is at (1,1,1,1) and the production terms cover the same nonlinearity range S, Fig.3.1(b).

The shift of the stable/unstable boundary is quantified by the shift of its vertex in the direction of the feeding nonlinearity. The point on the stable/unstable boundary with the lowest average feeding nonlinearity (F_{min}) is plotted in Fig.3.8 for all boundaries in type 1 and 2 specific models and segregated by topology. The stabilizing effect of the omnivorous link in these specific models and the typical generalized models (F_i equal) is evident. The

average F_{min} decreases by 0.15 when going from food chains to omnivorous webs; the relative change $\Delta F_{min}/(1-F_{min}^{chain})$ is 23%, one way to express the increase in stability. Figure 3.8 also reveals that the nonlinearity of production S for all the vertices is centered around $S = 0$, where the basal production rate has its maximum value (Fig. 3.1). Thus, the range of feeding nonlinearities that yield a stable equilibrium is the largest near peak basal production. The average S-value is about 0.0008 for food chains and about -0.0517 for omnivorous webs.

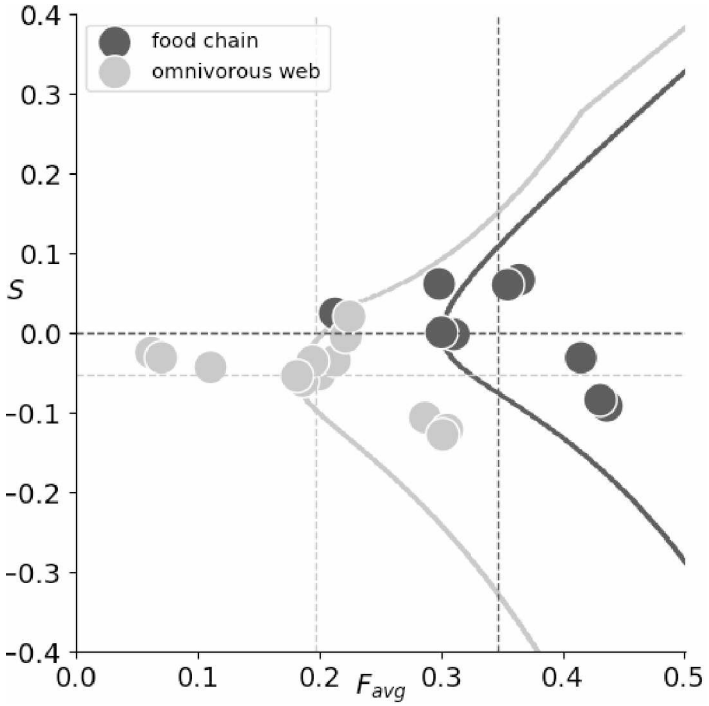

Figure 3.8: Lowest (average) feeding nonlinearity F_{min} that corresponds to a stable fixed point (e.g., red point in Fig.3.4) for type 1 and type 2 specific models together with the stable/unstable boundary from Fig.3.7(d) near F_{min}. The dashed lines intersect at the average coordinates for the food chains (dark grey) and the omnivorous webs (grey). There are fewer dark circles than light circles, since some food chains don't have coexisting stable fixed points.

3.10 Coexisting fixed points

Generalized modeling efficiently quantifies local stability of each nontrivial fixed point in infinitely many models, but which of the fixed points are in coexistence with others is unknown. A stable, single fixed point is globally stable in the absence of non-attracting manifolds or basin boundaries. Global stability can be challenging to prove in specific models, but is conceptually elusive/undefined in generalized modeling.

Since generalized models cannot determine the coexistence of fixed points, specific mod-

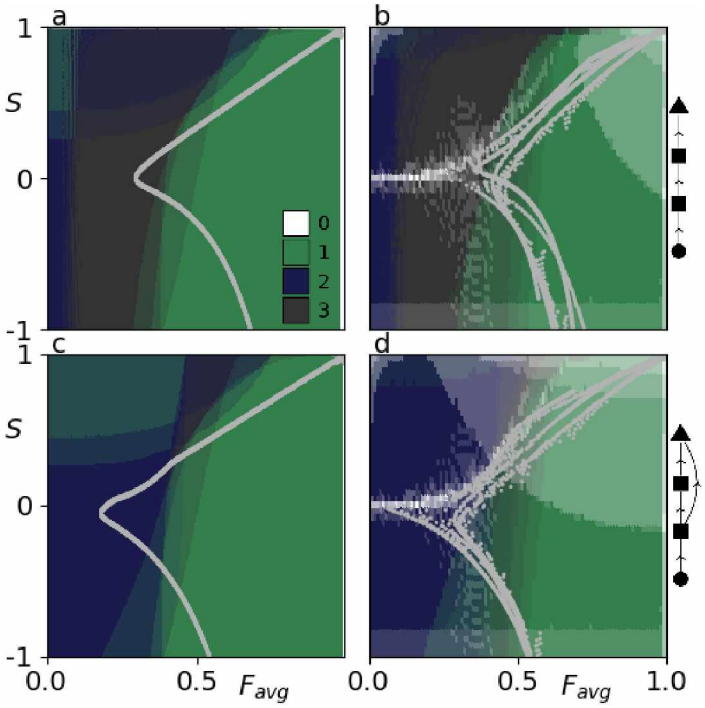

Figure 3.9: A superimposition of the number of nontrivial fixed points sorted by model type and topology: (a) type 1 food chain, (b) type 2 food chain, (c) type 1 omnivorous web, and (d) type 2 omnivorous web. The color coding represents the number of nontrivial fixed points. The grey points lie on the stable/unstable boundary. The production term, exponential equation, is excluded for type 1 models, since the space of nonlinearity is only partially covered by fixed points.

els are used to identify regions in the generalized parameter space where a single non-trivial fixed point is prevalent and regions where coexisting fixed points are prevalent. Such analysis with enough statistics from many specific models might provide supplementary information to generalized models where to likely expect coexistence or not. Figure 3.9 shows superimpositions of the number of nontrivial fixed points for type 1 and 2 specific models. For both topologies, the food chain and the omnivorous web, coexistence of nontrivial fixed points is common for small feeding nonlinearities, F_{avg} less than about one half. Most single fixed points have F_{avg} greater than one half and are also stable. Some stable fixed points with small feeding nonlinearities are coexistent fixed points and have a small basin of attraction. Coexistence of two stable fixed points is not found. Adding an omnivorous link to the food chain does not qualitatively change where coexistence occurs, but typically reduces the number of coexisting fixed points from three to two or two to one. The stabilizing shift of the stable/unstable boundary to lower feeding nonlinearities (Fig. 3.7) creates more stable fixed points in regions of coexistence.

In the nonlinearity regime with a stable, single fixed point, the feeding nonlinearities

are larger, representing more hungry predators. These four-species food webs might appear globally stable for an observer of a real system. From a mathematical point of view the stable, single nontrivial fixed point is not a globally stable fixed point, since coexisting trivial fixed points (saddles) exist that can be reached from non-typical initial conditions. Non-typical initial conditions, however, are not accessible in a real food web. Preliminary simulation results for the type 1 and 2 specific models show that trajectories with various initial conditions reach the stable nontrivial fixed point. Therefore, ecosystem persistence in form of a chaotic or periodic, coexisting attractor is not evident. In rare exceptions, for parameters close to the stable/unstable boundary, trajectories do not approach the nontrivial stable fixed point. Further studies would need to investigate this in more detail.

3.11 Feeding nonlinearities and stability

Generalized modeling often assumes equal feeding nonlinearities F_i for each predator across trophic levels to reduce the dimensionality of the generalized parameter space (Gross et al.; 2009; Yeakel et al.; 2014; Awender et al.; 2021). Plitzko et al. (2012) determines the distribution of F_i in steady state in specific 30-species food webs generated with the niche model (Williams and Martinez; 2000). They find that stable fixed points typically have larger feeding nonlinearities for larger trophic levels. Similar to Plitzko et al. (2012), we analyze the distribution of F_i in the type 1 and 2 specific models and find distributions that are sensitive to production forms.

Figure 3.10(a) shows stable fixed points distributed in the nonlinearity-of-feeding space (F_2, F_3) for three basal production forms. Logistic production yields stable fixed points with comparatively smaller feeding nonlinearities and (predominantly) $F_2 < F_3$ in the type 1 omnivorous web. Production due to the exponential map and Bellow's map in the type 2 food chain yield stable fixed points that cover a larger range of feeding nonlinearities and the ranking of F_2 and F_3 is less distinct. The corresponding histograms of feeding nonlinearities F_2, F_3, and F_4 are presented in Figs.3.10(b)-3.10(d). The exponential map [Fig.3.10(b)] yields a histogram with no clear ranking in F_i for stable fixed points; its shape is similar to most histograms for type 1 and 2 specific models with other combinations of production term and topology. The histogram for the logistic case [Fig. 3.10(c)] exhibits a unique shape with feeding nonlinearities predominantly ranked as $F_2 < F_4 < F_3$; the order with respect to peak location of F_3 and F_4 is switched in comparison to Plitzko et al. (2012).

When the production term is Bellow's map, the histograms for each trophic level are the same [Fig. 3.10(d), $S \approx 0$], which is also a unique result. All the stable points that are near maximal production growth ($S = 0$) have sets of equivalent feeding nonlinearities $F_i = F$,

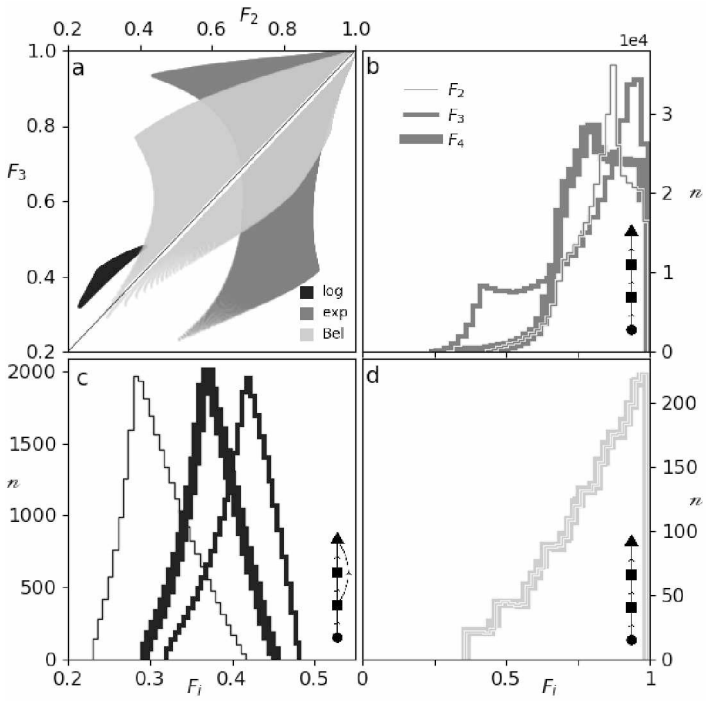

Figure 3.10: (a) Stable fixed points positioned by the nonlinearities of feeding, F_2 and F_3, for (black) the type 1 omnivorous web with logistic production [data from Fig. 3.3(f)], (dark grey) the type 2 food chain with exponential map production, and (grey) for the type 2 food chain with Bellow's map (b=2) production. The diagonal line is for reference. Histograms of the nonlinearities of feeding for each predator (F_2, F_3, F_4) for the data from panel (a) for (b) the exponential map, (c) the logistic case, and (d) the Bellow's map. n is the number of points per bin. For (d), only data with $|S| < 0.001$ corresponding to the white line in panel (a) are used.

Fig. 3.10(a).

This section compares the typical assumption in generalized models that feeding nonlinearities are equal for all species with the actually occurring feeding nonlinearities in the specific food web models. The results show that occurring feeding nonlinearities depend on the specific functional forms for production and have broad distributions; feeding nonlinearities are equal in the special case of fixed points at maximum production for Bellow's map.

3.12 Weighting of links in steady state

In the omnivorous web, species 2 is preyed upon by species 3 and 4, and species 4 is a predator of species 2 and 3 (Fig. 3.2). Thus, the biomass flow from x_2 is divided onto the two paths. In generalized ecological models the weighting between two such links is often assumed to be an even split. Other approaches incorporate variability in the link

strengths, such as random choices drawn from a distribution (Gross et al.; 2009) or scaling the weightings such that more probable links have higher flows (Yeakel et al.; 2014). It is investigated whether such assumptions are consistent with the actually occurring weights in the specific models at steady state.

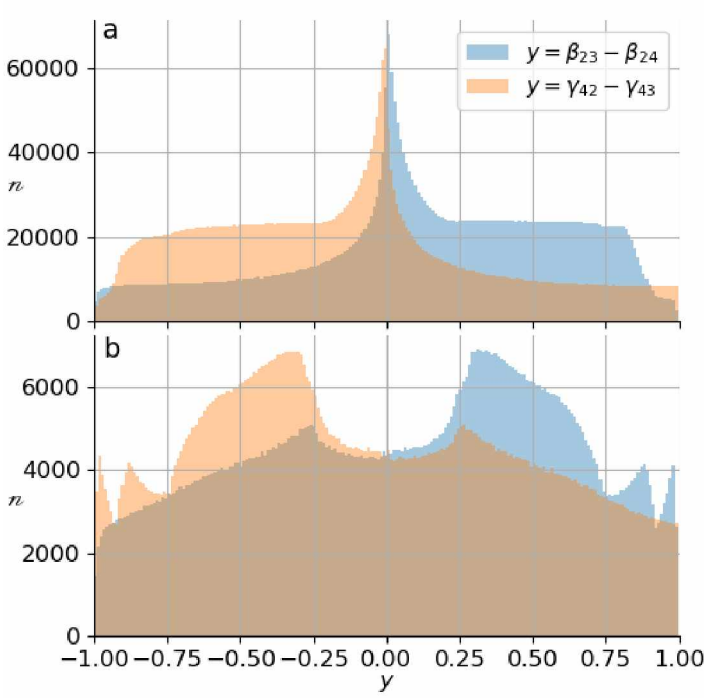

Figure 3.11: Histograms of proportionate biomass growth and proportionate biomass loss (y) in type 2, specific omnivorous webs with various production terms. n is the number of fixed points per bin for the (a) 200-bin histogram that includes all fixed points (about 3.54 million fixed points with about 25% of them stable), and for the (b) 200-bin histogram that only includes the stable fixed points. $y = \beta_{23} - \beta_{24}$ (transparent blue) represents the difference in proportionate loss of biomass from x_2 to x_3 and x_2 to x_4, and $y = \gamma_{42} - \gamma_{43}$ (transparent orange) represents the difference in proportionate growth of biomass x_4 from predation of x_2 and x_3. The productions terms include Bellow's equation (b=6,10), exponential map, and Bellow's map (b=2,10). The third color represents the data where both histograms overlap.

Proportionate link strengths are extracted from the type 2 specific models at steady state. The proportionate flows out from the biomass x_2 are β_{23} and β_{24}, which are non-negative and sum up to one; similarly for the proportionate flows into x_4, γ_{42} and γ_{43}. Figure 3.11(a) shows the distribution of the difference of proportionate flow out of x_2, $\beta_{23} - \beta_{24}$, and the distribution of the difference of proportionate flow into x_4, $\gamma_{42} - \gamma_{43}$, for all fixed points. The fixed points show any possible scenario of relative weighting, i.e., the differences in the scale parameters cover the entire range from [-1, 1]. The most common scenario has perfectly even flows out from x_2, but most of these fixed points are unstable. The most common scenario

for stable fixed points [Fig. 3.11(b)] has about twice the flow going from x_2 to x_3 than from x_2 to x_4, $\beta_{23} - \beta_{24} = 0.3$ or $(\beta_{23}, \beta_{24}) = (0.65, 0.35)$. Overall, networks with larger flows from x_2 to x_3 compared to x_2 to x_4 are more likely to result in stable steady states. These results can inform assumptions in future generalized modeling efforts.

The difference of weightings on predatory gains for x_4, $\gamma_{42} - \gamma_{43}$, show a symmetric distribution to that of the difference of weightings on predatory loss of x_2, $\beta_{23} - \beta_{24}$. More outflow from biomass x_2 to x_3 results in proportionately more inflow of biomass into x_4 via x_3. This symmetry in the distribution of out-flows from the bottom predator and the distribution of in-flows to the top predator needs to be explored in future studies; it might not exist in larger, more connected webs.

3.13 Conclusion

It is not possible to empirically determine complete descriptions of processes and parameters controlling biomass flow in real ecological systems. Specific models (e.g., coupled-ODE models) assume explicit functional forms and initial conditions to discuss trajectories and dynamics in abstractions of the ecological system. Generalized models make no such assumptions and efficiently capture the stability of nontrivial steady states for an infinite number of specific ecological models (Gross et al.; 2009). However, specific models provide information on trajectories, coexistence of fixed points, and more complex attractors, while generalized models can not. This study compares results and ecological implications from generalized modeling and specific modeling in a four-species trophic network where the top predator is omnivorous or not.

Generalized parameters, with a particular focus on feeding and basal production nonlinearities in this study, can span all plausible dynamic scenarios, but some of this parameter space may not be accessible to a particular specific model. Nevertheless, generalized modeling and specific modeling reveal some common ecological interpretations. Stable fixed points generally exist for hungry predators, a condition when the prey density is less than the half saturation of the predatory growth (larger feeding nonlinearities). Stable fixed points culminate over a range of feeding nonlinearities when the basal production rate is near its maximum (nonlinearity of production near zero). In short, good conditions for stability arise when basal growth rate approaches a maximum and nutrient flows to predators are fettered. These stability trends are qualitatively similar for the various production processes.

Adding an omnivorous link to the food chain has a stabilizing effect. The range of stable fixed points extends to smaller feeding nonlinearity parameters, which means that steady states with larger prey populations relative to the half-saturation constant in the

predatory response functions become stable. This finding is consistent across specific and generalized models and the two topologies. The role of omnivory for food web stability is an important area of research and studies report that increasing omnivory can have a stabilizing or destabilizing effect (Vandermeer; 2006; Awender et al.; 2021). Awender et al. (2021) show that adding omnivory to short food chains with three or four species has a stabilizing effect, while increasing omnivory in longer food chains is destabilizing.

Previous studies have reported that enrichment either stabilizes or destabilizes ecosystems(Roy and Chattopadhyay; 2007; Gross et al.; 2004; Awender et al.; 2021) with the later known as paradox of enrichment (Rosenzweig; 1971). The system is enriched by increasing the amount of limiting nutrients for basal growth, which effectively increases the carrying capacity. The four species food chain and the omnivorous web reveal that fixed points can stabilize from enrichment when the basal species are in a resource-deprived environment but become unstable when the basal species are in a more resource-rich environment. While a specific model exhibits a defined path of enrichment, a generalized model has infinitely many hypothetical paths of enrichment that may or may not be accessible by a specific model. Smaller prey densities relative to their predator's half-saturation constants (in generalized and specific models) also drive fixed points into the stable region where feeding nonlinearities are increased. Real systems are driven into this condition by the hampering of hunting conditions or less nutritious prey, a concept prevalent in a conglomerate of mesocosm experiments (Roy and Chattopadhyay; 2007; Harrison; 1995).

Generalized modeling approximates the distribution of flows to and from a multi-degree network node, assuming links with equal weights, or random weights, or weights that are scaled with link probability (Gross et al.; 2009; Yeakel et al.; 2014). In the specific model, however, the fixed points of the omnivorous web reveal any possible scenario of relative weighting. The most likely scenario has the flow to the top predator equally divided between the two flows, but most of these fixed points are unstable. The most likely scenario for stable fixed points has two-thirds of the flow go to the nearest trophic level and one-third of the flow go to the top, skipping a level. These results from the specific model can inform future generalized modeling efforts.

Global stability can be challenging to prove in specific models, but is conceptually elusive/undefined in generalized modeling. Specific models are used to identify regions in the generalized parameter space with one or more non-trivial fixed points. A stable fixed point is often the only nontrivial fixed point for larger feeding nonlinearities, representing ecosystems with hungry predators. For an observer such ecosystems might appear globally stable, since non-typical initial conditions are not accessible in a real food web. Coexistence of nontrivial fixed points is common for small feeding nonlinearities, i.e., when prey densities are larger

than predator's half-saturation constants. Further studies are needed to explore coexistence patterns in larger webs and different specific models with the goal to derive statistical information on coexistence that might be relevant for the interpretation of generalized models.

The four-species webs might behave similar to some larger and more complex food webs if the four species are interpreted as trophospecies that combine species with similar ecological function into one unit. If omnivory is uncommon enough, larger food webs are stratified to create a network of trophospecies to resemble the trophic levels of food chains. For example, one study shows that webs consisting of thirty basal species and thirty top predators and no intermediate predators have the same stability profile as a two species food chain (Gross et al.; 2005; Awender et al.; 2021), alluding to the scientific fertility simpler networks have in the development of foundational principles governing food web dynamics. Adding further complexity to these models is imperative for the refinement of these principles.

3.14 References

Abrams, P. A. and Walters, C. J. (1996). Invulnerable prey and the paradox of enrichment, *Ecology* **77**(4): 1125.

Allesina, S. and Tang, S. (2012). Stability criteria for complex ecosystems, *Nature* **483**: 205.

Awender, S., Wackerbauer, R. and Breed, G. A. (2021). Stability of generalized ecological-network models, *Chaos* **31**(2): 023106.

Bellows, T. (1981). The descriptive properties of some models for density dependence, *J. Anim. Ecol.* **50**(1): 139.

Cohen, J., Briand, F. and Newman, C. (1986). A stochastic theory of community food webs. III. Predicted and observed lengths of food chains, *P. Roy. Soc. B-Biol. Sci.* **228**(1252): 317.

Cook, L. (1965). Oscillation in the simple logistic growth model, *Nature* **207**(4994): 316.

Drossel, B. and McKane, A. J. (2003). Modelling food webs, *Handbook of graphs and networks: From the genome to the internet*, Wiley-VCH Verlag GmbH & Co. KGaA, Weinheim, p. 218.

Fussmann, G. F. and Heber, G. (2002). Food web complexity and chaotic population dynamics, *Ecol. Lett.* **5**(3): 394.

Genkai-Kato, M. and Yamamura, N. (1999). Unpalatable prey resolves the paradox of enrichment, *P. Roy. Soc. B-Biol. Sci.* **266**(1425): 1215.

Gounand, I., Mouquet, N., Canard, E., Guichard, F., Hauzy, C. and Gravel, D. (2014). The paradox of enrichment in metaecosystems, *Am. Nat.* **184**(6): 752.

Groß, T. (2004). *Population dynamics: General results from local analysis*, PhD thesis, Universität Oldenburg.

Gross, T., Ebenhöh, W. and Feudel, U. (2004). Enrichment and foodchain stability: The impact of different forms of predator–prey interaction, *J. Theor. Biol.* **227**(3): 349.

Gross, T., Ebenhöh, W. and Feudel, U. (2005). Long food chains are in general chaotic, *Oikos* **109**(1): 135.

Gross, T. and Feudel, U. (2004). Analytical search for bifurcation surfaces in parameter space, *Physica D* **195**(3-4): 292.

Gross, T. and Feudel, U. (2006). Generalized models as a universal approach to the analysis of nonlinear dynamical systems, *Phys. Rev. E* **73**(1): 016205.

Gross, T. and Feudel, U. (2009). Local dynamical equivalence of certain food webs, *Ocean Dyn.* **59**(2): 417.

Gross, T., Rudolf, L., Levin, S. A. and Dieckmann, U. (2009). Generalized models reveal stabilizing factors in food webs, *Science* **325**(5941): 747.

Harrison, G. W. (1995). Comparing predator-prey models to Luckinbill's experiment with Didinium and Paramecium, *Ecology* **76**(2): 357.

Jansen, V. A. (1995). Regulation of predator-prey systems through spatial interactions: A possible solution to the paradox of enrichment, *Oikos* p. 384.

Kuehn, C. and Gross, T. (2013). Nonlocal generalized models of predator-prey systems, *Discrete Contin. Dyn. Syst. - B* **18**(3): 693.

Kuehn, C., Siegmund, S. and Gross, T. (2013). Dynamical analysis of evolution equations in generalized models, *IMA J. Appl. Math.* **78**(5): 1051.

Lade, S. J. and Niiranen, S. (2017). Generalized modeling of empirical social-ecological systems, *Nat. Resour. Model.* **30**(3): e12129.

Lafferty, K. D., Dobson, A. P. and Kuris, A. M. (2006). Parasites dominate food web links, *PNAS* **103**(30): 11211.

May, R. M. (1972). Will a large complex system be stable?, *Nature* **238**: 413.

Mougi, A. and Nishimura, K. (2007). A resolution of the paradox of enrichment, *J. Theor. Biol.* **248**(1): 194.

Mulder, C. and Hendriks, A. J. (2014). Half-saturation constants in functional responses, *Glob. Ecol. Conserv.* **2**: 161.

Newman, M. (2018). *Networks*, Oxford University Press.

Pimm, S. L., Lawton, J. H. and Cohen, J. E. (1991). Food web patterns and their consequences, *Nature* **350**(6320): 669.

Plitzko, S. J., Drossel, B. and Guill, C. (2012). Complexity–stability relations in generalized food-web models with realistic parameters, *J. Theor. Biol.* **306**: 7.

Rosenzweig, M. L. (1971). Paradox of enrichment: Destabilization of exploitation ecosystems in ecological time, *Science* **171**(3969): 385.

Roy, S. and Chattopadhyay, J. (2007). The stability of ecosystems: A brief overview of the paradox of enrichment, *J. Biosci.* **32**(2): 421.

Sinha, S. and Sinha, S. (2005). Evidence of universality for the May-Wigner stability theorem for random networks with local dynamics, *Phys. Rev. E* **71**(2): 020902.

Stiefs, D. (2009). *Relating generalized and specific modeling in population dynamical systems*, PhD thesis, Universität Oldenburg.

Stiefs, D., Gross, T., Steuer, R. and Feudel, U. (2008). Computation and visualization of bifurcation surfaces, *IJBC* **18**(08): 2191.

Stiefs, D., Venturino, E. and Feudel, U. (2009). Evidence of chaos in eco-epidemic models, *Math. Biosci. Eng.* **6**(4): 855.

Stouffer, D. B. and Bascompte, J. (2010). Understanding food-web persistence from local to global scales, *Ecol. Lett.* **13**(2): 154.

Vandermeer, J. (2006). Omnivory and the stability of food webs, *J. Theor. Biol.* **238**(3): 497.

Veilleux, B. (1979). An analysis of the predatory interaction between Paramecium and Didinium, *J. Anim. Ecol.* **48**(3): 787.

Williams, R. J. and Martinez, N. D. (2000). Simple rules yield complex food webs, *Nature* **404**(6774): 180.

Winemiller, K. O. and Polis, G. A. (1996). Food webs: What can they tell us about the world?, *Food Webs*, Springer, p. 1.

Yeakel, J. D., Pires, M. M., Rudolf, L., Dominy, N. J., Koch, P. L., Guimarães, P. R. and Gross, T. (2014). Collapse of an ecological network in Ancient Egypt, *PNAS* **111**(40): 14472.

Yeakel, J. D., Stiefs, D., Novak, M. and Gross, T. (2011). Generalized modeling of ecological population dynamics, *Theor. Ecol.* **4**(2): 179.

Chapter 4 How Realistic Features Affect the Stability of an Arctic Marine Food Web Model

4.1 Introduction

Ecosystems are large, nonlinear dynamical systems that embody the interactions among community members and the abiotic environments that contain them. They are characterized with immense complexity from species richness, interconnectedness, and nonlinear processes that describe the flows of matter and energy to and from constituents. Until recently, work to understand and manage wild populations has focused on individual populations, but in the past few decades it has become increasingly clear that understanding the mechanics of ecosystems is essential for sustainable exploitation and conservation of ecosystem members, either collectively or individually (Plagányi; 2007).

Arctic ecosystems are of special interest for ecosystem modeling, because they are naturally among the least biodiverse, making them good candidates for more realistic mathematical representations. These depauperate systems are also special in that the organisms composing them are often uniquely adapted to the extreme conditions of cold temperatures and sea ice; and subject to long periods of day and night, and fast transitions of intense seasonality.

Ecosystems in the far north provide cultural and provisioning services to the human communities that live there. The resources of marine ecosystems are the most important natural resource to Alaska native subsistence and commercial harvest in the Arctic. For example, the harvest of bowhead whales accounts for more of the harvested biomass by weight than all the combined land mammals in the North Slope Federal Subsistence Region (Smith et al.; 2017). The Arctic is also at the front lines of climate change, and has seen more intense warming than any other region on Earth (Serreze and Barry; 2011). Arctic species with high degrees of specialization to polar conditions are most likely to face adverse effects from a changing environment. Understanding Arctic ecosystems and their dynamics is thus important for predicting the consequences of a changing climate on the system level and acquiring effective insight for conservation.

Ecosystems are often represented both conceptually and mathematically as interconnected networks called food webs. Such mathematical representations are useful to both theoretical and empirical ecology. Ecosystem network models are composed of nodes (species or aggregate trophic units) linked by consumer-resource interactions; some coupling can be from non-transfer interactions as well, such as competition. In this study, some links rep-

resent flows of resources (matter or energy) into or out of the system (natural mortality and primary production), but most represent energy transfers between species within the community (predator-prey interactions).

Realistic network representations of diverse ecosystems can become extremely complicated and include thousands of links between hundreds of trophic nodes. Even in simpler systems representing a few tens of nodes and a few hundred links, empirical biomass or flow estimates are unlikely to be available. In these circumstances, a relatively new modeling approach has been introduced known as "generalized modeling"(Gross and Feudel; 2006; Kuehn et al.; 2013). Generalized modeling is a powerful modeling technique that does not require specific functional formulations of processes nor initial conditions of the system. By contrast, in conventional dynamics modeling approaches, both the mathematical functional forms and their parameters must be specified. Instead of specifying exact mathematical forms to describe the various ecological processes, the terms that represent the ecosystem processes are merely classified into a series of gain or loss terms. A normalizing coordinate transformation maps the unknown fixed points (equilibria) to a known, rescaled fixed point from which local stability and bifurcation information is extracted. The transformed parameterization comprises the relative weighting of the flows between each process and the functional nonlinearities of each process at these fixed points, collectively referred to as generalized parameters.

In this analysis, we use generalized modeling to explore the impact of various ecosystem characteristics on overall stability of the Southern Beaufort Sea (SBS) ecosystem. We assess how incorporating foraging traits of ecosystem members, constraining the connections from habitat modularity, and adjusting predatory weights impacts the stability regions in the nonlinearity space of the systems' production processes and node-to-node transfers. We also assess how the addition or removal of a single species from SBS food webs is potentially stabilizing or destabilizing Lastly, we introduce a method to add "ecosystem background noise" in food web models to assess the collective impacts of numerous latent ecosystem members on overall stability, with the idea that ecosystem models often focus on abundant species and/or species of particular management interest.

4.2 The Beaufort Sea Food Web

The region of the Arctic Ocean directly adjacent to Alaska's North Slope and Canada's most western Arctic is the Southern Beaufort Sea (SBS). This sea freezes completely over in the winter, but the timing, thickness, and extent of the sea ice varies from year to year. Sea ice is a critical force in this ecosystem; it controls the plankton blooms and its presence

is critical for ice-obligate species, including walrus, polar bear, arctic cod and most of the region's seals. Sea ice also serves as a geographical northern boundary for many species, including killer, grey and humpback whales. Sea ice degradation and recession is changing this boundary, permitting the possible invasion and colonization of the system by subarctic and temperate species, allowing them to penetrate farther north and reside for longer periods (Breed et al.; 2013; Divine; 2016). The SBS also hosts a declining polar bear subpopulation, serves as a migratory corridor and breeding location for bowhead whale, and its fish biomass is predominately arctic cod (Thorsteinson and Love; 2016; Smith et al.; 2017).

In the analyses presented here, we use the SBS ecosystem as a motivating example and model ecosystem. Food webs representing the SBS were constructed from a species pool comprising thirty species or trophospecies, groups of species with similar ecological function that are collectively represented by one state variable. These thirty were selected with the expectation that they have the greatest ecological significance. Each species or trophospecies node has an associated set of ecological attributes, including a specified body mass and a set of habitats to which the species is most tightly associated within the larger ecosystem. The overall ecosystem has five modules, defined by habitat, that physically prevent some network connections as some species do not share the same habitat. Table 4.1 displays these species along with their mass and habitat associations. Table 4.1 also includes a plot of the size spectrum of masses in kilograms, which spans nearly 13 orders of magnitude.

Body size is a key trait because it strongly controls the probability one species will consume another, and a great deal of work has been undertaken to understand how body size spectra impact food web structure (Woodward et al.; 2005; Stouffer et al.; 2011). Predators are usually 1 to 4 orders of magnitude larger than their prey. Prey less than one order of magnitude smaller than predators are difficult or dangerous to capture, while prey smaller than four orders of magnitude can require too much effort for the small caloric rewards. Structuring a food web based solely on body size can predict the majority of real ecosystem links. As these representations are modified to incorporate increasingly detailed the foraging traits of ecosystem members (where available), the predictions become increasingly accurate (Rohr et al.; 2010).

Given that body size spectra are a key element structuring ecosystems, we begin our modelling effort by representing the probability p_{ij} a link is present between any two ecosystem members as a function of the predator-to-prey body-mass ratio m_i/m_j,

$$p_{ij} = p_{ij}(m_i, m_j) = \text{logit}^{-1}(a_i + b_i \ln\mu_{ij} + c_i \ln^2\mu_{ij}) \tag{4.1}$$
$$\mu_{ij} = \ln\left(d_i \frac{m_i}{m_j}\right)$$

Table 4.1: Thirty species in the model SBS ecosystem sorted by estimated average mass, the set of habitats most frequented by each species, and the masses plotted on a logarithmic scale. The killer whale is added as introductory species. (Thorsteinson and Love; 2016; Smith et al.; 2017; Majewski et al.; n.d., 2017; Gray et al.; n.d.; Loseto; 2008).

	Name	Latin name	Mass [kg]	Habitats
30	Bowhead Whale	*Balaena mysticetus*	4.9×10^4	1,2
29	Beluga	*Delphinapterus leucas*	1.4×10^3	3
28	Pacific Walrus	*Odobenus rosmarus divergens*	1.0×10^3	2,3,4
27	Polar Bear	*Ursus maritimus*	4.0×10^2	1,2,3
26	Bearded Seal	*Erignathus barbatus*	2.5×10^2	2,4
25	Ringed Seal	*Pusa hispida*	7.5×10^1	2,4
24	Dolly Varden	*Salvelinus malma*	2.2×10^0	1,2,3
23	Arctic Cisco	*Coregonus autumnalis*	1.0×10^0	1,2,3
22	Shorthorn Sculpin	*Myoxocephalus scorpius*	1.0×10^0	4
21	Bering Cisco	*Coregonus laurettae*	8.6×10^{-1}	1,2,3
20	Saffron Cod	*Eleginus gracilis*	6.5×10^{-1}	4,5
19	Bering Flounder	*Hippoglossoides robustus*	4.3×10^{-1}	4
18	Fourhorn Sculpin	*Myoxocephalus quadricornis*	3.1×10^{-1}	3,4
17	Arctic Smelt	*Osmerus dentex*	2.8×10^{-1}	1,2
16	Nebulous Snailfish	*Liparis bathyarcticus*	7.6×10^{-2}	4
15	Polar Eelpout	*Lycodes polaris*	7.0×10^{-2}	4
14	Arctic Cod	*Boreogadus saida*	6.3×10^{-2}	1,2,4,5
13	Arctic Sand Lance	*Ammodytes hexapterus*	3.7×10^{-2}	1,2,5
12	Arctic Staghorn Sculpin	*Gymnocanthus tricuspis*	3.5×10^{-2}	4
11	Slender Eelblenny	*Lumpenus fabricii*	2.8×10^{-2}	4
10	Pacific Capelin	*Mallotus catervarius*	5.5×10^{-3}	3
9	Hamecon	*Artediellus scaber*	5.3×10^{-3}	4,5
8	Ninespine Stickleback	*Pungitius pungitius*	2.0×10^{-3}	1,4
7	Snow Crab	*Chionoecetes opilio*	1.8×10^{-3}	4,5
6	**Large Crangonid Shrimps**		1.7×10^{-4}	4
5	**Amphipods**		1.6×10^{-4}	1
4	**Euphausiids**		8.2×10^{-5}	1,4,5
3	**Bivalves**		4.5×10^{-5}	4
2	**Mysids**		2.6×10^{-5}	1,4,5
1	**Copepods**		2.0×10^{-8}	1
	Killer Whale	Orcinus orca	3.5×10^3	1,2,3,4,5

Habitats	
1	Oceanic
2	Neritic
3	Littoral
4	Benthic
5	Shelf/Midwater

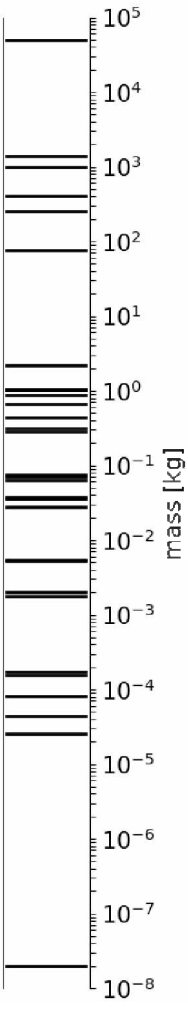

where $\text{logit}^{-1}(x) := e^x/(1+e^x)$. The linking probability p_{ij} is the probability that x_i preys on x_j (Fig. 4.1). Though the body mass ratio is a good starting point, linking probabilities also depend on the foraging traits of x_i, which can be specialized to avoid certain prey or target prey larger or smaller than that predicted from body mass ratios alone.

Here, we estimate the connections only from the perspective of the predators' foraging traits or feeding specialization; hence, the constants of Eq. (4.1), which represent the traits, apply only when a node is acting as the predator. The constants a_i, b_i, c_i, d_i are determined from x_i's foraging traits. In the base model, we apply the assumption that every species has the same foraging traits, and set $(a_i, b_i, c_i, d_i) = (a, b, c, d)$ for all ecosystem members i. The

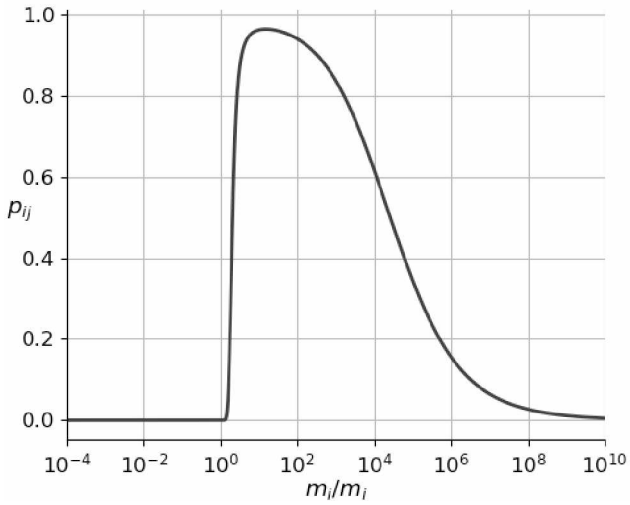

Figure 4.1: General linking probability p_{ij} versus predator prey mass ratio m_i/m_j for the standard parameters $(a_i, b_i, c_i, d_i) = (1.41, 3.73, -1.87, 1)$ in Eq. (4.1). For any potential prey item one to four orders of magnitude smaller than the predator, there is at least a 60% chance for a link.

choice of parameters used here is adopted from the parameters used in Yeakel et al. (2014). This base model has each of the species with the same feeding parameters, all members have the same chance for connection with any other species, and with no prey preference other than that determined by body mass ratios.

4.3 Food Web Dynamics

The mathematical framework of generalized ecological models was initially developed in Gross and Feudel (2006) and is summarized here. The state of an ecological network with N species at time t, $\boldsymbol{x}(t) \in \mathbb{R}^N$, is represented as a network of connections between species, with x_i representing the biomass of species i and $x_i \geq 0$. The state evolves by a growth rate from production $\mathscr{S}$ and predation $\mathscr{F}$, and a loss rate from predation $\mathscr{L}$ and other mortality $\mathscr{M}$,

$$\dot{x}_i(t) = \mathscr{S}_i(x_i) + \eta_i \mathscr{F}_i(T_i, x_i) - \mathscr{M}_i(x_i) - \sum_j \mathscr{L}_{ij}(\boldsymbol{x}). \tag{4.2}$$

η_i is an assimilation coefficient. The predatory loss $\mathscr{L}_{ij}$ of prey i from predator j is proportional to the predatory growth of the predator $\mathscr{F}_j$ and the fraction with which prey i

contributes to the resources of predator j,

$$\mathscr{L}_{ij}(\boldsymbol{x}) = \frac{C_{ji}(x_i)}{T_j(\boldsymbol{x})}\mathscr{F}_j(T_j, x_j). \tag{4.3}$$

T_j is the total prey resources destroyed by predator x_j,

$$T_j(\boldsymbol{x}) = \sum_k C_{jk}(x_k), \tag{4.4}$$

where C_{jk} is the contribution from x_k to the diet of x_j.

4.3.1 Generalized Ecological Model

Starting with Eq. (4.2) and normalizing the state vector to an unknown, nontrivial fixed point $\boldsymbol{x}^*$, and each unknown growth or loss process of the form $\mathscr{G}$ to its value at the fixed point $\mathscr{G}^* \equiv \mathscr{G}(\boldsymbol{x}^*)$, gives following rescaled variables and functions,

$$\chi_i = \frac{x_i}{x_i^*}, \qquad g(\boldsymbol{\chi}) = \frac{\mathscr{G}(\mathbb{X}^*\boldsymbol{\chi})}{\mathscr{G}^*}, \qquad t_i = \frac{T_i}{T_i^*} = \sum_k \gamma_{ik} c_{ik}(\chi_k), \tag{4.5}$$

where $\gamma_{ij} = C_{ij}^*/T_i^*$ and $\mathbb{X}^*$ is a diagonal matrix, $\mathbb{X}_{ij}^* = \boldsymbol{x}_i^*\delta_{ij}$. This normalization maps the unknown fixed point $\boldsymbol{x}^*$ to a known fixed point $\boldsymbol{\chi}^* = (1, 1, \ldots, 1)$, and the unknown process to a known process value at the fixed point, $g(\boldsymbol{\chi}^*) = 1$ in the rescaled system. The N equations of motion in non-dimensionalized form are

$$\dot{\chi}_i = \alpha_i\left(\sigma_i s_i(\chi_i) + \phi_i f_i(t_i, \chi_i) - \mu_i m_i(\chi_i) - \lambda_i \sum_j \beta_{ij} \frac{c_{ji}(\chi_i)}{\sum_k \gamma_{jk} c_{jk}(\chi_k)} f_j(t_j, \chi_j)\right). \tag{4.6}$$

The time scale parameter (turnover rate) α_i is determined from the steady state, where the total influx (growth) is equal to the total outflux (loss),

$$\alpha_i = \frac{\mathscr{S}_i^* + \eta_i \mathscr{F}_i^*}{x_i^*} = \frac{\mathscr{M}_i^* + \sum_j \mathscr{L}_{ij}^*}{x_i^*}. \tag{4.7}$$

The primary scale parameters that describe the relative weighting of the main process flows of the network at the steady state are

$$\sigma_i = \frac{\mathscr{S}_i^*}{\alpha_i x_i^*}, \qquad \phi_i = \frac{\eta_i \mathscr{F}_i^*}{\alpha_i x_i^*}, \qquad \mu_i = \frac{\mathscr{M}_i^*}{\alpha_i x_i^*}, \qquad \lambda_i = \frac{\sum_j \mathscr{L}_{ij}^*}{\alpha_i x_i^*}. \tag{4.8}$$

The secondary scale parameters that describe the relative weighting between the sums of predatory out- or in-flows at steady state are

$$\beta_{ij} = \frac{\mathscr{L}^*_{ij}}{\sum_k \mathscr{L}^*_{ik}}, \qquad \gamma_{ij} = \frac{C^*_{ij}}{T^*_i}. \tag{4.9}$$

The local dynamics near the fixed point is governed by the Jacobian matrix $\mathbb{J}^*$ evaluated at the fixed point. The diagonal elements are

$$J_{ii}|_* = \alpha_i \left[\sigma_i s_i^{(\chi_i)} + \phi_i (f_i^{(t_i)} \gamma_{ii} c_{ii}^{(\chi_i)} + f_i^{(\chi_i)}) - \mu_i m_i^{(\chi_i)} - \lambda_i \beta_{ii} f_i^{(\chi_i)} - \lambda_i \sum_k \beta_{ik} c_{ki}^{(\chi_i)} (1 + \gamma_{ki} (f_k^{(t_k)} - 1)) \right], \tag{4.10}$$

and the off-diagonal elements are

$$J_{ij}|_* = \alpha_i \left[\phi_i f_i^{(t_i)} \gamma_{ij} c_{ij}^{(\chi_j)} - \lambda_i \beta_{ij} f_j^{(\chi_j)} - \lambda_i \sum_k \beta_{ik} c_{kj}^{(\chi_j)} \gamma_{kj} (f_k^{(t_k)} - 1) \right]. \tag{4.11}$$

The exponent parameters (nonlinearity parameters) of the form $g^{(\xi)}$ in the Jacobian are defined as

$$g^{(\xi)} \equiv \left. \frac{\partial g(\boldsymbol{\chi})}{\partial \xi} \right|_{\boldsymbol{\chi}=\boldsymbol{\chi}^*}, \tag{4.12}$$

with $\xi \in \{\chi_i, t_i\}$. They describe the nonlinearity of process $\mathscr{G}(\boldsymbol{x})$ [Eq. (4.2)] with respect to ξ at the fixed point and are measures of elasticity.

4.3.2 Generalized Parameters for the Base Model

Steady state stability [Eqs. (4.10) and (4.11)] depends on the time scale parameter α_i [Eq. (4.7)], the scaling parameters [Eqs. (4.8,4.9)], the exponent parameters [Eq. (4.12)], and the topology of the web. Making assumptions on body-size distribution, proportion of biomass flows, nonlinearities of growth and loss processes, and the predatory links between species determines these generalized parameters without the need for specifying initial conditions or specific functional forms.

The characteristic time scale, α_i, is a species' turnover rate or the reciprocal of an individual's average lifetime. Allometric regressions show that this attribute, as well as many other processes such as respiration and water absorption, is well predicted by species' body mass, $\alpha_i = m_i^{-0.3}$ (Hendriks; 1999).

The primary scale parameters [Eq. (4.8), summarized in Table 4.2] describe the proportional biomass flow between different source processes and between different loss processes,

Table 4.2: Primary scale parameters [Eq. (4.8)] for top, intermediate, and basal species.

Species type	σ_i	ϕ_i	μ_i	λ_i
top	0	1	1	0
intermediate	0	1	0	1
basal	1	0	0	1

each forming the convex combination $\sigma_i + \phi_i = 1$ and $\lambda_i + \mu_i = 1$. E.g., the proportion of predatory gain to that of total gain is $\phi_i = 1 - \sigma_i$. For a species without prey (basal species) the production process is assumed to be the only source process, $\sigma_i = 1$. For a species with predators all loss is assumed to be due to predation, $\lambda_i = 1$. For a species with no predators (top predator) all loss is due to other mortality (Gross and Feudel; 2006), $\mu = 1$.

The secondary scale parameters describe the relative weighting of predatory out-flows β_{ij} and the relative weighting of predatory in-flows γ_{ij}. β_{ij} is the portion of the flux that predator j takes from prey i relative to all predatory loss of i. If all predatory loss terms are equal, β_{ij} only depends on the number of predators C_i that species i has.

$$\beta_{ij} = 1/C_i, \quad \gamma_{ij} = 1/R_i. \tag{4.13}$$

Similarly, if all predatory gain terms for predator i are equal, γ_{ij} only depends on the number of prey items R_i of predator i. If i does not prey on j, then $\gamma_{ij} = 0$, and analogously, if j is not a predator of i, then $\beta_{ij} = 0$.

The production process $\mathscr{S}$ is often approximated with the logistic growth model, but many homologous functional forms follow the same nonlinearity range (Awender et al.; 2023). The nonlinearity of production $s_i^{(\chi_i)}$ approaches one as the (basal) population approaches zero, since production grows linearly with population for low populations. The nonlinearity decreases as basal population increases due to increased intraspecific competition. For the production processes with a defined carrying capacity, the nonlinearity approaches -∞ as the population approaches its carrying capacity. The nonlinearity of production is chosen within the range $s_i^{(\chi_i)} \in [-1, 1]$ to exclude systems with basal populations close to their carrying capacity.

Predatory growth processes $\mathscr{F}$ are often represented with a growth function that depends on tactics and attributes of the species regarding evasion or capture. The predatory response is the per capita growth and saturates at high prey density. Implying processes similar to Holling's type functional responses, the nonlinearity of predation with respect to prey population (nonlinearity of feeding) is chosen within the range $f_i^{(t_i)} \in [0.5, 2]$. The lower limit excludes food webs with high prey availability, since prey abundance is scarce in Arctic food webs, especially at steady state. The upper limit includes predator responses that

incorporate hunting skill requirements or evasive prey behavior, motivated from a Holling's type III response. The predatory growth is assumed to be linearly proportional to the predator biomass, $f_i^{(\chi_i)} = 1$.

Mortality processes $\mathscr{M}$ are often modeled as linear or quadratic functions, e.g., in Lotka-Volterra predator and competition models, but non-integer exponents between one and two might more accurately represent nature (Edwards and Bees; 2001; Lan and Li; 2008). In this study, the nonlinearity of mortality is set to $m_i^{(\chi_i)} = 1.6$, consistent with Gross et al. (2005).

The contribution C_{ij} of prey species j to the diet of predator i is assumed to be proportional to the abundance of prey (Gross and Feudel; 2006). The nonlinearity of contribution $c_{ij}^{(\chi_j)} = 1$ if species i is a predator of species j, and $c_{ij}^{(\chi_j)} = 0$ otherwise.

4.3.3 Measuring Stability

Two generalized parameters that determine food web dynamics are varied in this study, the nonlinearity of production $s_i^{(\chi_i)}$ and the nonlinearity of feeding $f_i^{(t_i)}$. The stability of one web, P (Awender et al.; 2021), is given by the percentage of stable equilibria out of 900 fixed points that evenly span the nonlinearity space, $s_i^{(\chi_i)} \in [-1, 1]$ and $f_i^{(t_i)} \in [0.5, 2]$. A completely unstable web is defined by $P = 0$.

The stability of a set of webs, typically a set of topologies, is quantified by $P_{avg}(y)$. It averages the web stability P over a range of networks with attribute y, with y (for example) representing network size N or network connectance C. Other measures of stability that apply to particular results are introduced in their context.

4.4 Impact of Refined Species Characteristics on Stability

In the "base model" the probability for a predatory link exclusively depends on the predator to prey body-mass ratio and follows the same function, Fig. 4.1, for all species; predatory in-flows (and out-flows) are equally weighted, Eq. (4.13). Realistic species characteristics based on phylogeny, prey preference and habitat compartmentalization are introduced to modify the base model and to assess their impact on network stability.

4.4.1 Adjusting the Base Model

§ Foraging Traits

Body size is a fundamental trait predicting a predator-prey interaction probability and strength for many species (Akin and Winemiller; 2008). However, models constrained only with body size predict the structure of real food webs with only limited accuracy. Better

prediction requires constraining with additional species-specific traits, where they are available (Naisbit et al.; 2012; Rohr et al.; 2010; Williams et al.; 2010). In this study, we only consider predator-specific traits and refer to them as "foraging traits".

The evolutionary history has shaped a diverse set of species in which a relatively small number of species underwent specialized behavioral and physiological adaptations that shift, expand, or restrict their foraging niche. For instance, not every predator has the same mouth-to-body size ratio. The bowhead whale, for example, is the largest species in the Southern Beaufort Sea (SBS) food web and generally considered to have considerable ecosystem importance. If we use only its body size to predict which species it is likely to ingest as food, we would predict its most likely prey is any of the large mammals in the SBS. However, we know bowhead whales are equipped with specialized feeding morphology, having evolved baleen and an oversized mouth to feed on very small but enormous energetic supply of plankton, which are far smaller than mass ratios would predict. Figure 4.2 compares bowhead whale prey size spectra to other species.

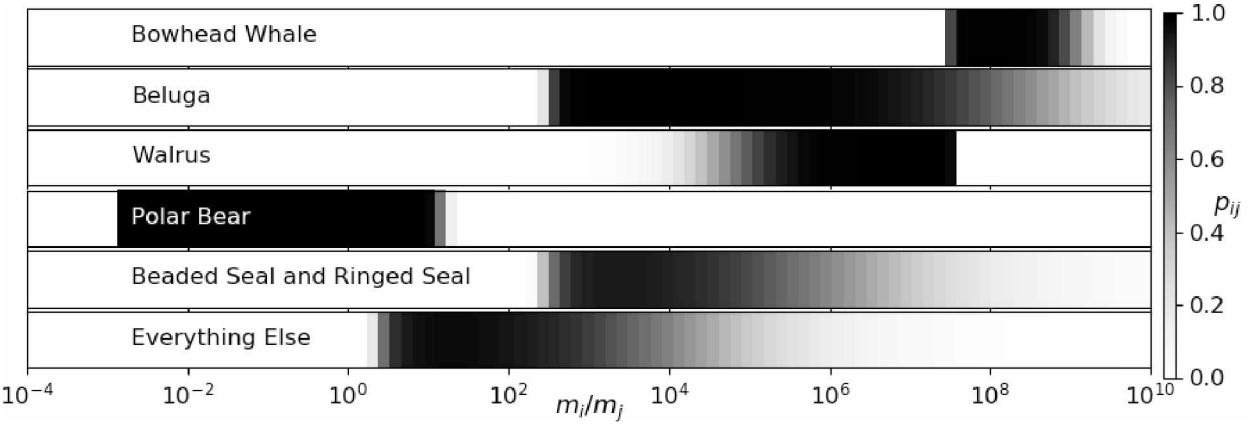

Figure 4.2: Linking probability, p_{ij}, that species i will prey on species j based on their body-mass ratio m_i/m_j, Eq. (4.1). The parameters a_i, b_i, c_i, d_i for the species are (1, 12, -8, 1e-7) bowhead whale, (0.4, 8.9, -3.3, 1e-2) beluga, (6, 3, -3, 5e7) pacific walrus, (70, 14, -20, 1e3) polar bear, (0.4, 4, -1.8, 1e-2) bearded seal and ringed seal, and the standard parameters (1.41, 3.73, -1.87, 1) for everything else (Fig. 4.1). For the walrus, m_i/m_j is also exchanged with m_j/m_i due to its preference of primarily eating mollusks(Dehn et al.; 2007).

In our system, six species are classified as "specialized species" and they each have unique linking probabilities [Eq. (4.1)] in comparison to the standard species in the base model, Fig. 4.2. These six species are the filter-feeding megafauna (bowhead whale), gape-limited cetacean and pinnipeds (beluga, walrus, bearded and ringed seal) and the super predator (polar bear). The gape-limited species have relatively small mouth-to-body size ratios and their linking probabilities are shifted to smaller prey. A "super predator" is a predator that feeds on the largest species in the system. The polar bear, being the only land species, is

an example that only eats the mammals in our model; we exclude any fish prey that may otherwise be of an appropriate mass for foraging. The linking probabilities of every species in a foraging traits model are shown in Figure 4.2.

§ Adjusting Weights of Predator-Prey Links

Once network links are probabilistically determined from body-mass ratios [Eq. (4.1)], the secondary scale parameters describing relative weights between predatory in-flow γ_{ij} or out-flow β_{ij}, Eq. (4.9), can be assigned. In the base model, flows into a predator are evenly distributed across all prey species connected to that predator. E.g., a predator connected to two prey species receives 50% of predation gain from each prey for its growth. Similarly, the outflow from a prey species into all of its predators is equally weighted.

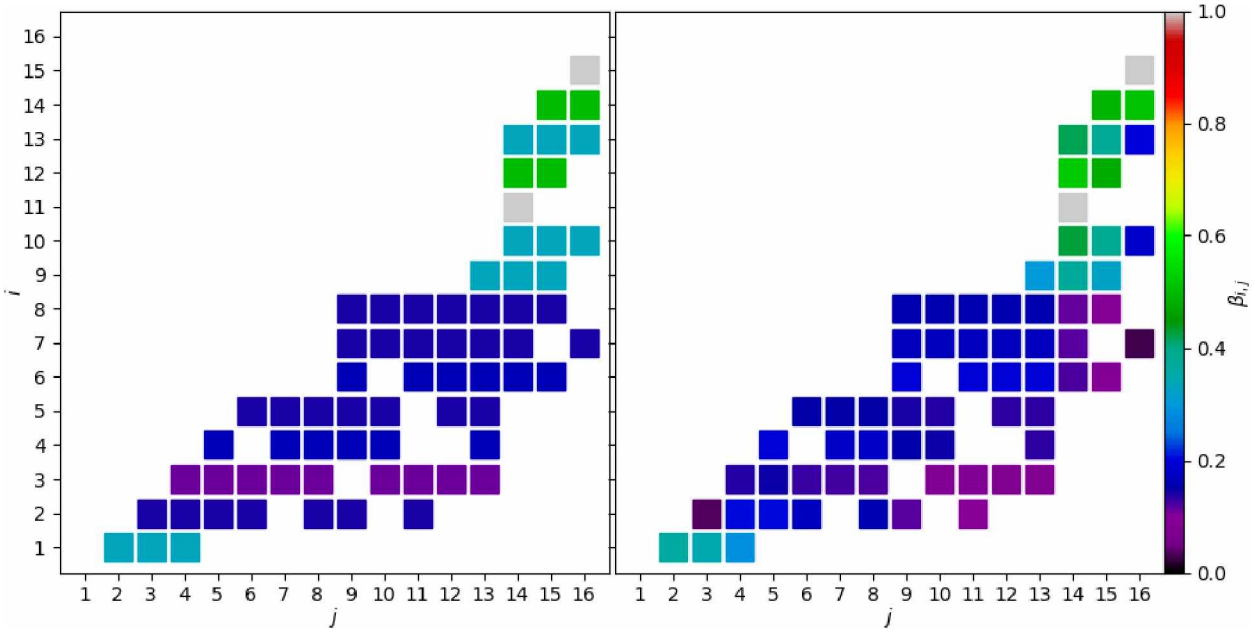

Figure 4.3: Proportional flows of predatory loss β_{ij} from prey i to predator j in a 16-species network with a) even weights (base model) and b) after adjusting the weights [Eq. (4.14)]. The indices are not species identifiers as in Table 4.1. The colored squares represent links and the value of β_{ij}.

In the adjusted weights model, link weights are proportional to the linking probability, p_{ij} [Eq. (4.1)]. This may better represent a predator's prey preference by enhancing the link weight for prey that are closer to the optimal prey body size (Yeakel et al.; 2014). The relative weights for predatory in-flow γ_{ij} and out-flow β_{ij} are defined as

$$\gamma_{ij} = \frac{p_{ij}}{\sum_\kappa p_{i\kappa}} \quad \text{and} \quad \beta_{ij} = \frac{p_{ji}}{\sum_k p_{ki}}, \tag{4.14}$$

where κ is in the set of prey items for x_i (in-degree of node x_i) and k is in the set of predators of x_i (out-degree of node x_i). Note, $\sum_n \gamma_{i,n} = \sum_n \beta_{i,n} = 1$, with n in the entire set of N species.

Figure 4.3 depicts the structural change of a network before and after adjusting the weights β_{ij}. For predatory outflow with equal weights the colors within a row are equal, while including prey preference can induce significant changes in the weights. This example has a rather large discrepancy, about 28%, in the norm of each weight matrix with elements β_{ij}. More typical examples for 16-species networks have a closer to 10-15% discrepancy.

§ Habitat Constraints

To our knowledge, no generalized modeling efforts have considered topologically structuring ecological networks into connected modules that represent the kind of modularity caused by habitat specialization from environmental differences across land or seascapes. Different habitats are spatially segregated within the larger ecosystem. Most species frequent a subset of available habitats, which inhibits some members from one habitat to interact with members from another habitat. Based on the limited number of species and the most encompassing and frequent habitat descriptions, we classify five habitat types within our larger ecosystem model, Table 4.1. Near or at the ocean surface, the photic zone is segmented into three zones based on distance to the coast; from farthest to closest, they are oceanic (open ocean), neritic (shelf), and littoral (tidal, sub-tidal) zones. The remainder of the marine ecosystem is divided into benthic (sea floor) and midwater habitats.

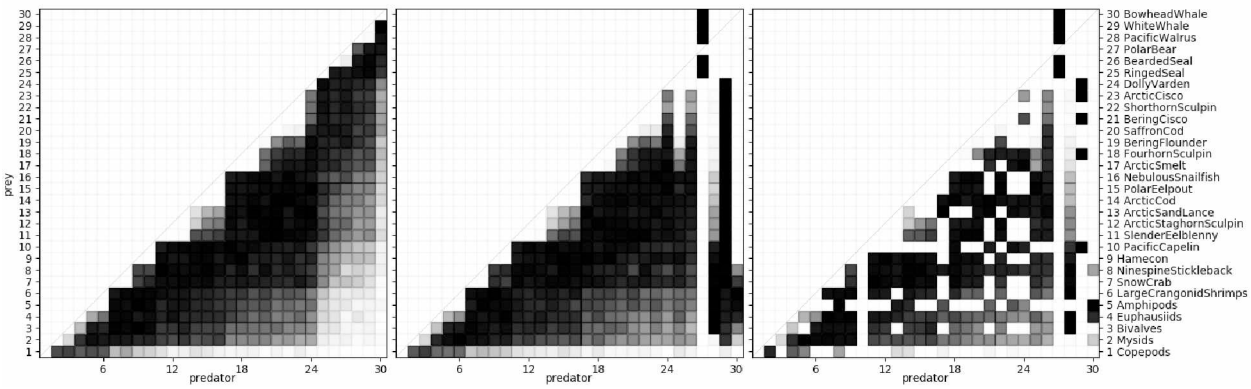

Figure 4.4: 30-species adjacency matrices superimposed from 100 topologies for (a) the base model [Eq. (4.1)], (b) the base model with foraging traits (Fig. 4.2), and (c) the base model with habitat constraints [Table 4.1] and foraging traits. A darker color represents more link occurrences and white represents no occurrences.

Habitat constraints are imposed with the assertion that any two species obey the linking probability [Eq. (4.1)] if they are members of a common habitat. If they do not have a

Table 4.3: Stability measures for the different models: Total average stability $\overline{P}$ over 280,000 webs (independent of network size) for each model, and corresponding relative changes $\Delta\tilde{P}_y$ in integral web stability [Eq. (4.16)] for y being N, C, or R. The N column is exact, while the C and R columns show averages from arbitrary binning into 10 to 30 intervals (Fig. 4.6).

Model	$\overline{P}$	$\Delta\tilde{P}_y$[%]		
Base	0.26	N	C	R
Foraging Traits	0.30	17	2	-21
Adjusted Weights	0.31	20	6	21
Habitats	0.38	49	11	16
Full	0.45	82	49	4

habitat in common the linking probability is set to zero. Thus habitat constraints decrease the total number of realized connections in a network. This is graphically expressed by the frequency of link occurrences in accumulated adjacency matrices (Fig. 4.4). While adding foraging traits of specialized species to the base model rearranges elements in the matrix (Fig. 4.4b), a decrease in connectance is inferred once the habitat constraint is imposed (Fig. 4.4c). Since some species are members of multiple habitats, cross-habitat links occur to generate a connected network with a degree of modularity instead of disjoint modules. The link occurrence density in Fig. 4.4 also reflects the linking probability curves from Fig. 4.2 for the individual species.

4.4.2 Results

Network stability is discussed for five models, the "base model" (Sec. 4.3.2), the "foraging traits model" (Sec. 4.4.1), the "adjusted weights model" (Sec. 4.4.1), the "habitat constraints model" (Sec. 4.4.1), and the "full model", which combines all three realistic characteristics into a single model. A data set of 280,000 webs, consisting of 10,000 webs for each size from N=3 to N=30, is generated for each model.

The total average stability, $\overline{P}$, is the average of P, a single web's proportion of stable equilibria (Sec. 4.3.3), over all 280,000 webs (independent of network size) for a given model. Each realistic feature increases network stability in terms of $\overline{P}$ in comparison to the stability of the base model, summarized in Table 4.3. While adjusting foraging traits or weights increases stability by 15% to 19%, the habitat constraints increase stability by 46%. The full model has almost twice as many stable equilibria than the base model.

Figure 4.5 shows network stability $P_{avg}(N)$ as a function of network size N for the different models, averaging over 10,000 webs for each N. Each refined species characteristics, whether it is foraging traits, prey preference, of habitat constraints, leads to an increase in web stability $P_{avg}(N)$ over a particular range of network sizes and an overall gain in network

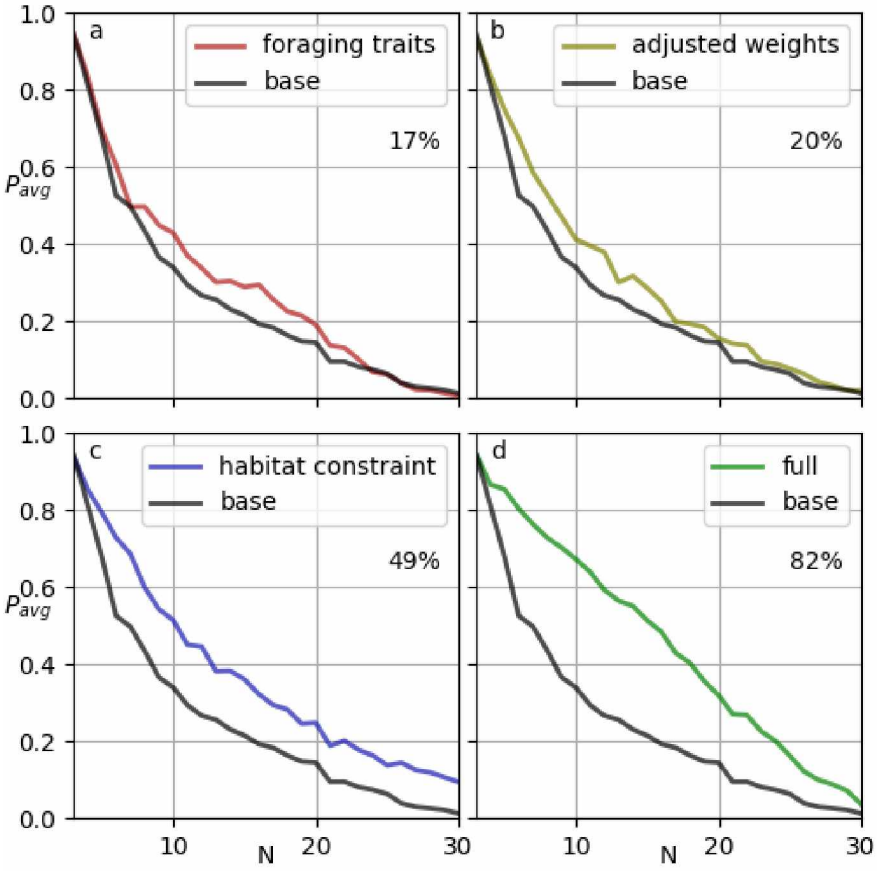

Figure 4.5: Comparing average stability, P_{avg}, of the base model to the added-feature models against network size N for a) the "foraging traits model", b) the "adjusted weights model", c) the "habitat constraints model", and d) the "full model". The text shows the percent change of the areas under the curves. 10,000 webs are used for each network size, $N \in [3, 30]$, resulting in 280,000 webs for each model.

stability. The largest individual gain in stability is reached from habitat compartmentalization, Fig. 4.5(c); integrating over all network sizes the stability is increased by about 50% in comparison to the base model. Combining all the refined species characteristics in the full model, the number of stable webs almost doubled in comparison to the base model, Fig. 4.5(d).

The average web stability P_{avg} is also affected by different aspects of network topology. The connectance C represents the overall density of links in a network, the proportion of possible connections that actually occur. Webs with small connectances are less stable for the "full model" than for the base model, and webs with large connectances are more stable for the full model, Fig 4.6(a). The findings for the "habitat model" are similar to the "full model", while the "foraging traits model" and the "weights model" show little difference in $P_{avg}(C)$ to the base model. $P_{avg}(C)$ closely agrees for all models at intermediate connectances

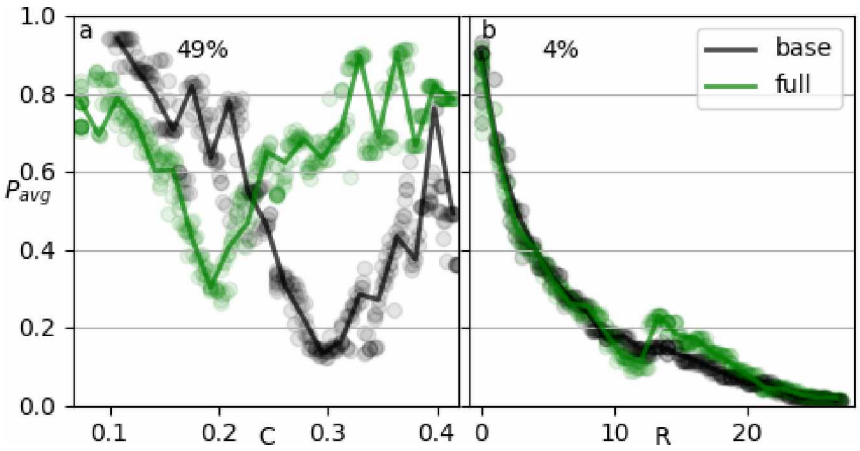

Figure 4.6: Comparing average stability, P_{avg}, of the "full model" to the base model against a) connectance C and b) intermediate-to-top predator ratio R, using all webs from Fig. 4.5. A lower value in R corresponds to fewer mesopredators in the network. The average stability depends on the number of bins; the solid curves correspond to 22 bins, and the scattered data correspond to between 10 and 30 bins. The text shows the average integral percent change from all the different binning choices.

around $C = 0.25$. Connectedness between predators is expressed by the number of intermediate predators (mesopredators) to the number of top predators, R. The intermediate-to-top predator ratio R largely agrees for the "full model" and the base model, but shows a small increase of $P_{avg}(R)$ for $13 < R < 20$ and a small decrease for $10 < R < 13$ for the "full model", Fig. 4.6(b). Deviations from the stability of the base model vary for each "added-feature model". For the "foraging traits model", $P_{avg}(R)$ decreases for $0 < R < 10$, for the "adjusting weights model" $P_{avg}(R)$ increases for all R, and for the "habitat constraints model" $P_{avg}(R)$ increases for $12 < R$ with minimal difference elsewhere.

The integral web stability is defined as

$$\tilde{P}_y = \int_a^b P_{avg}(y)dy, \tag{4.15}$$

with y being network size N, connectance C, or intermediate-to-top predator ratio R, and a, b the bounds of the domain of y such that $\tilde{P}_y$ represents the area under the corresponding curves in Figs. 4.5 and 4.6. Relative changes in $\tilde{P}_y$ between the base model and any of the four models with realistic modifications are given by

$$\Delta\tilde{P}_y = (\tilde{P}_{y,\text{model}} - \tilde{P}_{y,\text{base}})/\tilde{P}_{y,\text{base}}, \tag{4.16}$$

and summarized in Table 4.3. For each realistic feature and all network specifiers N, C, and R the integral web stability $\tilde{P}_y$ increases in comparison to the base model, except for the

"foraging traits model" with respect to the predator ratio R.

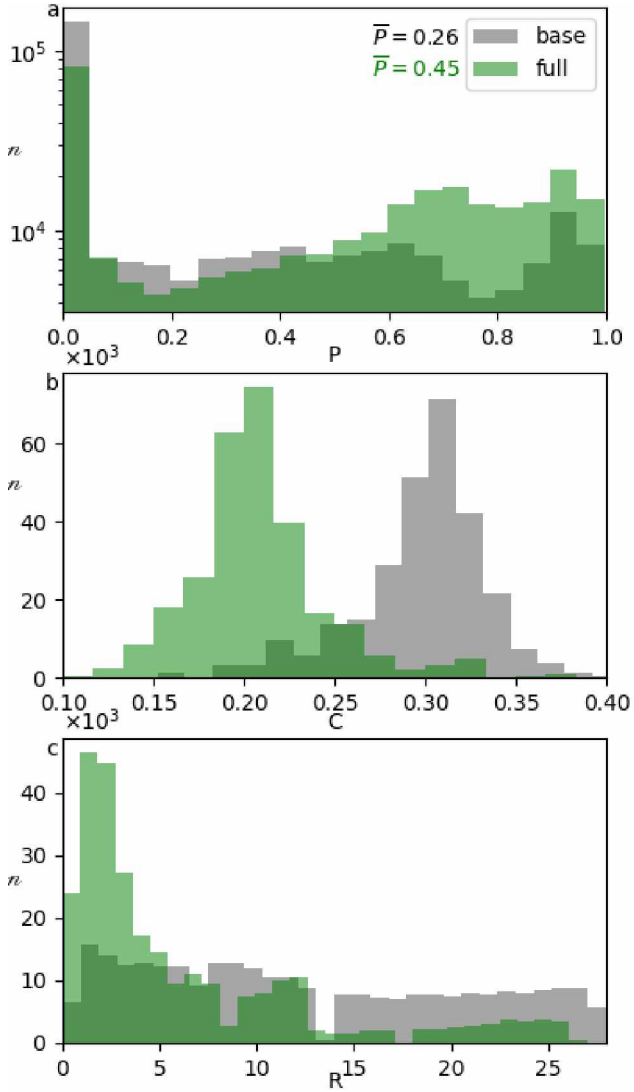

Figure 4.7: Comparative number histograms from 280,000 web realizations of the base model and the full model for a) a web's proportion of stable equilibria P, b) connectance C, and c) intermediate-to-top predator ratio R. The total average stability $\overline{P}$ is written in (a).

In an attempt to explain why webs tend to be more stable when realistic characteristics are in effect, we study histograms of a web's proportion of stable equilibria, P, connectance, C, and intermediate-to-top predator ratio, R, for 280,000 realizations of the base model and the full model, Fig. 4.7. These histograms reveal that the base model has significantly more completely unstable webs ($P = 0$) and larger connectances than the full model. Additionally, the distribution of intermediate-to-top predator ratios is relatively even in the base model, but heavily concentrated toward smaller ratios in the full model.

It is well established that more connected networks tend to be less stable (May; 1972;

Gross and Feudel; 2006). Incorporating habitat constraints decreases the number of realized links and therefore connectance, and thus habitat compartmentalization presents one way real ecosystem networks might have lower connectances and therefore higher stability. The habitat constrained model has a similar distribution of connectances than the full model [Fig. 4.7(b)], but with a slightly larger median. This is consistent with lower average web stability in the habitat constrained model in comparison to the full model, but both models' stability is significantly higher than for the base model, Table 4.3.

The other important topological feature that positively impacts stability is a lower intermediate-to-top predator ratio R (Awender et al.; 2021). Decreasing the number of intermediate predators relative to the number of top predators tends to increase overall system stability for the full model versus the base model, Fig. 4.7(c). The simulations also reveal (not shown) that the foraging trait model has more web realizations with $R < 5$ than with $6 < R < 23$, and the habitat constraints model has more realizations with $R < 14$ than with large ratios, $R > 14$. The prevalence of smaller intermediate-to-top predator ratios for both models and their increase in overall stability is consistent with the stability trend about R.

The decrease in mean connectance and mean intermediate-to-top predator ratio helps to explain why the webs become more stable, but they do not explain the increase in stability from adjusting the weights since that modification does not affect these measures.

4.5 Impact of Species Introduction and Removal on Stability

Arctic sea-ice extent has been trending downward for nearly four decades, resulting in 30% less ice in the month of September (Box et al.; 2019). As ice declines, ice-obligate species such as polar bear, arctic cod, and walrus are likely to decline and/or become extirpated from some areas of the Arctic, and thus would no longer be members of the ecosystem in those regions. Sea-ice loss also permits more temperate species to move into Arctic habitats (Moore and Huntington; 2008). One such prominent, recent addition to some Arctic regions are killer whales; declining sea ice has allowed these southern visitors to penetrate farther north and stay longer during summers (Higdon and Ferguson; n.d.). Also, sea-ice loss and generally warmer sea waters may allow more southerly distributed forage fish species, such as saffron cod to become formidable competitors to arctic cod (Deary et al.; 2021).

To understand how ecosystems might be impacted by such species introductions and removals, we construct a series of generalized models to assess how changes in species composition affect patterns of ecosystem stability, Fig 4.8. Specifically, we assess the impacts of loss of polar bear by sorting webs into groups with and without polar bears and evalu-

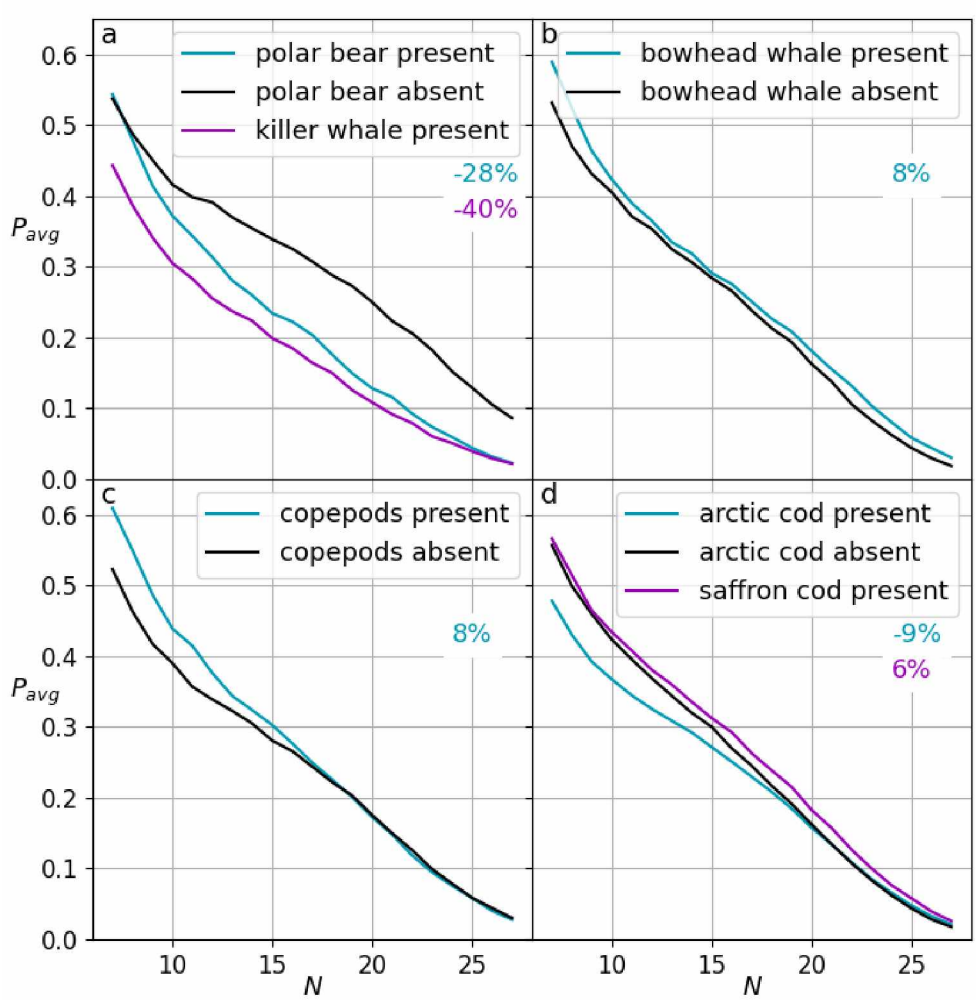

Figure 4.8: Comparing the average stability of webs P_{avg} grouped by network size N for webs with and without select species. a) webs with polar bear (green), webs without polar bear (black), and webs with killer whale instead of polar bear (red), b) webs with bowhead whale (green) and without bowhead whale (black), c) webs with copepods (green) and without copepods (black), and d) webs with arctic cod and no saffron cod (green), webs without either cod (black), and webs with saffron cod and no arctic cod (red).

ate differences in average stability with respect to network size. Additionally, we compare networks where killer whales are replacing polar bears as top predators, Fig 4.8a.

The removal of polar bears results in a strong increase in food-web stability for networks with ten or more species, Fig 4.8a. As a top predator, polar bear feed on other large mammals (e.g. seals, walrus) in the ecosystem, which in turn primarily feed on smaller species such as fish and bivalves. In the absence of polar bears, these seal and walrus mesopredators become top predators (Fig 4.9). In effect, the loss of polar bears from an ecosystem with multiple large mesopredators creates a system that is effectively more diverse in top predators, which lowers the intermediate-to-top predator ratio, R. In theoretical ecosystems, lowering R

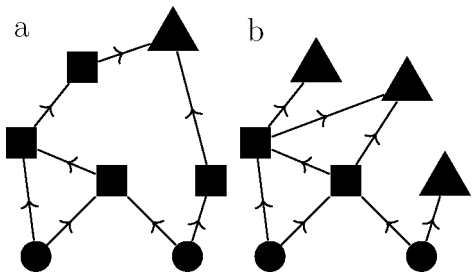

Figure 4.9: An example of a significant decrease in the intermediate/top predator ratio, R, due to the absence of a super predator. a) A 7-species topology present in the set of webs with a polar bear, $R = 4/1$, and b) a 7-species topology present in the set without the polar bear, $R = 2/3$. The symbols represent top predators (triangle), intermediate predators (square), and basal species (circle).

improves overall system stability (Awender et al.; 2021).

When killer whales are added to replace polar bears, the increase in stability is reversed. Here, killer whales are assumed to be a standard species with normal size-selective predatory behavior [Eq. (4.1)]. As killer whales are large, they become a new, single top predator able to prey upon most of the largest ecosystem members, and the system has a lower diversity of top predators. This effectively lowers the intermediate-to-top predator ratio R considerably, and stability declines markedly. Our findings imply that a lack of a fierce top predator (super predator: killer whale or polar bear) produces more stable equilibria from the effect of generating less completely unstable webs ($P = 0$).

Similarly, the ratio of intermediate to basal species also impacts stability and in real webs may be a useful indicator of average stability. The very small copepods may serve a similar function as a super predator, but imposing stability from a perspective of flows coming into the system rather than out. In our SBS webs, when copepods are present, fewer basal species appear in the generated ecosystem networks. Removing copepods results in a decline in average stability for smaller webs, $N < 16$, but has no effect on larger webs (Fig. 4.8 c).

Finally, we explore the impact of replacement of arctic cod with saffron. Removal of arctic cod increases average stability for small networks, and the introduction of saffron cod overall increases average stability further (Fig 4.8 d). The presence of bowhead whale, too, creates more stable points over all N (Fig. 4.8 b). The effects of removal of bowhead whales, copepods, and replacement of arctic with saffron cod on stability, however, are much smaller than the impacts from the presence of super predators.

4.6 Impact of Background Species on Stability

A significant difficulty of accurate food web modeling, assuming enough computational power and time, is empirically sampling and enumerating all ecosystem members of real webs, along with their vital rates and ecological properties. Real webs often contain too many organisms with differing birth, death, and other vital rates and unique feeding behaviors, to collect and include such information for every species. In most ecosystems, however, the vast majority of these species represent minor members that contribute little to the total biomass and have minimal influence on ecosystem dynamics or function. Such members are typically not included in ecosystem models for they are assumed to have effectively no impact; however, ignoring their potential collective impact on stability may lead to incorrect conclusions, and they may have a moderating influence on the effects of major ecosystem members that are of explicit interest. Thus, in our final set of analyses, we assess if the collective impact of minor ecosystem members potentially impart ecosystem stability that differs from models which include only major ecosystem players and ignore all minor members.

Even the depauperate Arctic ecosystems we model here contain thousands of identifiable species, but biomass differences create an ecosystem primarily forced by a much smaller number of the most abundant species. Rare species with very small abundances interact by the same processes, but each of these thousands of minor species have essential no ecosystem impact when considered individually.

4.6.1 Adjusting the Model

A "background food web" is constructed with all thirty species from Table 4.1 and accumulating the predatory links from 1000 realizations of topologies that include habitat constraints and foraging traits with the goal to represent every practically possible predator-prey connection in the SBS model ecosystem, Fig. 4.4c. This background food web and the corresponding adjacency matrix is the same for each simulation. A "main food web" consists only of major species. It is composed of 15 random species that are connected based on foraging traits and habitat constraints.

Both food webs are combined to generate a 30 species web with major and minor species and main links and background links. The 15 species that are not major species are minor species ("background species"). The modifications to the scaling parameters for the main web that result from background links are determined; they affect the Jacobian matrix and thus the stability of the main web. The links that the background has that the main web does not are given proportional flows of predatory gain γ_{back} or predatory loss β_{back}, and set to a small positive number, $b \ll 1$,

$$\gamma_{ij}^{B} = \gamma_{\text{back}} = b, \qquad \beta_{ij}^{B} = \beta_{\text{back}} = b. \tag{4.17}$$

The links of the main web have proportional flow weights γ_{ij}^{M} and β_{ij}^{M}, in analogy to Eq. (4.13),

$$\gamma_{ij}^{M} = \frac{1 - bR_i^B}{R_i^M}, \qquad \beta_{ij}^{M} = \frac{1 - bC_i^B}{C_i^M}. \tag{4.18}$$

R_i^M is the number of main prey items to x_i and its number of background-prey connections is R_i^B. C_i^M is the number of main predators of x_i and its number of background-predator connections is C_i^B. The total number of predators to x_i is $C_i^M + C_i^B = C_i$ while its total number of prey items is $R_i^M + R_i^B = R_i$. If $\gamma_{ij}^M < \gamma_{\text{back}}$ or $R_i^M = 0$, then $\gamma_{ij} = 1/R_i$ for all predatory inflows to species i. If $\beta_{ij}^M < \beta_{\text{back}}$ or $C_i^M = 0$, then $\beta_{ij} = 1/C_i$ for all predatory outflows from i.

In special cases, the primary scaling parameters for the main web also need to be adjusted in the presence of background species. If x_i represents a basal species in the main web and an intermediate predator with the background, the growth parameters are adjusted to

$$\sigma_i = 1 - b, \qquad \phi_i = b. \tag{4.19}$$

If x_i represents a top predator in the main web but is an intermediate predator with the background, then the loss parameters become

$$\mu_i = 1 - b, \qquad \lambda_i = b. \tag{4.20}$$

All other parameters declarations are unchanged. The stability is computed from the Jacobian matrix for the main food web; it has elements J_{ij}, where i and j are main members. The deterministic noise from the minor species on the main web is the collective effect of the perturbed scale parameters from an increasing background pressure, b, that values between zero and 0.02. The upper limit for b is determined from the condition that the norm of the difference matrix of the main web's Jacobian with a background perturbation has at most a 10% discrepancy to the norm of the Jacobian when $b = 0$.

4.6.2 Results

This study considers 6710 main-web topologies, and each topology considers 900 different nonlinearity parameters. $P(b)$ describes the percentage of stable webs for a given main-web topology and a given background pressure b, with $b \in [0, 0.02]$.

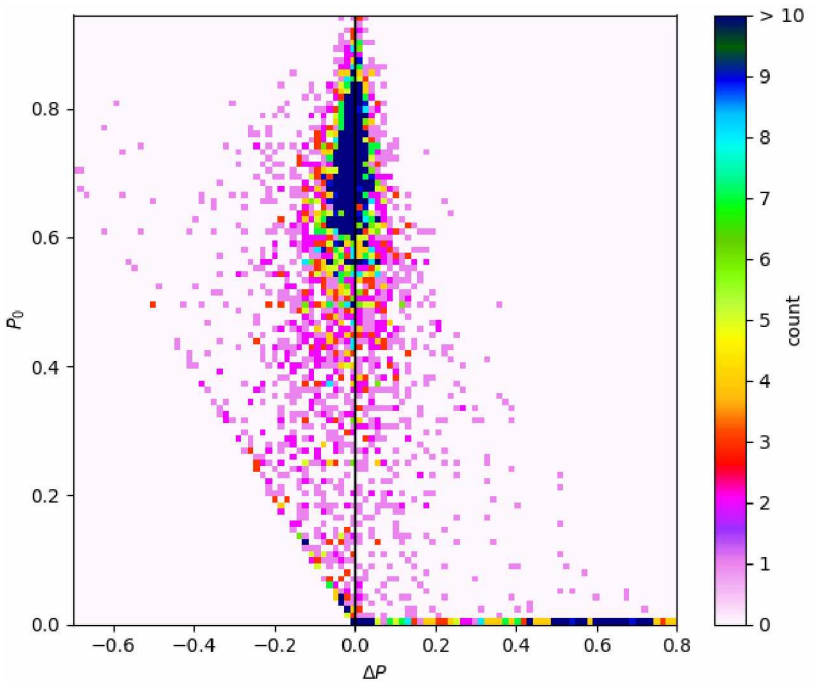

Figure 4.10: Main-web stability in the absence of background species, $P_0 = P(b = 0)$ in comparison to $P(b = 0.02)$ in the presence of background species. The number of main webs (color coded), out of 6710 topologies, is scattered by unperturbed stability P_0 and the change in stability, $\Delta P = P(b = 0.02) - P(b = 0)$.

The background pressure has varying perturbation effects on the main-web's stability. For some main webs, the stability $P(b)$ increases, for some it decreases, and for some it switches from completely unstable $P(b) = 0$ to having stable webs, $P(b) > 0$. Figure 4.10 shows the effect of background pressure of $b = 0.02$ for the 6710 webs. For most topologies the stability fluctuates within 10% when adding background species. Some webs have well over a 200% stability increase. About one third of the webs with a zero unperturbed stability, $P(b = 0) = 0$, are stabilized through the background pressure, i.e. $P(b = 0.02) > 0$. Also, about 2.5% of the webs that have a nonzero unperturbed stability, $P(b = 0) > 0$, are completely destabilized with the full perturbation, i.e. $P(b = 0.02) = 0$, visible in form of the diagonal line in Fig. 4.10.

The average stability $P(b)_{avg}$, which is $P(b)$ averaged over the 6710 main-web topologies, reveals a significant and steep increase of stability for already small background pressure b, Fig 4.11. The average stability exhibits a maximum value around $b = 0.003$ that represents an about 8% increase in average stability from the unperturbed web. This maximum is a consequence of two competing effects. Most of the completely unstable webs, $P(b = 0) = 0$, stabilize quickly on the b-scale, from very small background pressure on, $b \approx 10^{-4}$. This dominates the steep increase in $P(b)_{avg}$. Overall, increasing background pressure decreases

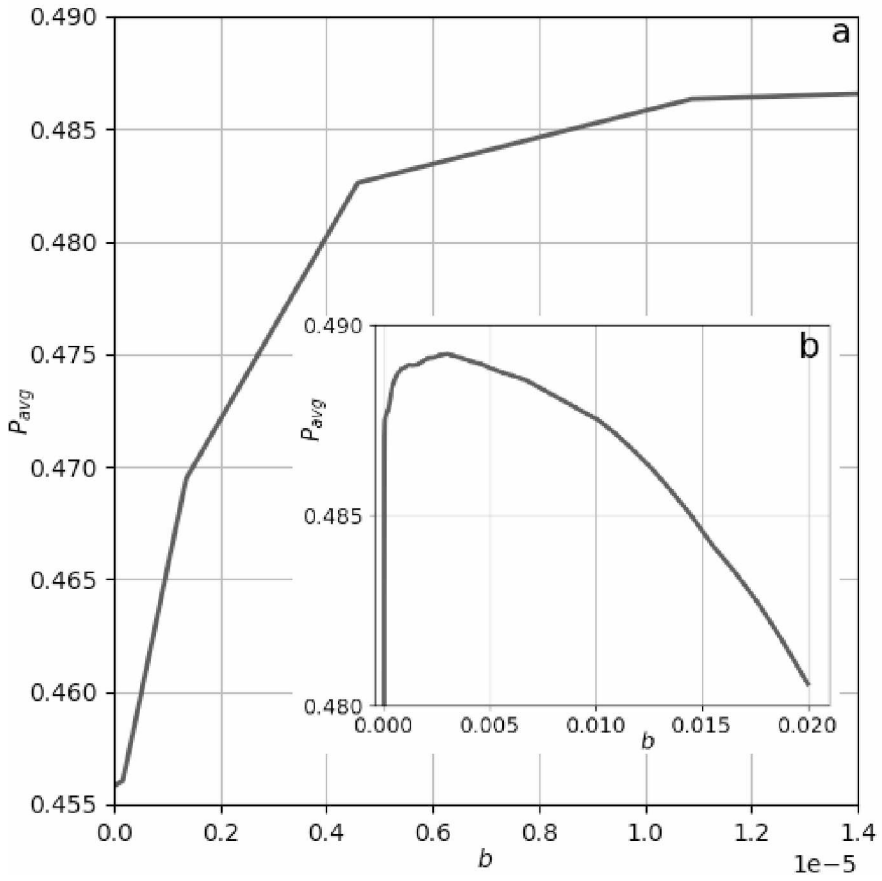

Figure 4.11: Average stability P_{avg} of main webs for 6710 main-web topologies as a function of background link weight b near $b = 0$ and for the entire b-range (inset). Without background species, $P_{avg}(b = 0) = 0.455$.

stability, although background pressure both increases stability on some main webs and decreases stability on others.

4.7 Conclusion

Discrepancies between theoretical and empirical evidence on food-web stability is common in ecological literature, especially about how empirical systems appear to exhibit greater stability properties than related mathematical simulations. Topics with such discourse, with particular application of generalized ecological models, are known as "paradox of enrichment" (Roy and Chattopadhyay; 2007) and "complexity-stability debate" (Belgrano et al.; 2005). A central ground that many believe holds the key to resolving such discrepancies lies in rhetoric about reductionistic versus holistic approaches (Polis; 1998). That is to say, refining models with more realistic detail to account for the complex intricacies of the nature and operation of ecological systems may bridge the gap between simulation and empirical observation. With

this premise, we investigate food-web models that resemble those found in an Arctic marine ecosystem and follow the stability implications after sequential refinements are incorporated as more realistic hypotheses are considered.

Thirty species from the Southern Beaufort Sea (SBS) are deliberately chosen based on high ecological significance in this Arctic marine environment. Over a million food webs are reconstructed from five different probabilistic food-web generating algorithms that take body-mass ratios as arguments. The first algorithm is the "base model" that permits predator-prey connections between any pair of species and every species has the same foraging behavior. Modifications to the algorithm are intended to better reflect reality. These modifications include specialized species that are known to form predator-prey connections that would not normally be predicted to exist, predator's prey preference that enhances the dependence on particular prey that should be more suitable and weakens dependence on prey that is less suitable, and restricting realized connections to be between species that share a common habitat. The stability of these systems is defined from the local stability of fixed points as a function of "nonlinearity" space, obtained with a powerful modeling technique known as generalized modeling (Gross and Feudel; 2006; Kuehn et al.; 2013).

In the base model (generic structuring algorithm), the webs are constructed with the assumption that every species shares the same general feeding trend of consuming species within a certain size range relative to that of the predator, this is referred to as the generic linking probability. In real food webs, specialized species diverge from the generic linking probability. For instance, a generalist would indicate an expansion of the linking probability to feed on a wider variety of prey body sizes, while a specialist would indicate a narrowing of the feeding trend. Only six species (the marine mammals) are developed as specialized species. The food webs that are realized with specialized feeders increase the total number of stable fixed points by 15%.

The second modification is an adjustment of the flow distribution to account for a predator's prey preference. In the base model, if a particular predator has multiple prey items (or a particular prey species has multiple predators), the in-flows (out-flows) of that particular species are evenly distributed. To incorporate prey preference, the balance of flows is redistributed to reflect that the most likely links hold the most weight and the less likely links hold the least weight. The food webs that are realized with prey preference increase the total number of stable fixed points by 19%.

The last modification to the base model uses five different species pools that represent five different marine habitats. Only species that share a common habitat can potentially form a link. This habitat constraint creates food webs with smaller connectances (link density), a measure with a negative relationship to stability in random and niche-model

networks (Gross and Feudel; 2006; May; 1972). The food webs that are realized with habitat constraints increase the total number of stable fixed points by 46%.

We find the food webs with more realistic structures have more stable fixed points than those from the less realistic (more generic) structuring algorithm. The largest increase in the number of stable fixed points is when all three modifications are used in conjunction, increasing the number of stable fixed points by 73%. Most of the increase in the number of stable fixed points arises from the creation of fewer completely unstable webs. The habitat constraint decreases connectance although it is inconclusive how much the decrease in connectance contributes to the increase in stable fixed points. Also, both specialized species and habitat constraints decreases the average intermediate-to-top predator ratio, another measure with a negative relationship to stability of ecological networks (Awender et al.; 2021). However, proportioning the weights to simulate prey preference has no effect on the structural measurements, connectance and predator ratio, yet stability still increases.

Arctic amplification is causing the Arctic to warm faster than the global-warming rate (Rantanen et al.; 2022). Rising temperatures in the Arctic causes less sea ice and warmer waters. Sea ice is a critical habitat for the many sympagic species populating the Arctic and serves as a physical barrier for many other species. Warmer waters change the efficiencies and rates of various biological processes of each species differently. Thus, as sympagic species experience habitat loss and some southern species compete better in the warmer waters, the ecosystem is anticipated to restructure by means of a changing species composition and redistribution of biomass. Motivated from this portent of a changing species composition, we investigate how the presence and absence of some species affect overall stability. Ice-obligate species (polar bear and arctic cod), mass-outliers (bowhead whale and copepods), and "invasive" species (killer whale and saffron cod) are investigated. The presence of each species has little effect to overall stability ($< 10\%$ change), except for the large-bodied predators. The polar bear's presence decreases overall stability by 28% and the killer whale's presence decreases stability by 40%. Although apex predators are thought to enhance biodiversity (Wallach et al.; 2015), super killers in general may have a destabilizing impact on fixed-point stability.

In spite of the harsh Arctic conditions, the real SBS ecosystem is much bigger than 30 species. For instance, one network node represents a trophospecies named bivalves, but there could be as many as 30 bivalve taxa (Carey Jr et al.; 1984) and thousands of zoobenthos in the SBS (Bluhm et al.; 2011). Dynamical ecological models often only include up to tens of species and try to include the most important players; however, infrequent or rare species or otherwise rare predator-prey interactions are a forcing on the focused system. We suppose a 15-species network, referred to as the main web, is subsumed by the larger 30-species

ecosystem that effectively represents all the possible links. The added links and added species that are needed to create the complete web from the main web are collectively referred to as the "background" network. The relative weighting of the links in the background network contribute the same weak characteristic perturbation strength. Applying this perturbation of a phantom network to over six thousand realized main webs stabilizes (more stable fixed points) a third of the completely unstable main webs from a weak perturbation strength. This perturbation strength can be one part in a hundred thousand (1×10^{-5}) yet increases average stability by 7%. Increasing the perturbation strength past three parts in a thousand (3×10^{-3}) begins a slow descent of the average stability, defining an optimal perturbation strength.

Suggested improvements or furtherance of this work - Improving the species composition for a more complete picture improves the accuracy about real webs and makes new research opportunities. The smallest organism in these models is zooplankton (copepods), thus, the ecological networks in this paper are animal communities. A smaller-bodied but diverse Arctic taxonomic realm is primary producers, ice algae and phytoplankton; other primary producers are seaweeds (Bluhm et al.; 2011). A few other species candidates are the widespread brittle star, subsistence hunters, and invading gray whale (Stafford et al.; 2007). Obtaining a more comprehensive design of the taxonomic realms opens another study with modularity (Newman; 2018) in ecological networks (Allesina; 2008). Different modules containing entire taxon groups (e.g. primary producers, zooplankton and sea-ice fauna, fish, marine mammals and seabirds, zoobenthos, etc. (Bluhm et al.; 2011)) can be identified. Not to be confused with the similar idea of trophospecies, the grouping of many taxa into a single network node. Focusing on taxon modules and keeping in mind how busy food webs can operate in the same way as simplified, counter-part webs or chains (Gross et al.; 2005; Awender et al.; 2021) is a prospect for interesting discoveries.

Other suggestions for improvements and furtherance include more accurate depiction of the actual food-web links and explicit incorporation of climate. More empirical studies of stomach contents and stable isotopes refine our knowledge of the actual predator-prey connections and their flow magnitudes. This would impel the development of more specialized species and reformation of the linking probabilities. Explicit use of a climatic function would create ecological networks that entangle the physical environment into the organism communities, a concept not yet explored with generalized models as far as we know. For instance, a sea ice function may represent ice-sea extent or thickness, and has a positive effect on ice-obligate species (Moore and Huntington; 2008) and a negative effect on others.

4.8 References

Akin, S. and Winemiller, K. O. (2008). Body size and trophic position in a temperate estuarine food web, *Acta Oecol.* **33**(2): 144.

Allesina, S. (2008). Cycling and cycling indices, *Ecosystem Ecology*, Elsevier.

Awender, S., Wackerbauer, R. and Breed, G. A. (2021). Stability of generalized ecological-network models, *Chaos* **31**(2): 023106.

Awender, S., Wackerbauer, R. and Breed, G. A. (2023). Combining generalized modeling and specific modeling in the analysis of ecological networks, *Chaos: An Interdisciplinary Journal of Nonlinear Science* **33**(3): 033130.

Belgrano, A., Scharler, U. M., Dunne, J., Ulanowicz, R. E. et al. (2005). *Aquatic food webs: an ecosystem approach*, Oxford University Press.

Bluhm, B. A., Gebruk, A. V., Gradinger, R., Hopcroft, R. R., Huettmann, F., Kosobokova, K. N., Sirenko, B. I. and Weslawski, J. M. (2011). Arctic marine biodiversity: An update of species richness and examples of biodiversity change, *Oceanography* **24**(3): 232.

Box, J. E., Colgan, W. T., Christensen, T. R., Schmidt, N. M., Lund, M., Parmentier, F.-J. W., Brown, R., Bhatt, U. S., Euskirchen, E. S., Romanovsky, V. E. et al. (2019). Key indicators of Arctic climate change: 1971–2017, *Environ. Res. Lett.* **14**(4): 045010.

Breed, G. A., Stichter, S. and Crone, E. E. (2013). Climate-driven changes in northeastern US butterfly communities, *Nat. Clim. Change* **3**(2): 142.

Carey Jr, A. G., Scott, P. H. and Walters, K. R. (1984). Distributional ecology of shallow southwestern Beaufort Sea (Arctic Ocean) bivalve mollusca, *Mar. Ecol. Prog. Ser.* p. 125.

Deary, A., Vestfals, C., Mueter, F., Logerwell, E., Goldstein, E., Stabeno, P., Danielson, S., Hopcroft, R. and Duffy-Anderson, J. (2021). Seasonal abundance, distribution, and growth of the early life stages of polar cod (Boreogadus saida) and saffron cod (Eleginus gracilis) in the US Arctic, *Polar Biol.* **44**(11): 2055.

Dehn, L.-A., Sheffield, G. G., Follmann, E. H., Duffy, L. K., Thomas, D. L. and O'Hara, T. M. (2007). Feeding ecology of phocid seals and some walrus in the Alaskan and Canadian Arctic as determined by stomach contents and stable isotope analysis, *Polar Biol.* **30**(2): 167.

Divine, L. M. (2016). *Trophic dynamics and stock characteristics of snow crabs, Chionoecetes opilio, in the Alaskan Arctic*, University of Alaska Fairbanks.

Edwards, A. M. and Bees, M. A. (2001). Generic dynamics of a simple plankton population model with a non-integer exponent of closure, *Chaos Solitons Fractals* **12**(2): 289.

Gray, B. P., Norcross, B. L., Beaudreau, A. H., Blanchard, A. L. and Seitz, A. C. (n.d.). Food habits of Arctic staghorn sculpin (Gymnocanthus tricuspis) and shorthorn sculpin (Myoxocephalus scorpius) in the northeastern Chukchi and western Beaufort Seas., *Deep Sea Res. Part II Top. Stud. Oceanogr.* **135**: 111.

Gross, T., Ebenhöh, W. and Feudel, U. (2005). Long food chains are in general chaotic, *Oikos* **109**(1): 135.

Gross, T. and Feudel, U. (2006). Generalized models as a universal approach to the analysis of nonlinear dynamical systems, *Phys. Rev. E* **73**(1): 016205.

Hendriks, A. J. (1999). Allometric scaling of rate, age and density parameters in ecological models, *Oikos* p. 293.

Higdon, J. W. and Ferguson, S. H. (n.d.). Loss of Arctic sea ice causing punctuated change in sightings of killer whales (Orcinus orca) over the past century, *Ecological Applications* **19**(5).

Kuehn, C., Siegmund, S. and Gross, T. (2013). Dynamical analysis of evolution equations in generalized models, *IMA J. Appl. Math.* **78**(5): 1051.

Lan, Y. and Li, Q.-G. (2008). Control of hopf bifurcation in a simple plankton population model with a non-integer exponent of closure, *Applied mathematics and computation* **200**(1): 220–230.

Loseto, L. L. (2008). Beaufort sea beluga whales: An ecological approach in examining diet and dietary sources of mercury.

Majewski, A. R., Atchison, S., MacPhee, S., Eert, J., Niemi, A., Michel, C. and Reist, J. D. (2017). Marine fish community structure and habitat associations on the Canadian Beaufort shelf and slope, *Deep Sea Res. Part I Oceanogr. Res. Pap.* **121**: 169.

Majewski, A., Walkusz, W., Lynn, B., Atchison, S., Eert, J. and Reist, J. (n.d.). Distribution and diet of demersal Arctic cod, Boreogadus saida, in relation to habitat characteristics in the Canadian Beaufort Sea., *Polar Biol.* **39**(6): 1087.

May, R. M. (1972). Will a large complex system be stable?, *Nature* **238**(5364): 413.

Moore, S. E. and Huntington, H. P. (2008). Arctic marine mammals and climate change: Impacts and resilience, *Ecol. Appl.* **18**(sp2): S157.

Naisbit, R. E., Rohr, R. P., Rossberg, A. G., Kehrli, P. and Bersier, L.-F. (2012). Phylogeny versus body size as determinants of food web structure, *P. Roy. Soc. B-Biol. Sci.* **279**(1741): 3291.

Newman, M. (2018). *Networks*, Oxford University Press.

Plagányi, É. E. (2007). Models for an ecosystem approach to fisheries.

Polis, G. A. (1998). Stability is woven by complex webs, *Nature* **395**(6704): 744.

Rantanen, M., Karpechko, A. Y., Lipponen, A., Nordling, K., Hyvärinen, O., Ruosteenoja, K., Vihma, T. and Laaksonen, A. (2022). The arctic has warmed nearly four times faster than the globe since 1979, *Commun. Earth Environ.* **3**(1): 1.

Rohr, R. P., Scherer, H., Kehrli, P., Mazza, C. and Bersier, L.-F. (2010). Modeling food webs: Exploring unexplained structure using latent traits, *Am. Nat.* **176**(2): 170.

Roy, S. and Chattopadhyay, J. (2007). The stability of ecosystems: A brief overview of the paradox of enrichment, *J. Biosci.* **32**(2): 421.

Serreze, M. C. and Barry, R. G. (2011). Processes and impacts of arctic amplification: A research synthesis, *Glob. Planet. Change* **77**(1-2): 85.

Smith, M. A., Goldman, M. S., Knight, E. J. and Warrenchuk, J. J. (2017). *Ecological Atlas of the Bering, Chukchi, and Beaufort Seas*, Audubon Alaska.

Stafford, K., Moore, S., Spillane, M. and Wiggins, S. (2007). Gray whale calls recorded near Barrow, Alaska, throughout the winter of 2003-04, *Arctic* p. 167.

Stouffer, D. B., Rezende, E. L. and Amaral, L. A. N. (2011). The role of body mass in diet contiguity and food-web structure, *J. Anim. Ecol.* **80**(3): 632.

Thorsteinson, L. K. and Love, M. S. (2016). Alaska Arctic marine fish ecology catalog.

Wallach, A. D., Ripple, W. J. and Carroll, S. P. (2015). Novel trophic cascades: Apex predators enable coexistence, *Trends Ecol. Evol.* **30**(3): 146.

Williams, R. J., Anandanadesan, A. and Purves, D. (2010). The probabilistic niche model reveals the niche structure and role of body size in a complex food web, *PloS one* **5**(8): e12092.

Woodward, G., Ebenman, B., Emmerson, M., Montoya, J., Olesen, J., Valido, A. and Warren, P. (2005). *Body-size determinants of the structure and dynamics of ecological networks*, Academic Press, p. 179.

Yeakel, J. D., Pires, M. M., Rudolf, L., Dominy, N. J., Koch, P. L., Guimarães, P. R. and Gross, T. (2014). Collapse of an ecological network in Ancient Egypt, *PNAS* **111**(40): 14472.

Chapter 5 Conclusion

Introduced by Thilo Gross, Ulrike Feudel, and Wolfgang Ebenhöh in 2004, generalized modeling is a relatively new approach for the analysis of dynamical systems. Its power lies in its ability to analyze systems that are large and complex, and where it is generally not possible to know or explicitly define every process in the system. Generalized modeling has been especially developed for analyses of ecological networks. Real ecological systems are extremely large and can comprise thousands of interacting species for which biomass estimates, flow magnitudes, and interaction-process functionality are impractical or impossible to measure for every connection. Such measurements would be needed for conventional dynamical-system modeling techniques. Generalized modeling, in contrast, does not require the position of fixed points in the state space of the system, but assumes such points exist and transforms the state variables by normalizing them to the fixed point. The subsequent transformed parameters are interpretable and become the relative weighting among processes and the "nonlinearity" of each process. The relative weightings are interpreted as the proportion a particular process contributes to the total flow of like-processes and the nonlinearity of a process, or exponent parameter, are measures of a process's sensitivity. In this thesis, the linearized stability of fixed points from generalized ecological networks is used to explore how ecosystem features impact functioning and stability of the systems.

Generalized Models for Ecological Insight - There is a perennial interest in understanding how enrichment impacts food web dynamics, especially as many food webs world wide experience anthropogenic eutrophication. There is also motivation for understanding the impact of increased productivity in exploited systems, as increasing the productive capacity of the food web increases the abundance of an exploited species. The first mathematical analyses exploring the effects of "enrichment" began with Rosenzweig in 1971, where he warned that attempting to increase food yield by increasing the supply of a limiting resource may have devastating consequences to the stability of the system (Rosenzweig; 1971). However, in real systems, this destabilizing effect from enrichment remains largely unobserved (Roy and Chattopadhyay; 2007). Nonetheless, most mathematical food-web models have shown that the destabilization of a steady state occurs when the system is enriched, pushing the system into a fluctuating state. However, many recent theoretical explorations of ecosystem behavior have demonstrated stability behavior after enrichment that differs from the destabilization Rosenzweig warned of, as the complexities of the real systems on which now theoretical analyses are based are better understood and those details are taken into account (Gross et al.; 2004; Awender et al.; 2021). Many theoretical studies have found that the presence of less

profitable prey (inedible, unpalatable, invulnerable, etc.) effectively reduces the amplitude of oscillations or renders unstable condition unreachable from enrichment (Genkai-Kato and Yamamura; 1999; Abrams and Walters; 1996). Alternatively, empirical studies have proposed that the hampering of the ability of a predator to exploit prey could induce stability (Veilleux; 1979; Luckinbill; 1973), later supported with a mathematical analysis and theoretical reasoning (Harrison; 1995).

From this dissertation, the impacts from enrichment are examined by building food webs containing anywhere from 2 to 60 species and using these model webs to test how the stability of a fixed point changes due to enrichment mechanisms. Such fixed points are traced as they change coordinates and enter different dynamical stability regimes. The stability profiles (bifurcation diagram) can be sensitive to different topologies in large networks, however, most stability profiles assumed one of the few general patterns. Among these patterns, and belonging to a considerable proportion of the topologies, is a stable region centrally located within the nonlinearity space indicating that a theoretical path of enrichment will cross through the stable region thereby describing systems that are stabilized by enrichment in a resource-deprived environment and subsequently destabilized as the systems become "overly enriched". Using a four-species food web as a specific, deterministic model and transferring the fixed points into a generalized modeling context such that actual paths of enrichment can be determined (which cannot be done in the generalized modeling framework). In that case, the stable region is not in a centrally-isolated location like the profiles discussed previously. Instead, the stable region has a centrally-located protrusion and, with the right system parameters, paths move across the protrusion to describe the same stabilizing-then-destabilizing effect as the system is enriched. Additionally, the four-species food webs (Chapter 3) and the thousands of large webs (Chapter 2) support the observed phenomena (Roy and Chattopadhyay; 2007) that predators in a hunting-hampered environment or offered less profitable prey favor a stable steady state. This is inferred from the fixed points having a large value for the nonlinearity (sensitivity) of the predator response, a condition that generally favors a stable steady state. As hunting conditions or nutritional quality of prey is made less profitable, a larger prey population is required to support the same predator growth as when conditions were more profitable, effectively increasing the half saturation of a predator response. When prey populations are fixed, increasing the half-saturation constant increases the sensitivity of the predator's response. Predator responses are most sensitive when prey populations are lowest, thus hungry predators may be indicative of a stable steady state.

Southern Beaufort Sea Ecosystem - In Chapter 3, a series of generalized models is developed to explore the Southern Beaufort Sea Ecosystem. This is motivated by ecosystem changes that are underway and expected under climate change. Arctic sea-ice extent has

been trending downward for nearly 4 decades, resulting in 30% less ice from the months of September in 2019 from initial recording year (1980) (Box et al.; 2019). As ice declines, ice-obligate species such as polar bear, arctic cod, and walrus are likely to decline and/or become extirpated from some areas of the Arctic, and thus would no longer be members of many Arctic marine ecosystems. A reduction in the sympagic (associated with ice) habitat is also permitting more temperate species to move into Arctic habitats (Moore and Huntington; 2008). One such pertinent, recent addition to some Arctic regions related to sea-ice loss have been killer whales. As sea ice declines, it allows these southern visitors to penetrate farther north and stay longer (Higdon and Ferguson; n.d.). Sea-ice loss and warmer sea surface temperatures are also believed to allow more southerly distributed forage fish species, such as saffron cod, to become formidable competitors to arctic cod and other endemic ecosystem members (Deary et al.; 2021).

A changing climate is a portent of ecosystem restructuring and changes in Arctic community composition. In ecology, trophic cascade theory encapsulates the notion of key ecosystem players, the idea that some members of the ecosystem play an extraordinary role that dramatically influences overall ecosystem function or the state of the system. Examples of such key species may include those of interest in invasion biology and large-bodied apex predators. Invasive species may cause extinctions of native species through competitive exclusion (Mooney and Cleland; 2001) while the presence of super predators is thought to enhance biodiversity by limiting population irruptions of both native and non-native species permitting coexistence (Wallach et al.; 2015). To identify species with powerful ecological influence is to permit efficacious prediction of climate warming impacts and better develop appropriate conservation policy under climate change.

Thus, in Chapter 3, thirty species are carefully selected that are estimated to be the most ecologically significant in the functioning of the Southern Beaufort Sea ecosystem, mostly based off of recorded abundances and biomasses in wild catches and stomach contents. They compose a species pool that spans over 12 orders of magnitude of body masses. We selected a few candidate species that may serve important functions to the ecosystem in the Beaufort Sea and investigate the stability differences from their presence and absence. The chosen included those with unique qualities, such as: Super predators (polar bear and killer whale), body mass outliers (bowhead whale and copepods), and a known species with a notably high biomass dominance and a partly sympagic life history (arctic cod). From the GM approach, biomass has no notion and the only explicitly-modeled species traits are foraging traits, body mass, and frequented habitats. In any case, no major impact is detected from the bowhead whale, copepods, or cod; however, a large destabilizing impact is observed when either super predator is present.

In addition to the species compositions, the effects of other realistic system features on stability are explored. These include the aforementioned foraging traits which predict the existence of a particular predator-prey connection. The foraging traits typically follow a general trend that most species forage for prey within the same body-size range relative to that of the predator. Specialized feeding traits allow species to prey more frequently or less frequently than would otherwise be predicted from the general body-mass ratio trend. An amiable example would be baleen whales, the largest species feeding on some of the smallest ones. Another incorporated realistic feature is adjusting the relative weightings between a species' outflows or inflows based on how close the relationships are to the optimal mass ratio. As a last extension to better replicate nature, we organize the food-web structure to simulate the modularity of ecological networks due to habitats and niches. For this, we set the probability of any two species forming a connection to zero if they do not share a habitat in common. Each realistic modification to the food webs results in a net stabilizing effect.

Advantages of Generalized Modeling - Over the past several decades, a variety of abstract analysis methods of dynamical systems have been introduced. Random matrix models is one approach that randomly generates the studied systems. One renowned piece (May; 1972) that labels a random matrix with a mean value of zero minus the identity matrix as the Jacobian of an ecological network and finds an unstable system when the product of the square of the variance of the random matrix, size, and connectance, becomes large enough. This product feature is often referred to as the "complexity" of a system, thus this work illustrates how structural complexity is inherently a destabilizing feature of random systems. The only way to incorporate the physics into random matrix models, one must control the probability distribution from which the random samples are drawn to replicate the details and intricacies of real systems. In the work of May, this is touched on by modularizing the system into three disjoint submatrices, leaving all other elements of the larger matrix zero (i.e. no link) and finds that these networks can be stable for larger complexity. Generalized modeling (GM) is considered an abstract analysis as well, but instead of random matrices, the elements of the linearized system are founded by ecological motivation and constraints and can be reduced to fit any specific model with the same class of equations of motion. GM transforms the more tangible state variables and system parameters to a more abstract framework, but it preserves the Jacobian (Kuehn et al.; 2013) so we really do draw inferences from real fixed points of the ecological networks. By comparison, conventional modeling is considered more computationally limited and relies heavily on accurate empirical estimates of system parameters, and often varies a single system parameter for insight into the different dynamical regimes and interpretation. That GM is far more computationally efficient and minimally reliant on empirical observations affords much greater versatility.

Understanding Food Webs as Complex Dynamical Systems - In this thesis and in analyses published elsewhere, chaotic dynamical regions in the space of model ecosystem parameters can be found even in small, simple food webs, along with two-tori, three-tori, and multiple attractors (Hastings and Powell; 1991; Gross et al.; 2005) (Chapter 3). The dynamical regions show sensitivity to small changes in topology: For example, adding a single link to a network with 258 connections and connectance of 0.3 altered the bifurcation diagram so much that it made a completely unstable web across the parameter space into a largely stable one (Awender et al.; 2021). In another example, introducing a very weak perturbation on food webs, that simulates the effect of a larger weakly-interacting ecological network subsuming the food web, creates large stable regions in the parameter space from completely unstable webs when the perturbation strength is null. In the latter example, increasing the characteristic strength of the perturbation continues to impart a net stabilizing impact until further increase begins a destabilizing effect, leaving an optimal characteristic strength that maximizes the average size of stable regions in the system's generalized parameter space.

On the other hand, despite sometimes extreme sensitivity resulting from small structural changes, there is notion of topological equivalence in food webs. Early on in GM research, it was noticed that food webs with distinct trophic levels (i.e. no omnivory) have identical bifurcation diagrams, i.e. the same local dynamics throughout the system's generalized parameter space, as food chains with the same number of trophic levels (Gross and Feudel; 2009). Furthermore, when food webs have omnivorous species but the omnivory is regularly dispersed to every species, equivalence patterns in the bifurcation diagrams also emerge (Awender et al.; 2021).

Overall Perspective and Outlook for Future Development - Just as mathematical models that include ever increasing levels of realistic detail begin to predict patterns observed in real systems as they become enriched, so too, may the stability of highly complex (large and highly connected) mathematical systems better reflect what is hypothesized from empirical observation. An addition to the models presented in this dissertation, a viable next consideration would be to incorporate more species types, especially of those that complete cycles in the network. Ecological cycles of material, such as water and carbon dioxide, are required for long-term self-sustainability of life. The anti-symmetric forms between the chemical reactions of photosynthesis and cellular respiration is a powerful testament to the validity of this claim. Nutrient recycling from decomposers and nutrient waste reduction from detrivores would be species types for incorporating the cyclic nature of real systems into the community networks studied here. These have been incorporated into other ecosystem modeling frameworks, but have not yet been included in analyses using generalized modeling.

Generalized modeling is predominantly used for linearized stability analysis. Although

GM is computationally efficient and has practical use for the investigation of overarching features that favor stability and meta-analysis, more detail can be gathered from specific models, such as: transient dynamics, multiple fixed points, multiple attractors, identification of complex invariant sets, or global bifurcations. This appears to be a major limitation for GM research. How much insight could we possibly gain from knowledge of all the fixed points? Perhaps, the continued research that combines GM with specific models will make this more clear.

5.1 References

Abrams, P. A. and Walters, C. J. (1996). Invulnerable prey and the paradox of enrichment, *Ecology* **77**(4): 1125.

Awender, S., Wackerbauer, R. and Breed, G. A. (2021). Stability of generalized ecological-network models, *Chaos* **31**(2): 023106.

Box, J. E., Colgan, W. T., Christensen, T. R., Schmidt, N. M., Lund, M., Parmentier, F.-J. W., Brown, R., Bhatt, U. S., Euskirchen, E. S., Romanovsky, V. E. et al. (2019). Key indicators of Arctic climate change: 1971–2017, *Environ. Res. Lett.* **14**(4): 045010.

Deary, A., Vestfals, C., Mueter, F., Logerwell, E., Goldstein, E., Stabeno, P., Danielson, S., Hopcroft, R. and Duffy-Anderson, J. (2021). Seasonal abundance, distribution, and growth of the early life stages of polar cod (Boreogadus saida) and saffron cod (Eleginus gracilis) in the US Arctic, *Polar Biol.* **44**(11): 2055.

Genkai-Kato, M. and Yamamura, N. (1999). Unpalatable prey resolves the paradox of enrichment, *P. Roy. Soc. B-Biol. Sci.* **266**(1425): 1215.

Gross, T., Ebenhöh, W. and Feudel, U. (2004). Enrichment and foodchain stability: The impact of different forms of predator–prey interaction, *J. Theor. Biol.* **227**(3): 349.

Gross, T., Ebenhöh, W. and Feudel, U. (2005). Long food chains are in general chaotic, *Oikos* **109**(1): 135.

Gross, T. and Feudel, U. (2009). Local dynamical equivalence of certain food webs, *Ocean Dyn.* **59**(2): 417.

Harrison, G. W. (1995). Comparing predator-prey models to Luckinbill's experiment with Didinium and Paramecium, *Ecology* **76**(2): 357.

Hastings, A. and Powell, T. (1991). Chaos in a three-species food chain, *Ecology* **72**(3): 896.

Higdon, J. W. and Ferguson, S. H. (n.d.). Loss of Arctic sea ice causing punctuated change in sightings of killer whales (Orcinus orca) over the past century, *Ecol. Appl.* **19**(5).

Kuehn, C., Siegmund, S. and Gross, T. (2013). Dynamical analysis of evolution equations in generalized models, *IMA J. Appl. Math.* **78**(5): 1051.

Luckinbill, L. S. (1973). Coexistence in laboratory populations of Paramecium aurelia and its predator Didinium nasutum, *Ecology* **54**(6): 1320.

May, R. M. (1972). Will a large complex system be stable?, *Nature* **238**(5364): 413.

Mooney, H. A. and Cleland, E. E. (2001). The evolutionary impact of invasive species, *PNAS* **98**(10): 5446.

Moore, S. E. and Huntington, H. P. (2008). Arctic marine mammals and climate change: Impacts and resilience, *Ecol. Appl.* **18**(sp2): S157.

Rosenzweig, M. L. (1971). Paradox of enrichment: Destabilization of exploitation ecosystems in ecological time, *Science* **171**(3969): 385.

Roy, S. and Chattopadhyay, J. (2007). The stability of ecosystems: A brief overview of the paradox of enrichment, *J. Biosci.* **32**(2): 421.

Veilleux, B. (1979). An analysis of the predatory interaction between Paramecium and Didinium, *J. Anim. Ecol.* **48**(3): 787.

Wallach, A. D., Ripple, W. J. and Carroll, S. P. (2015). Novel trophic cascades: Apex predators enable coexistence, *Trends Ecol. Evol.* **30**(3): 146.